

# Climate and Environmental Remote Sensing

## 09 – *Carbon cycle and vegetation: Photosynthesis*

Wouter Dorigo, Matthias Forkel, Leander Mössinger



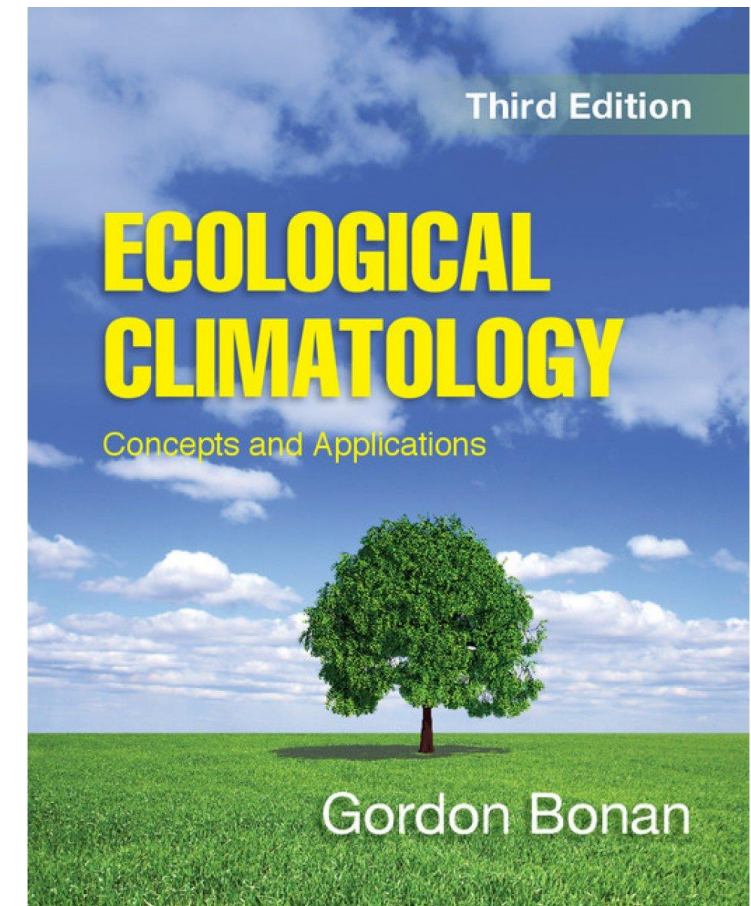
Forschungsgruppe Klima- und Umweltfernerkundung  
<http://climers.geo.tuwien.ac.at/>  
Vienna University of Technology  
Department of Geodesy and Geoinformation

# Schedule

Date	Topic / Holidays	Type	Presenter	Exercise	Deadlines
07.03.2019	Intro LV, Earth observation, The Earth system	Theory	WD		
14.03.2019	Earth and Climate system	Theory	WD		
21.03.2019	Earth and Climate system	Theory	WD		
28.03.2019	Earth and Climate system	Theory + introduction exercise 1	MF + LM	Exercise 1	
04.04.2019	Water cycle	Theory	WD		
11.04.2019	EGU conference	Time for exercise			
18.04.2019	Easter holidays	Time for exercise			
25.04.2019	Easter holidays	Time for exercise			
02.05.2019	Water cycle	Theory + introduction exercise 2	WD + LM	Pres./Exam 1; Exercise 2	
09.05.2019	Water cycle	Theory	WD		Report 1
16.05.2019	Living Planet Symposium	Time for exercise			
23.05.2019	Carbon cycle and vegetation	Theory	MF		
30.05.2019	Ascension (Christi Himmelfahrt)	Time for exercise		Presentation/Exam 2	
06.06.2019	Carbon cycle and vegetation	Theory + introduction exercise 3	MF	Exercise 3	Report 2
13.06.2019	Carbon cycle and vegetation	Theory	MF		
20.06.2019	Corpus Christi (Frohnleichnam)	Time for exercise			
27.06.2019	Climate models and projections	Theory	WD	Presentation/Exam 3	
04.07.2018		Deadline Reports			Report 3

# Topics and recommended reading

Topics in Part 3	Bonan et al. (2016)
08 – Global carbon cycle <ul style="list-style-type: none"><li>- Global carbon cycle and atmospheric CO<sub>2</sub></li><li>- Remote sensing of atmospheric CO<sub>2</sub></li><li>- Ecosystem carbon cycle</li><li>- Eddy covariance / Fluxnet</li></ul>	3.5 Biogeochemical cycles (Buchwitz et al. 2017) 20 Ecosystems
09 – Photosynthesis <ul style="list-style-type: none"><li>- Photosynthesis and light absorption</li><li>- Remote sensing of canopies (NDVI, LAI, FAPAR)</li><li>- Sun-induced fluorescence (SIF)</li><li>- Estimation of photosynthesis</li><li>- Ecosystem models</li><li>- Model evaluation</li><li>- Exercise 3</li></ul>	16 Photosynthesis, 17 Plant canopies (Huete et al. 2012) (Frankenberg & Berry 2019) 16 Photosynthesis, 17 Plant canopies (Prentice et al. 2007), 24.3 Global TBMs (Janssen & Heuberger 1995) 25.4 Model Evaluation
10 – Model-data integration, biomass and fire <ul style="list-style-type: none"><li>- Model-data integration</li><li>- Carbon cycle data assimilation systems</li><li>- Carbon turnover and biomass</li><li>- Remote sensing of tree height and biomass</li><li>- Fires</li></ul>	(Keenan et al. 2011) (Kaminski et al. 2013) 24.3 Net Primary Production and Plant Biomass



The Concentration and Isotopic Abundances of Carbon Dioxide in the Atmosphere  
By CHARLES D. KEELING, Scripps Institution of Oceanography, University of California, La Jolla, California  
(Manuscript received March 25, 1960)



**Abstract**  
A systematic variation with season and latitude in the concentration and isotopic abundance of atmospheric carbon dioxide has been found in the northern hemisphere. In Australia, however, no small but permanent increase in concentration has been found. Possible causes of these variations are discussed.

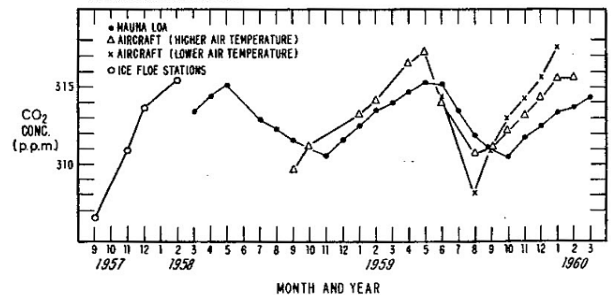
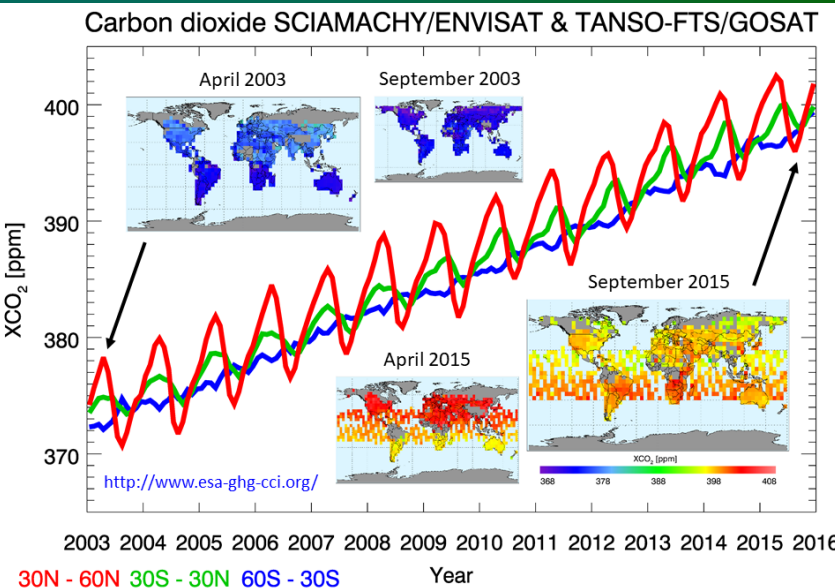
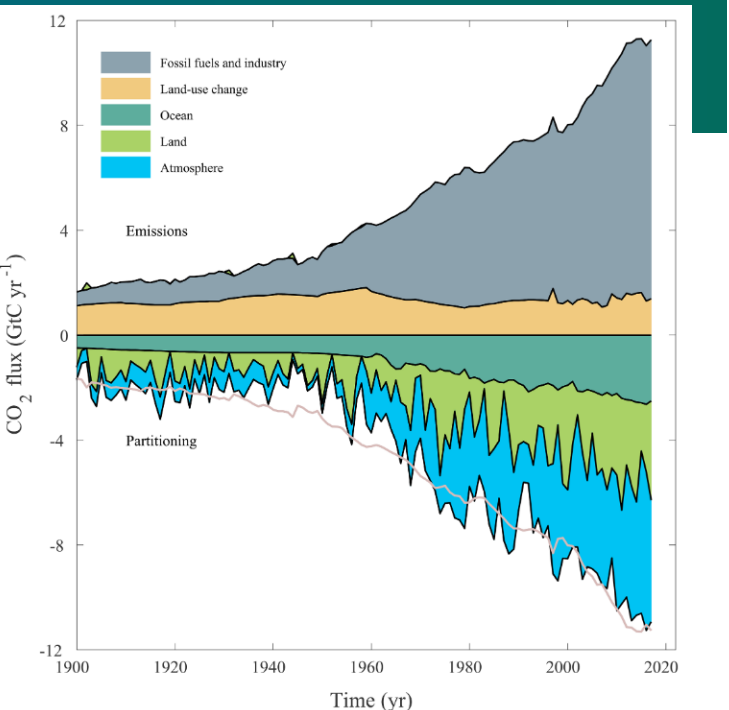
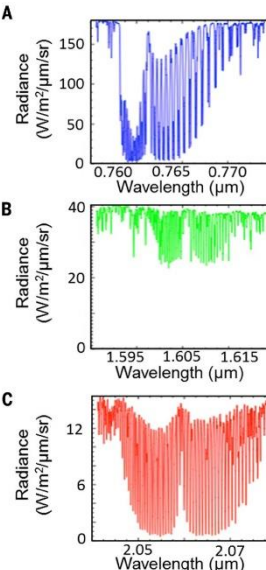
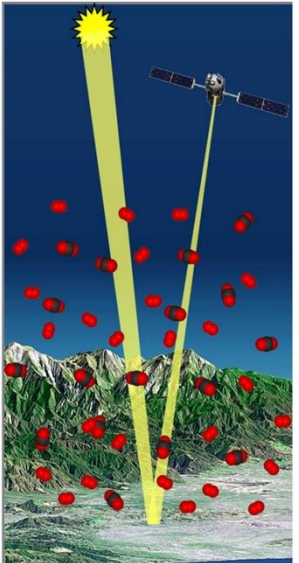
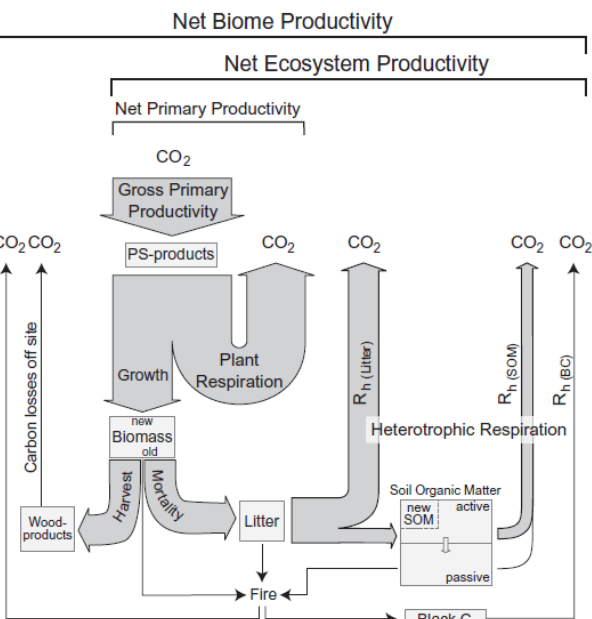
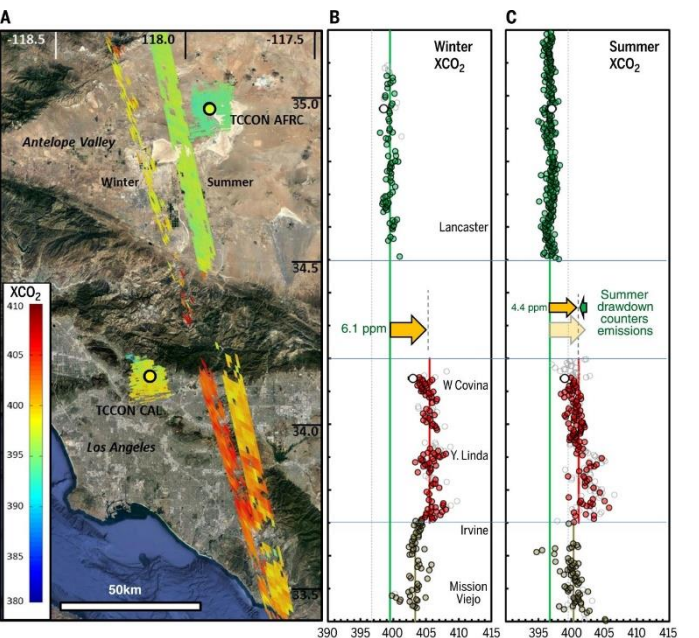


Fig. 1. Variation in concentration of atmospheric carbon dioxide in the Northern Hemisphere.

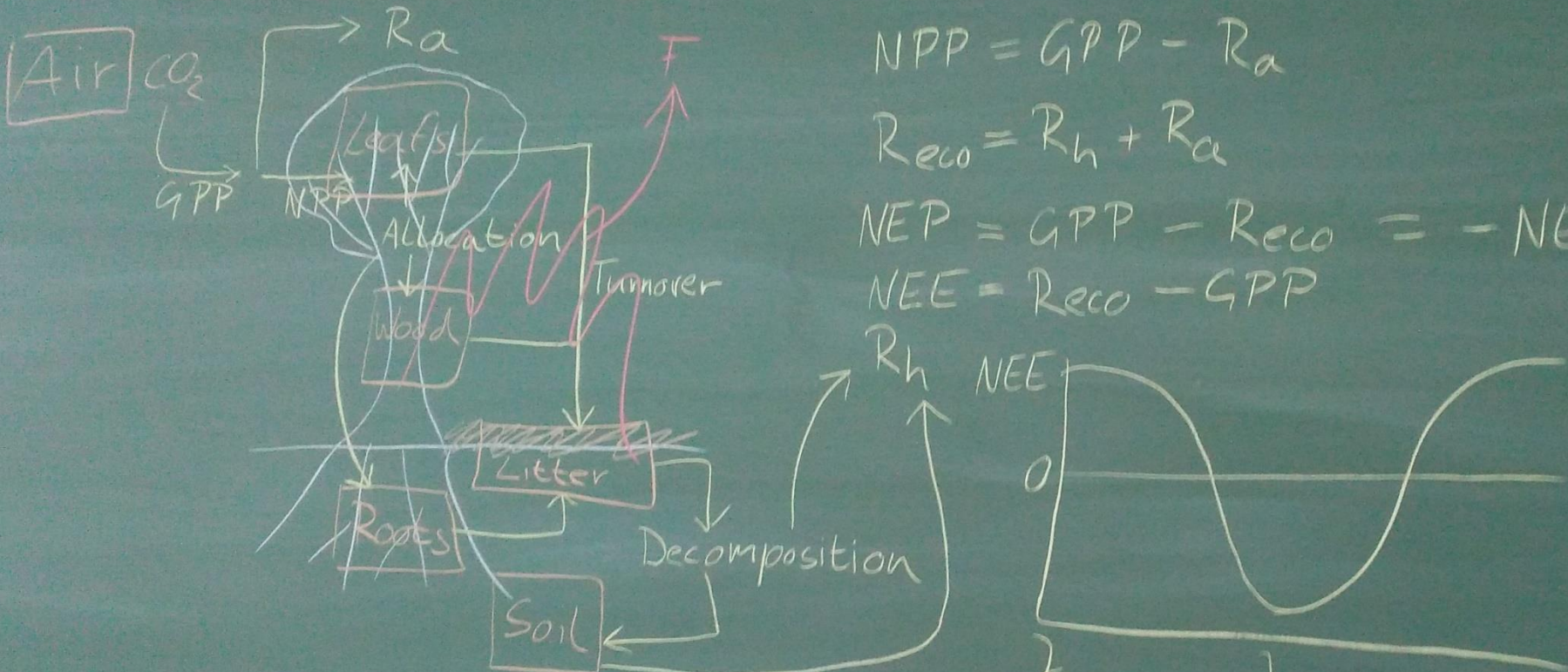
Tellus XII (1960), 2



2003 2004 2005 2006 2007 2008 2009 2010 2011 2012 2013 2014 2015 2016  
30N - 60N 30S - 30N 60S - 30S Year



# Ecosystem carbon cycle

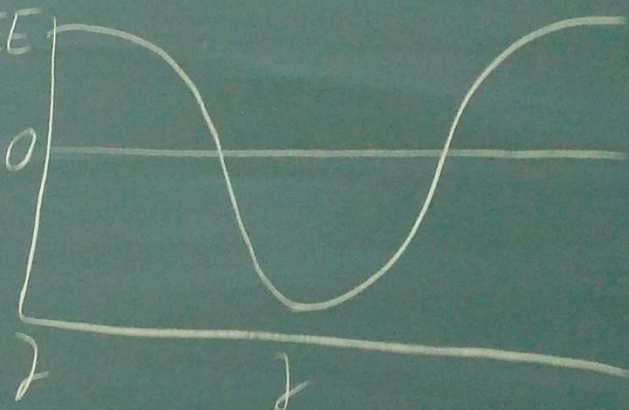


$$\text{NPP} = \text{GPP} - R_a$$

$$R_{\text{eco}} = R_h + R_a$$

$$\text{NEP} = \text{GPP} - R_{\text{eco}} = -\text{NEE}$$

$$\text{NEE} = R_{\text{eco}} - \text{GPP}$$



$$\text{NBP} = \text{NEP} - F$$

$$= \text{GPP}$$

$$-(R_a + R_h + F + LU)$$

$$\text{GPP} = 123$$

$$R_{\text{eco}} + F = 118.7$$

$$R_h = 1.7$$

$$R_a = 0.5 \times \text{GPP} = 61.5$$

$$\text{NPP} = 61.5$$

$$\text{NEP} = 6.5$$

$$\text{NBP} = 4.3$$

$$\text{Loss} = F + LU + \text{Rivers} = 5$$

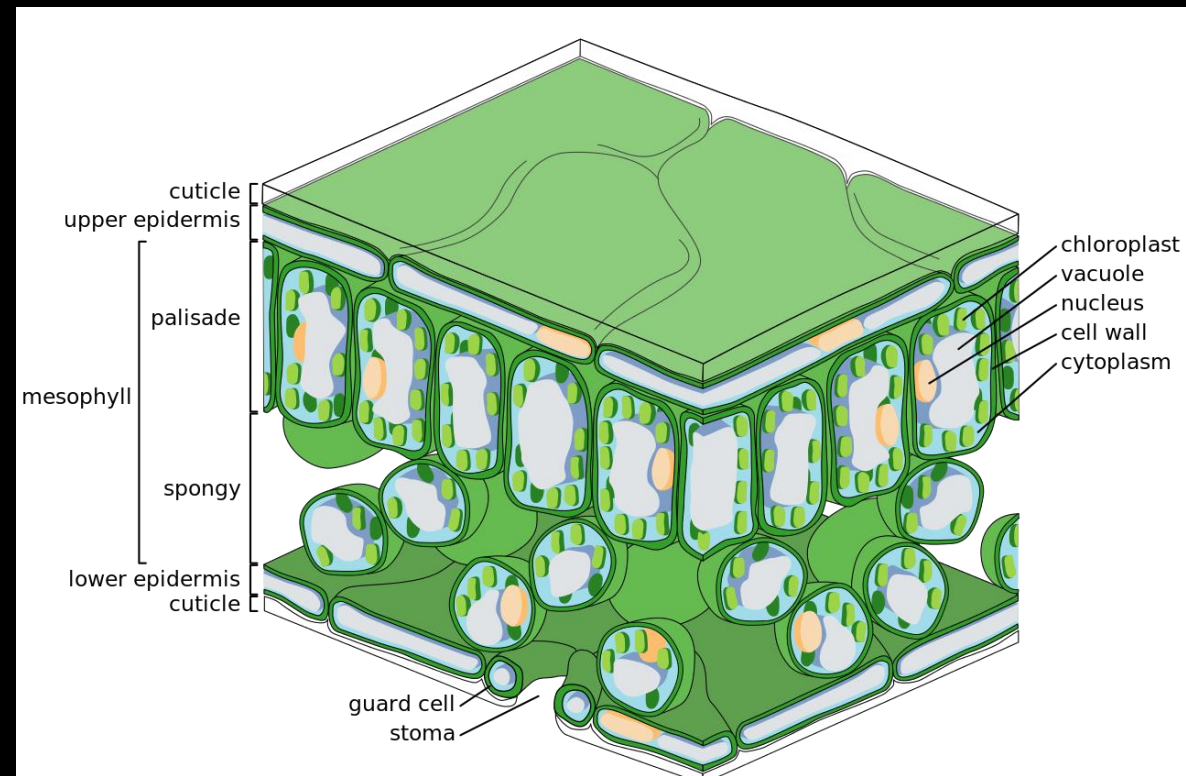
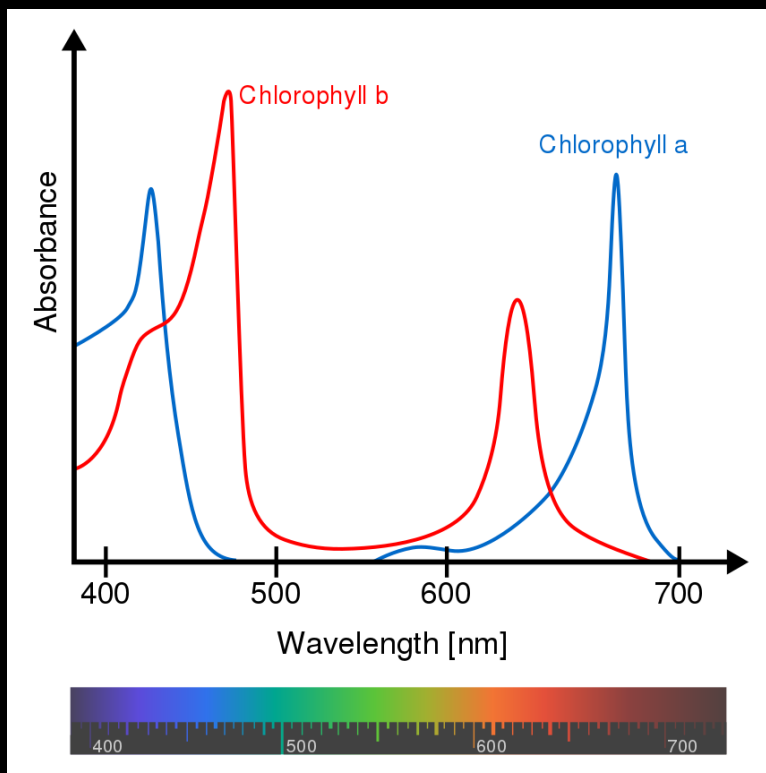
# Photosynthesis and light absorption

Black board

- What is the net chemical reaction of photosynthesis?
- Why are leafs green?

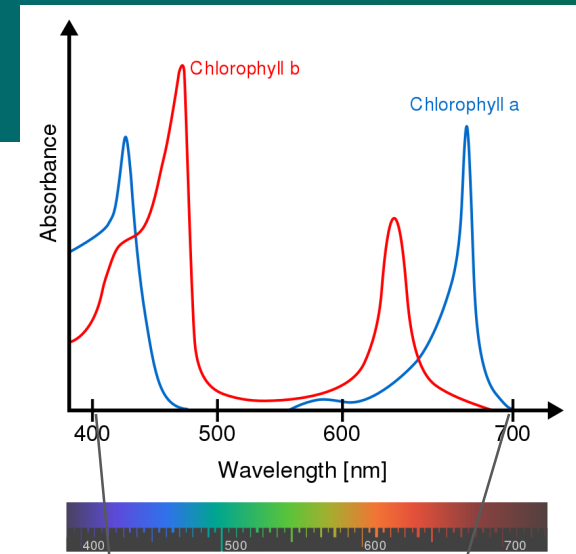
# Leaf photosynthesis

- What is the net chemical reaction of photosynthesis?  $6CO_2 + 6H_2O \xrightarrow{\text{light}} C_6H_{12}O_6 + 6O_2$
- Why are leafs green?

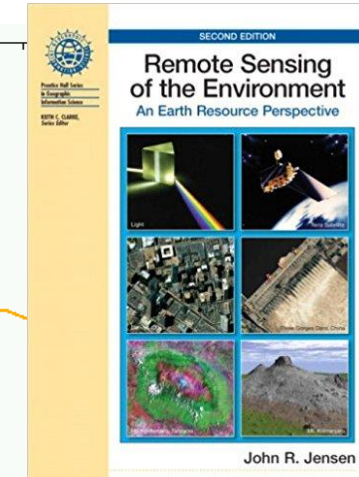
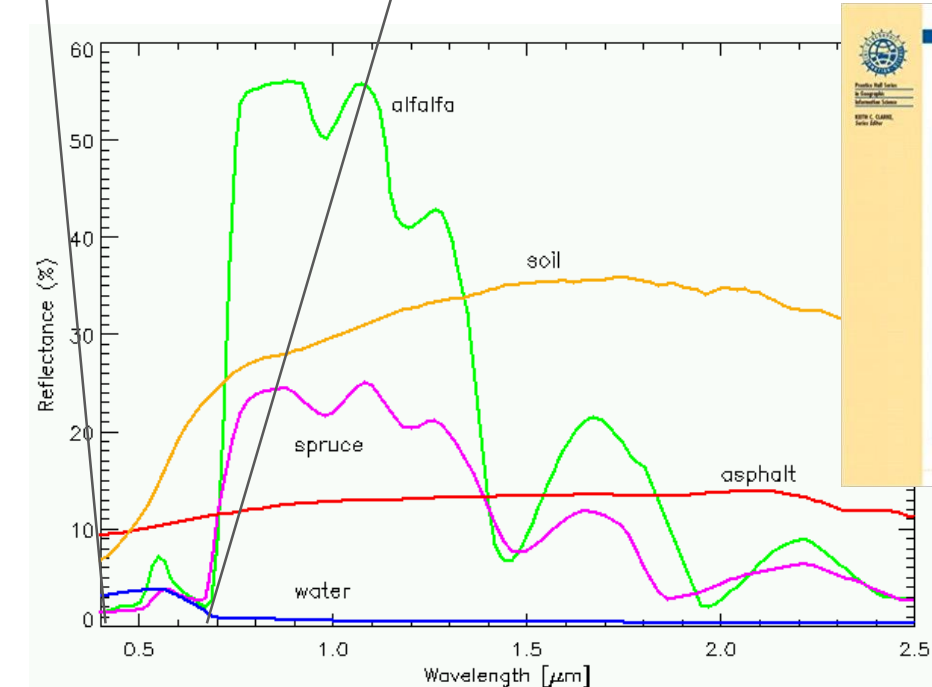


# Light absorption

- “Light”
  - › 400-700 nm (~ visible light)
  - › **PAR**: Photosynthetic active radiation
    - W m<sup>-2</sup>
    - PAR ~45-50% of incoming global solar radiation
  - › **PPFD**: Photosynthetic Photon Flux Density
    - Number of photons received by a surface during a time
    - mol m<sup>-2</sup> s<sup>-1</sup>
- **APAR**: absorbed photosynthetic active radiation
- **fAPAR**: fraction of APAR
  - › APAR = fAPAR \* PAR
  - › fAPAR depends on leaf albedo, leaf area



Wikimedia.org



# Leaf net photosynthesis

## Net photosynthesis

= Gross photosynthesis

- mitochondrial respiration

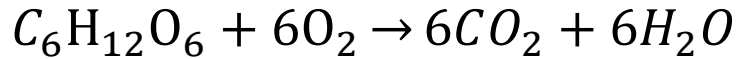


**Table 16.1** Maximum net photosynthesis with natural CO<sub>2</sub> availability, saturated light intensity, optimal temperature, and adequate water

Plant type	CO <sub>2</sub> uptake (μmol m <sup>-2</sup> s <sup>-1</sup> )
<i>Herbaceous</i>	
C <sub>3</sub>	
Grasses	5–15
Crops	20–40
C <sub>4</sub>	30–60
CAM	5–10
<i>Tree</i>	
Tropical broadleaf evergreen	
Sunlit leaves	10–16
Shaded leaves	5–7
Broadleaf deciduous	
Sunlit leaves	10–15
Shaded leaves	3–6
Needleleaf evergreen	3–6
Needleleaf deciduous	8–10

Source: From Larcher (1995, pp. 85–86).

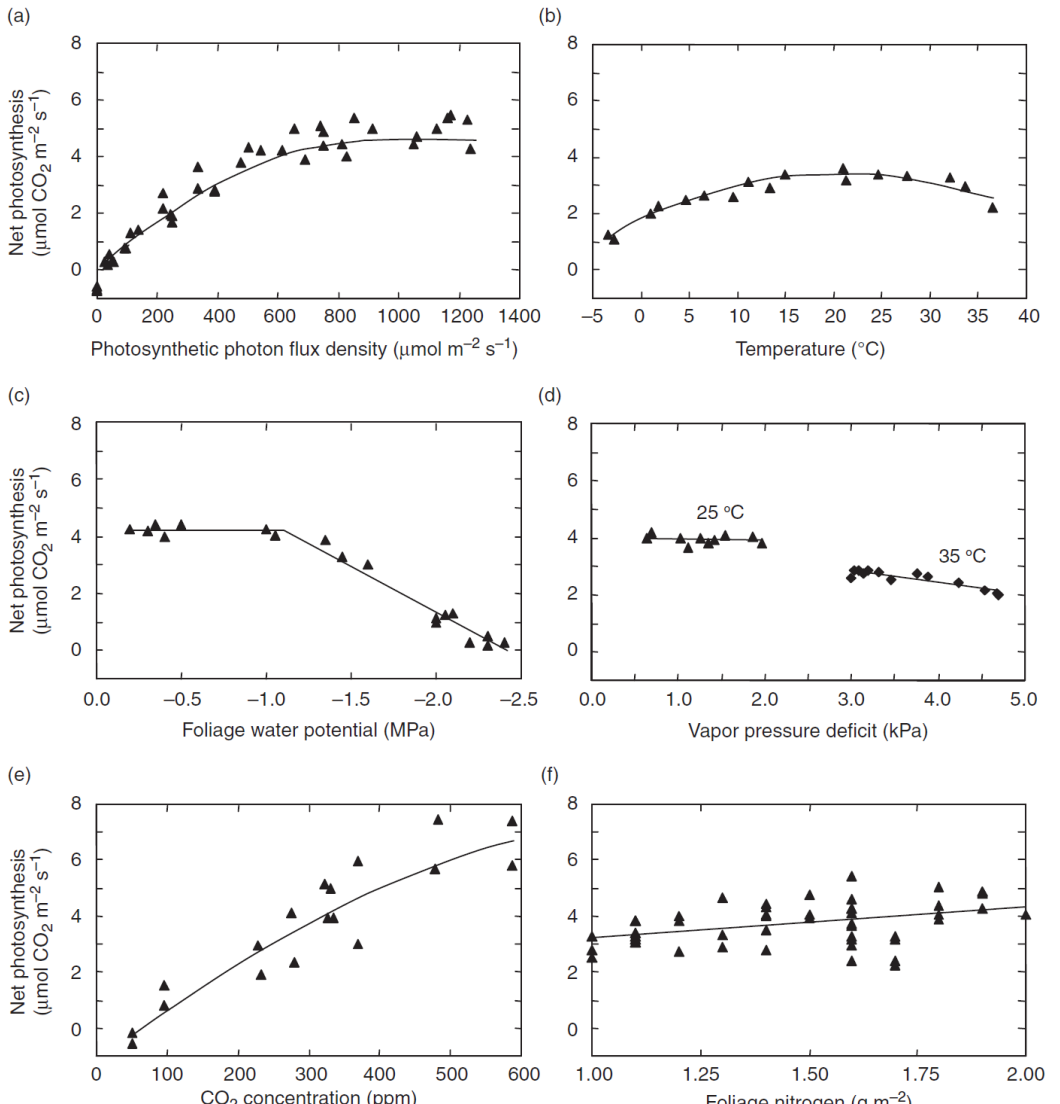


**Fig. 16.3** Environmental controls of net photosynthesis for jack pine trees. Net photosynthesis is shown in response to (a) photosynthetic photon flux density, (b) temperature, (c) foliage water potential, (d) vapor pressure deficit, (e) ambient CO<sub>2</sub> concentration, and (f) foliage nitrogen. Data from Dang et al. (1997a,b, 1998).

# Canopy photosynthesis

- Photosynthesis of all leafs → canopy photosynthesis = gross primary production (GPP)
- „Lambert-Beer law“

$$I(z) = I_0 e^{-K \cdot LAI(z)}$$

$I(z)$  ... irradiance at height  $z$

$I_0$  ... irradiance at top of canopy

LAI ... cumulative **leaf area index**

$K$  ... light extinction coefficient

- Light extinction coefficient  $K$ 
  - Depends on solar zenith angle and leaf orientation
  - Varies 0.2 – 1.9, typically 0.5
  - (Monsi and Saeki 1953)
- fAPAR as a function of LAI

$$fAPAR = 1 - e^{-K \cdot LAI}$$

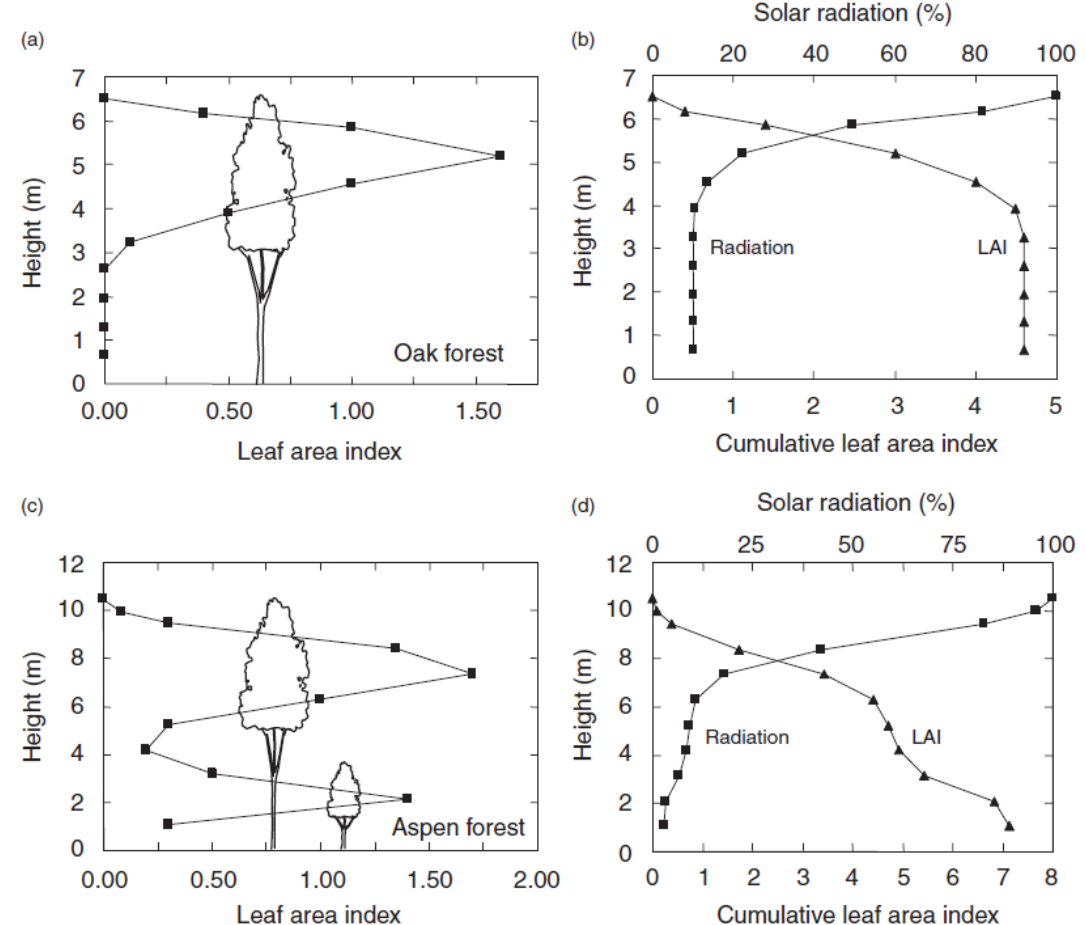


Fig. 17.1 Vertical profile of leaves in forests. The top panels show for an oak forest (a) the leaf area profile and (b) the cumulative leaf area and irradiance as a percentage of that at the top of the canopy. The bottom panels (c-d) show the same data for an aspen forest with understory. Data from Rauner (1976).

# Remote sensing of vegetation canopies

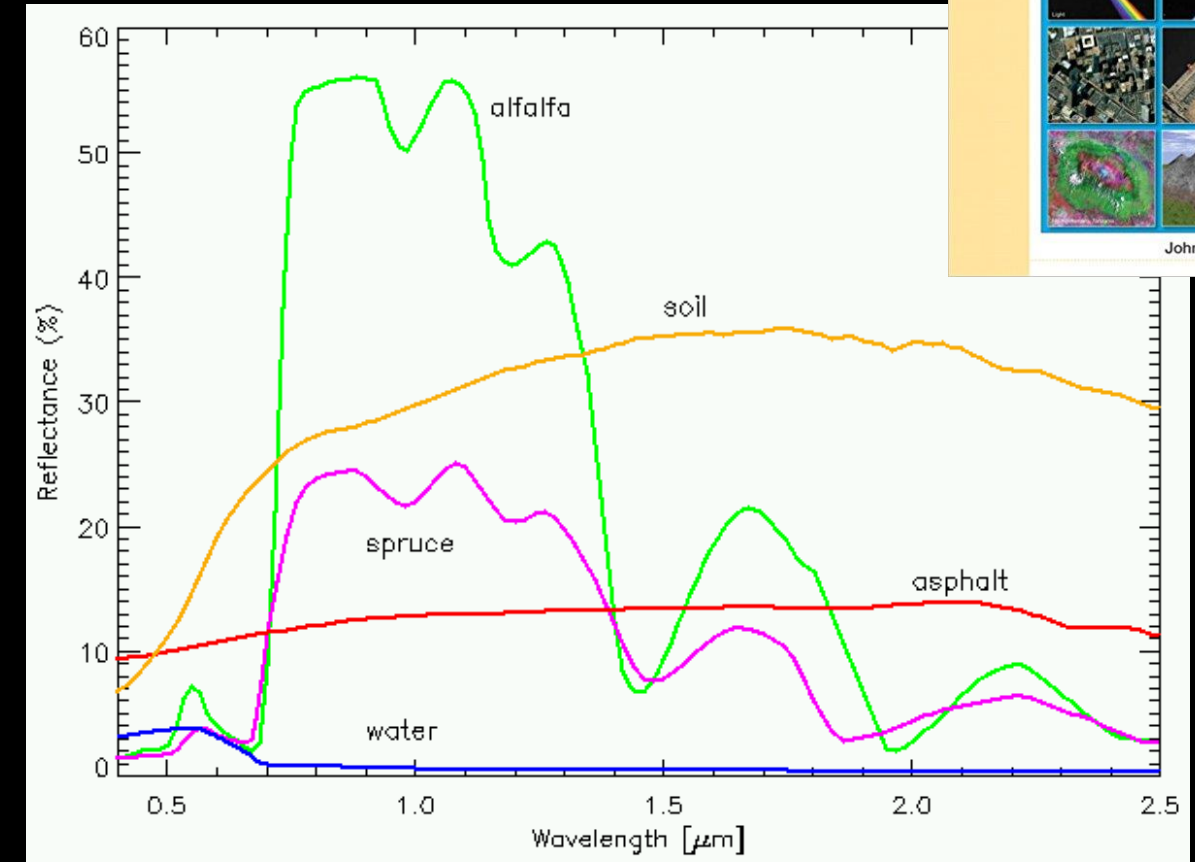
## “greenness”

### (NDVI, FAPAR, LAI)

# Spectral vegetation indices

Black board

- NDVI: Normalized difference vegetation index
- $NDVI = (NIR - Red) / (NIR + Red)$
- Calculate NDVI for the five surface types in the Figure.



# Spectral vegetation indices

The simple ratio (SR) measures the green foliage status of a canopy with a ratio of NIR reflectance with the chlorophyll-absorbing red reflectance (Rouse et al. 1973),

$$SR = \rho_{NIR} / \rho_{red} \quad (1)$$

where  $\rho$  is the reflectance in the NIR or red spectral region (600–700 nm). Similarly the water index (WI) is constructed as the ratio of NIR with a water-absorbing SWIR band, e.g., the Moisture Stress Index (MSI, Hunt and Rock 1989),

$$MSI = \rho_{NIR} / \rho_{SWIR} \quad (2)$$

There are also normalized VIs and WIs that constrain ratio values to within -1 and +1. The most popular is the normalized difference vegetation index (NDVI, Tucker 1979), a functionally equivalent variant of the Simple Ratio,

$$NDVI = (SR - 1) / (SR + 1) = (\rho_{NIR} - \rho_{red}) / (\rho_{NIR} + \rho_{red}) \quad (3)$$

The normalized difference WI (NDWI, Gao 1996) and land surface WI (LSWI, Xiao et al. 2004) are scaled ratios of NIR with a water absorption band at 1240 or 1600 nm, respectively,

$$NDWI = (\rho_{NIR} - \rho_{1240nm}) / (\rho_{NIR} + \rho_{1240nm}) \quad (4)$$

$$LSWI = (\rho_{NIR} - \rho_{1600nm}) / (\rho_{NIR} + \rho_{1600nm}), \quad (5)$$

Linear and optimized combinations of spectral bands are also used to measure foliage *greenness* and water status (Gobron et al. 2000; Huete and Glenn 2011). The enhanced vegetation index (EVI) is an example of optimized spectral band combinations that aim to minimize VI biases from canopy background and aerosol variations,

$$EVI = 2.5(\rho_{NIR} - \rho_{red}) / (L + \rho_{NIR} + C_1\rho_{red} - C_2\rho_{blue}), \quad (6)$$

where L is the soil adjustment factor, and  $C_1$  and  $C_2$  are the aerosol resistance weights. The coefficients of the EVI equation, as used with the coarse resolution Moderate Resolution Imaging Spectroradiometer (MODIS) and medium resolution Landsat sensor data, are  $L = 1$ ;  $C_1 = 6$  and  $C_2 = 7.5$  (Huete et al. 2002). An example of a MODIS EVI image over the Amazon basin is depicted in Figure 5.

*Geography Compass* 6/9 (2012): 513–532, 10.1111/j.1749-8198.2012.00507.x



## Vegetation Indices, Remote Sensing and Forest Monitoring

Alfredo R. Huete\*

Plant Functional Biology and Climate Change Cluster, School of Environment, University of Technology Sydney

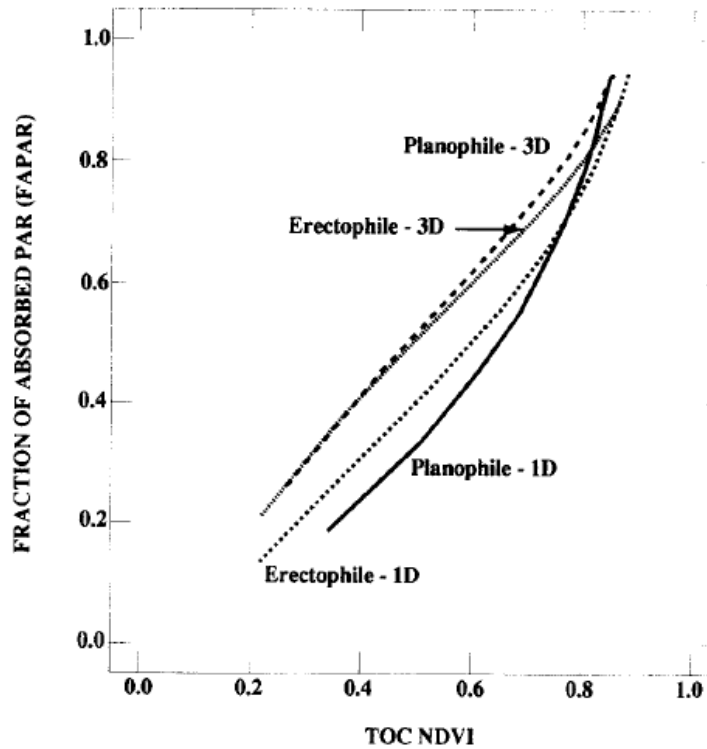
### MODIS Enhanced Vegetation Index



Fig. 5. MODIS EVI composited image of the Amazon basin during the 2005 July–October dry season (image courtesy Robert Simmon).

# NDVI and FAPAR

- Relation between NDVI and FAPAR is linear
- But depends on plant type, background (soil), solar zenith angle



**Figure 7.** The relationship between FAPAR and top of the canopy (TOC) NDVI in homogeneous (1D) and heterogeneous (3D) canopies with different leaf orientation distributions. The other problem parameters are as in the base case.

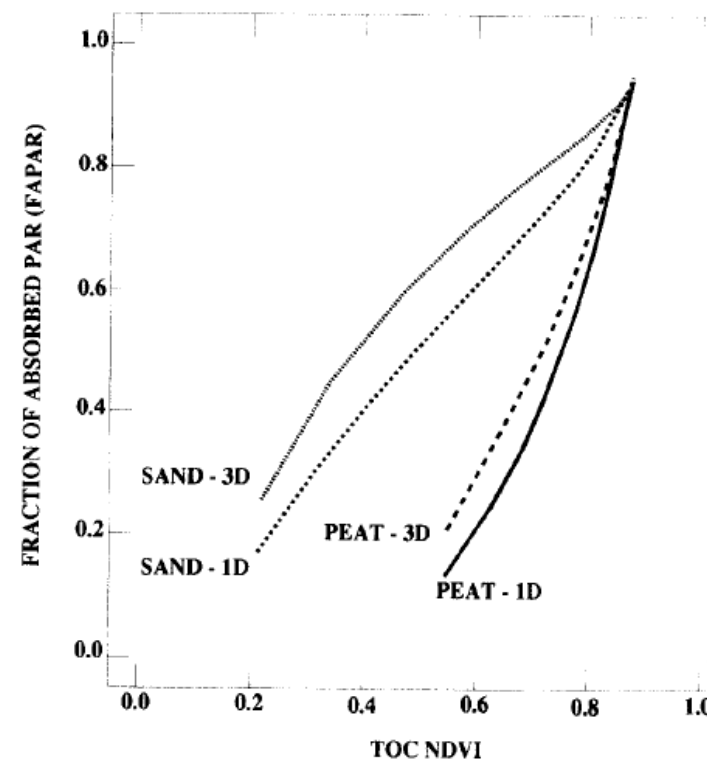


**Figure 8.** The relationship between FAPAR and top of the canopy (TOC) NDVI in homogeneous (1D) and heterogeneous (3D) canopies with different soil backgrounds. The other problem parameters are as in the base case.

## On the Relationship between FAPAR and NDVI

R. B. Myneni<sup>\*,†</sup> and D. L. Williams<sup>\*</sup>

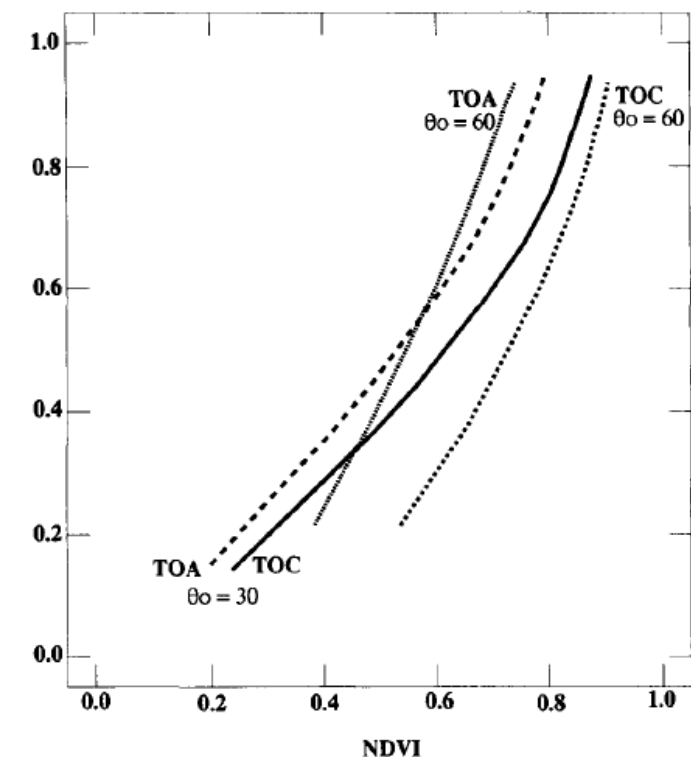


**Figure 9.** The relationship between FAPAR and NDVI in homogeneous canopies at different solar zenith angles  $\theta_0$ . Both top of the atmosphere (TOA) and top of the canopy (TOC) NDVIs are shown. The other problem parameters are as in the base case.

# NDVI and vegetation properties

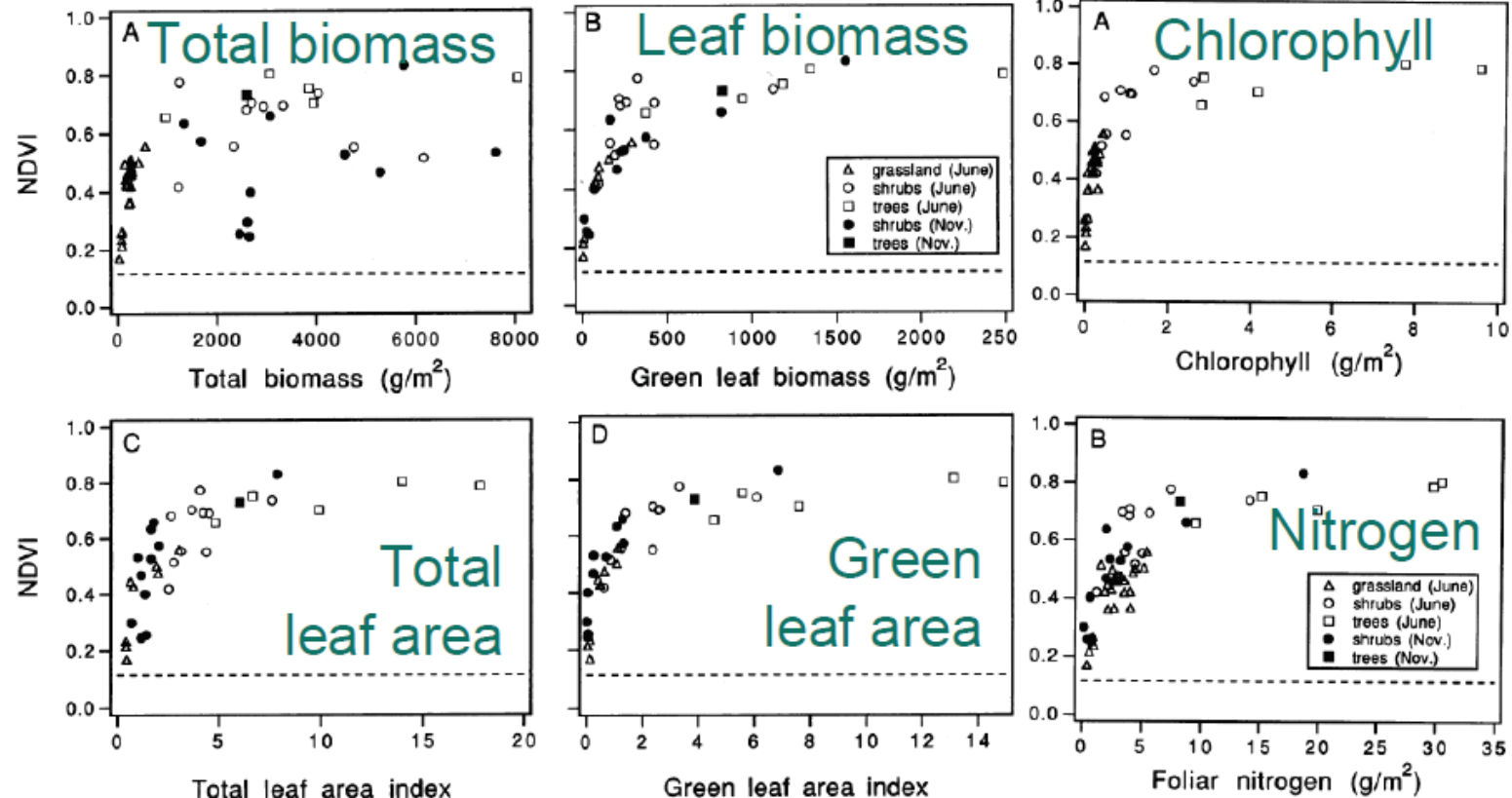


Fig.: Relationships biomass, chlorophyll, LAI, foliar nitrogen and NDVI (Gamon et al. 1995)

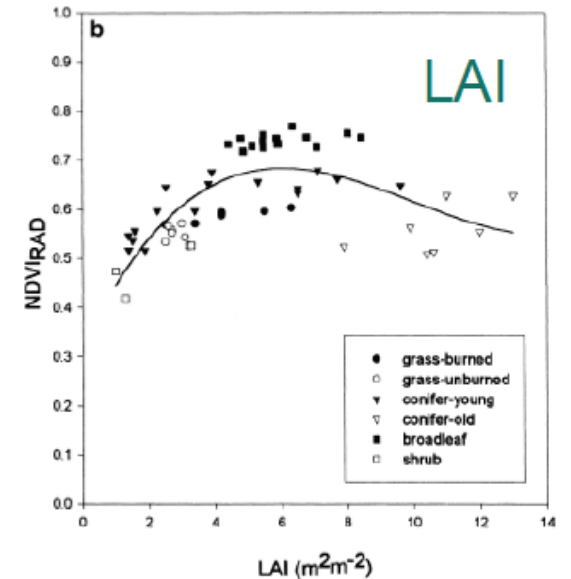
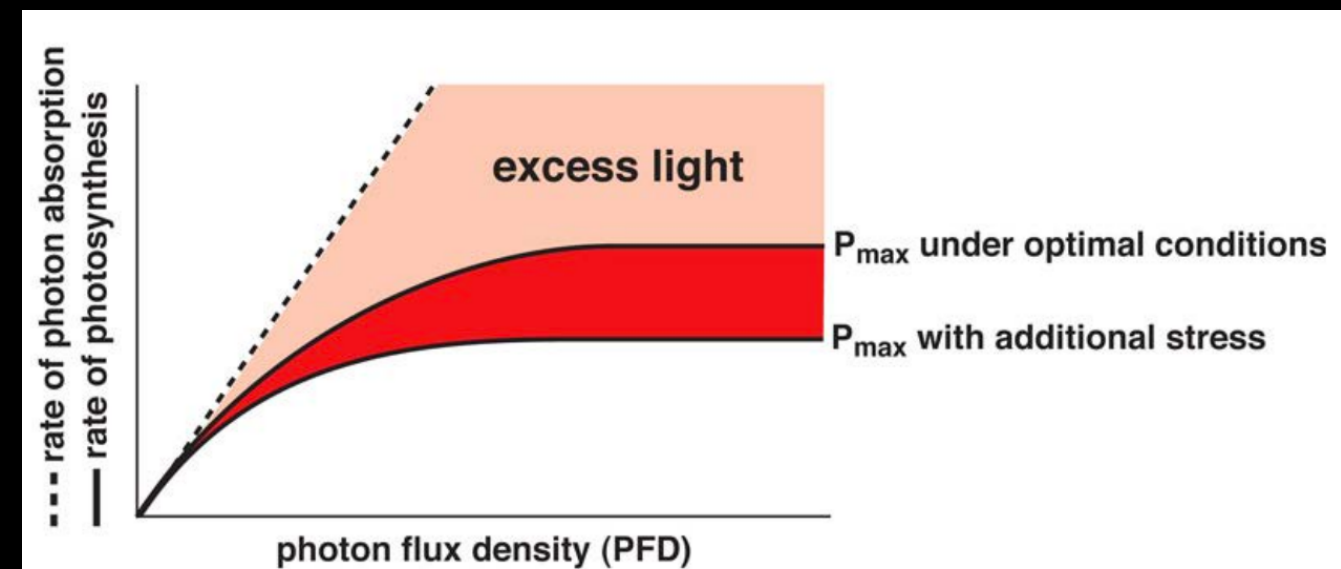
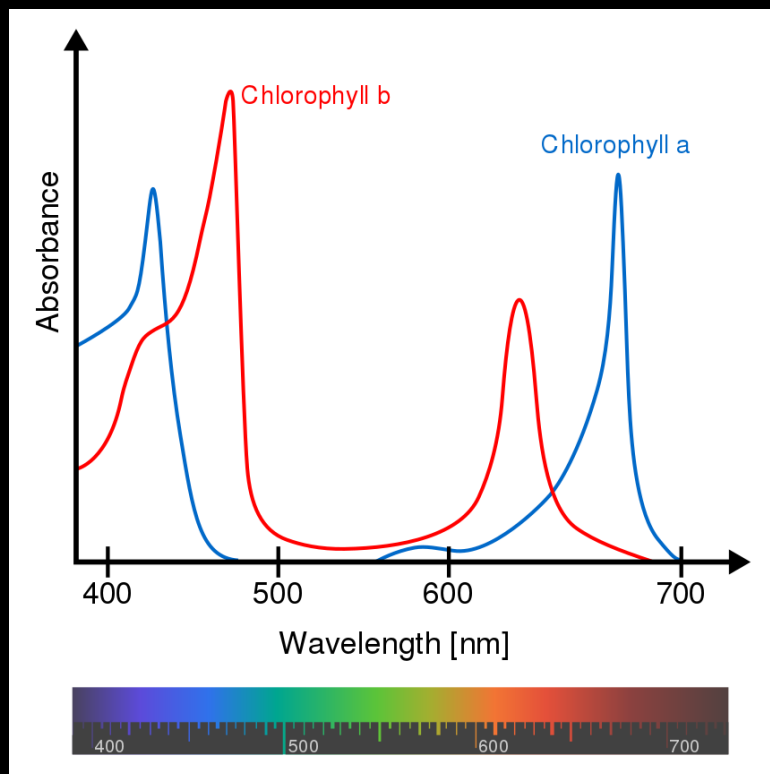


Fig.: Relationship between leaf area index and NDVI calculated on radiances (Turner et al. 1999)

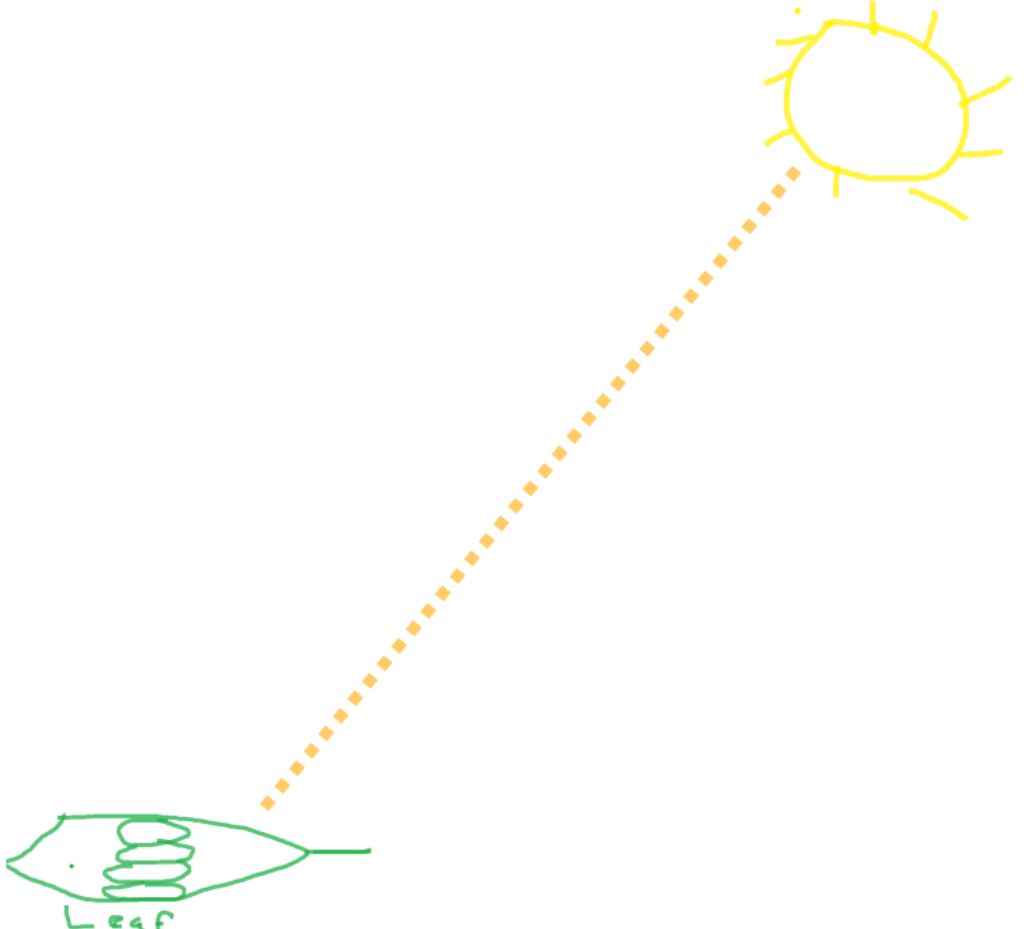
# Sun-induced fluorescence

# Leaf photosynthesis

- What happens with the absorbed light?



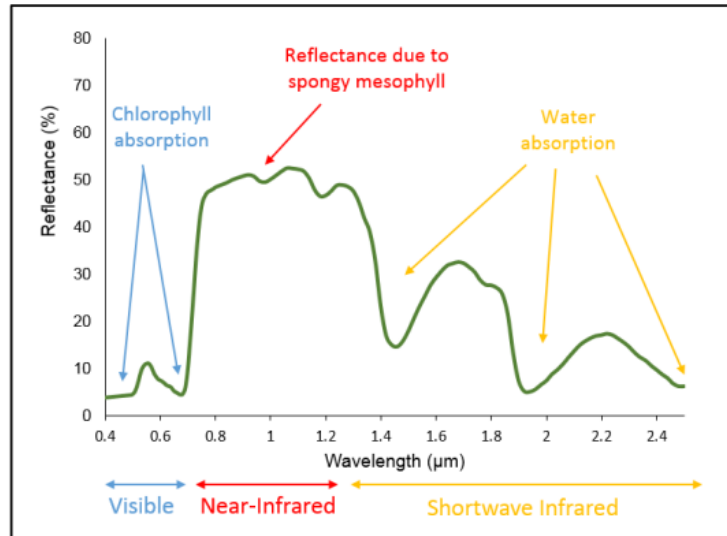
## The fate of a photon



12 Dec. 2018

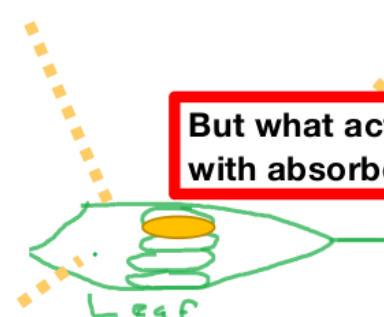
5

## The fate of a photon



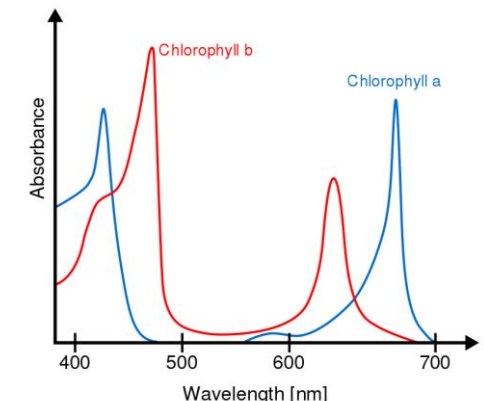
2. Reflection

3. Transmission

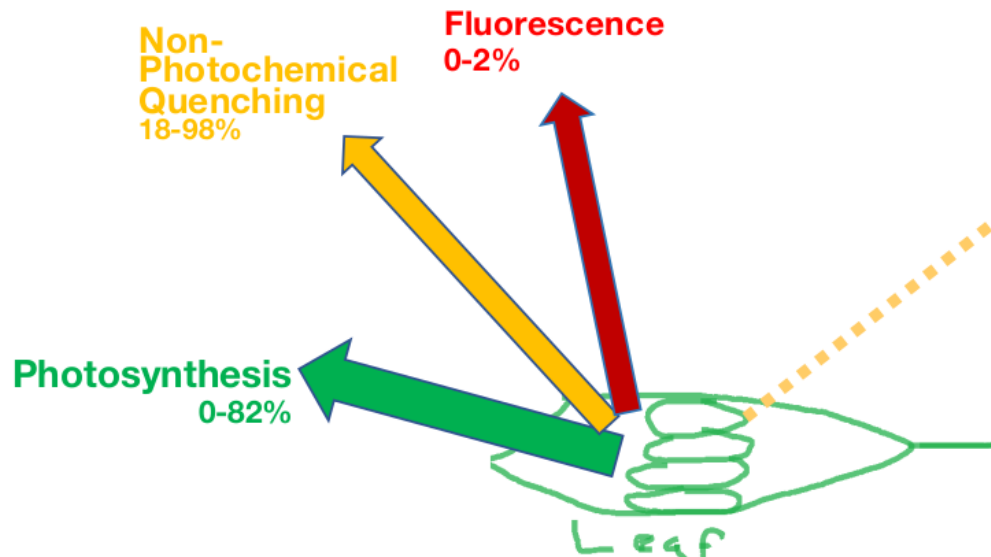


But what actually happens with absorbed photons?

1. Absorption

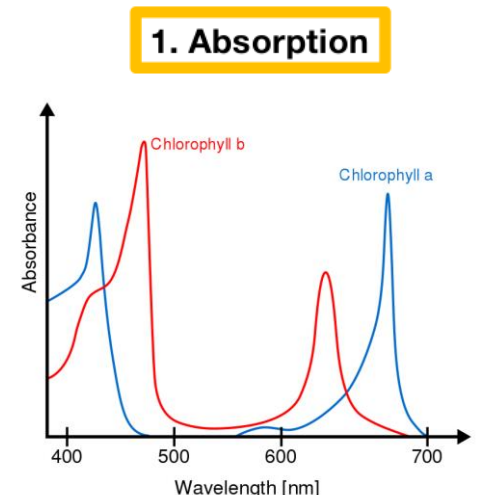


## The fate of an absorbed photon.



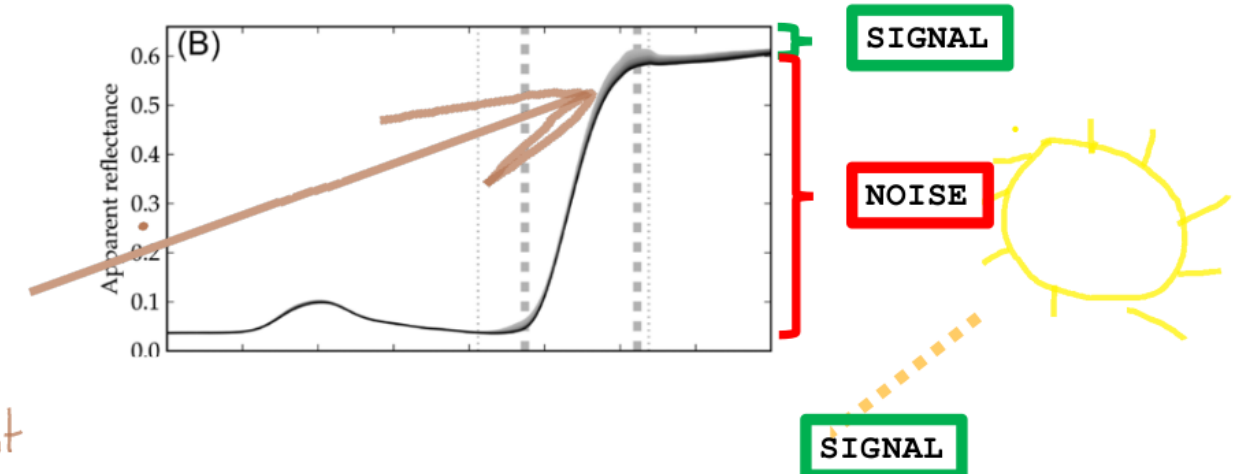
12 Dec. 2018

AGU SIF Workshop

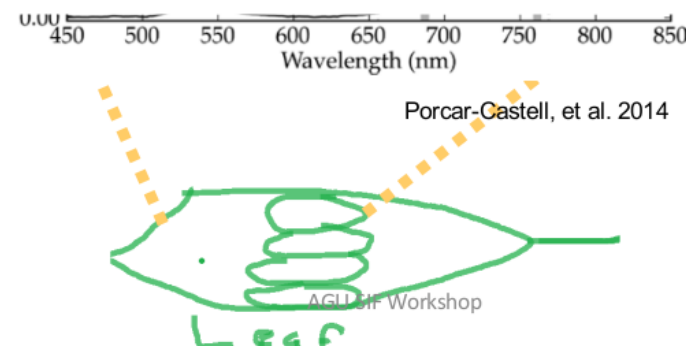


## How much is actually fluoresced?

That's great,  
But it's like  
<2% of the  
reflected light



### 2. Reflection

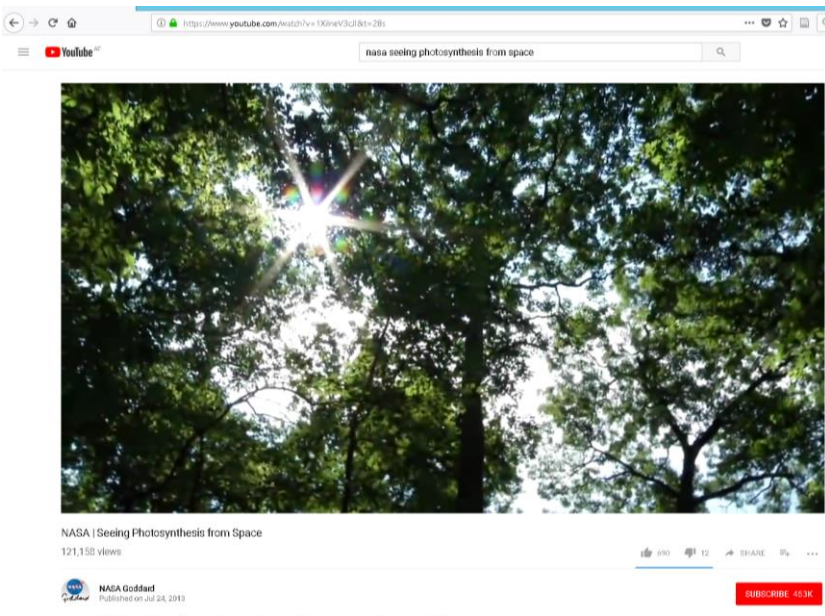


12 Dec. 2018

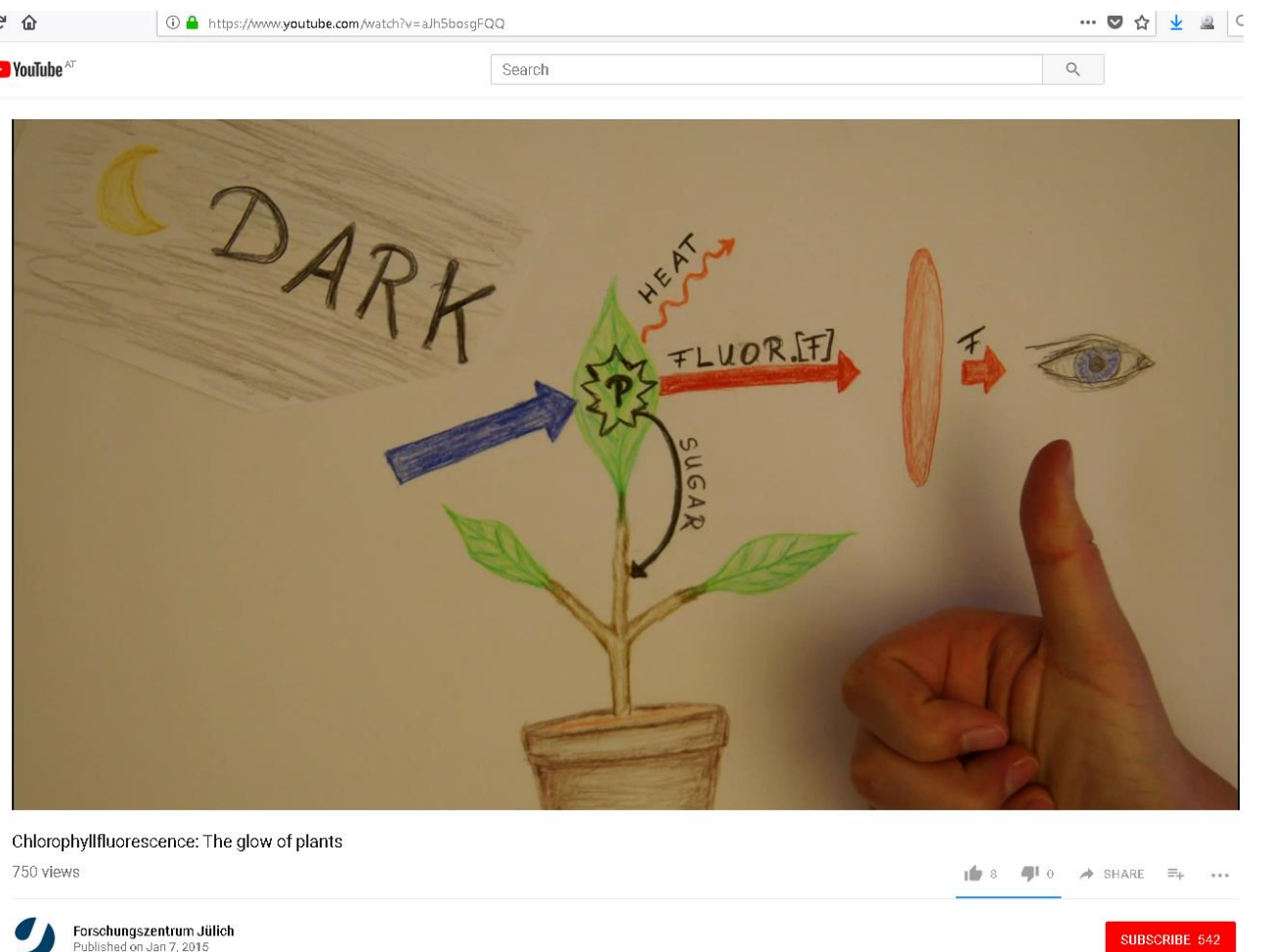
8

# Fluorescence

How can we observe chlorophyll fluorescence?



<https://www.youtube.com/watch?v=1XilneV3cJI&t=28s>



<https://www.youtube.com/watch?v=aJh5bosgFQQ>

# Sun-induced fluorescence

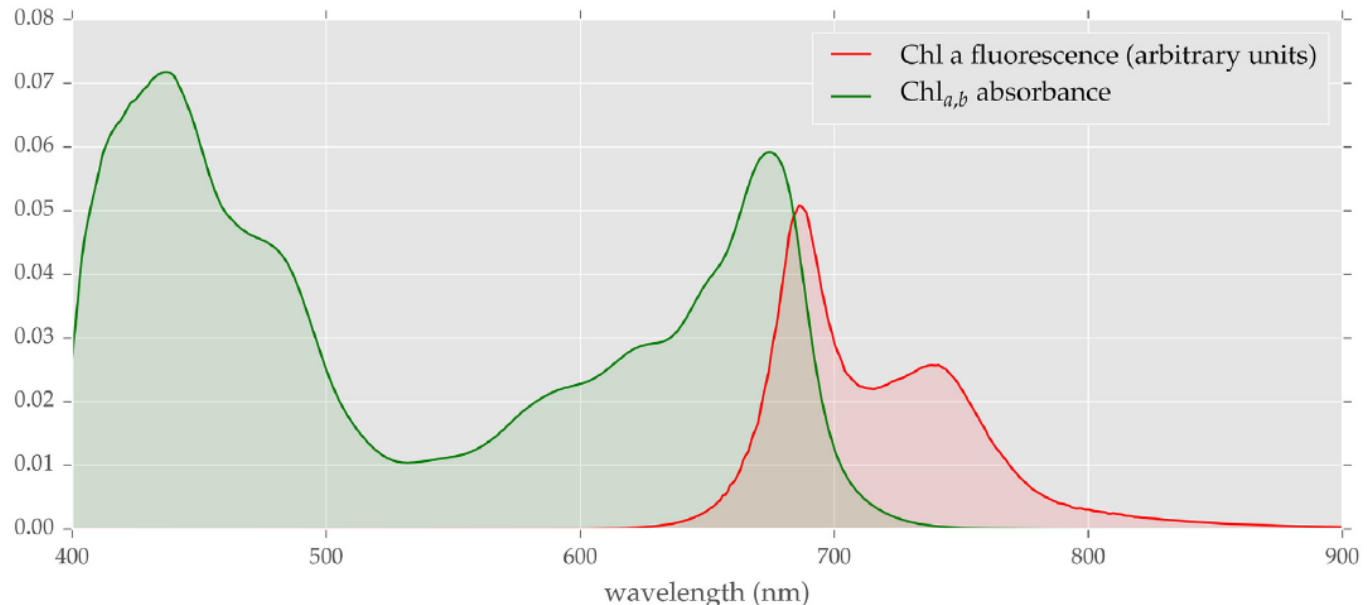


**Fig. 1** This graph depicts the absorbance of chlorophyll (both a and b) as well as a typical fluorescence spectrum in arbitrary units. The minimum in the absorbance around 550 nm gives rise to the green color of plants. Around 680 nm, there is an area of overlap, where SIF is increasing and chlorophyll absorption decreasing (a reason for the red edge in vegetation). Thus, the SIF wavelength range up to 700–720 nm is heavily affected by chlorophyll reabsorption, reducing the red peak at 685 nm (Gitelson et al., 1999).

## 3.10 Solar Induced Chlorophyll Fluorescence: Origins, Relation to Photosynthesis and Retrieval

C Frankenberg, California Institute of Technology, Division of Geological and Planetary Sciences, Pasadena, USA; and Jet Propulsion Laboratory, California Institute of Technology, Pasadena, USA

J Berry, Department of Global Ecology, Carnegie Institution for Science, Stanford, CA

© 2018 Elsevier Inc. All rights reserved.

3.10.1	Introduction	143
3.10.2	Origins of SIF	144
3.10.2.1	Quenching Mechanisms of Excited Chlorophyll	144
3.10.2.1.1	Summary	147
3.10.2.2	SIF at the Canopy Scale	147
3.10.3	Global SIF Observations	148
3.10.4	SIF Retrievals	149
3.10.4.1	Basic Principles of SIF	150
3.10.5	Additional Challenges from Space	156
3.10.5.1	Notes on Quality Control	158
3.10.6	Conclusions and Outlook	159
Acknowledgments		159
References		159

# Sun-induced fluorescence

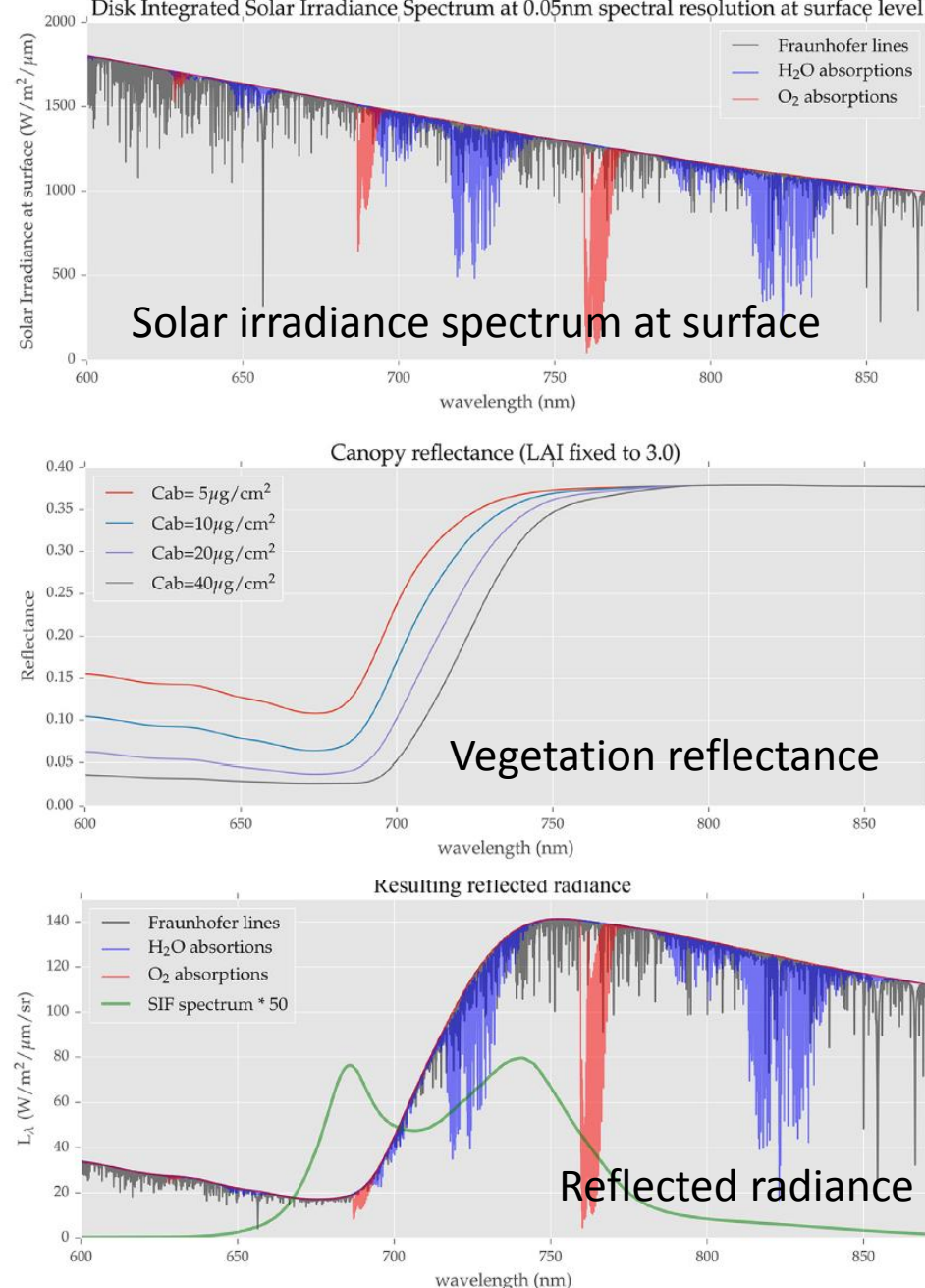


**Fig. 9** This graph shows the main contributors to a reflectance spectrum observed at the top of canopy in nadir view. The top panel shows the incoming solar radiation including solar and telluric absorption features (assuming an US standard atmosphere and 20 degrees SZA). The middle panel show typical reflectance spectra for a variety of chlorophyll contents at a fixed LAI. The bottom panel shows the resulting reflected spectrum, including an assumed solar induced fluorescence emission (SIF, scaled by a factor 50) that is added.

## 3.10 Solar Induced Chlorophyll Fluorescence: Origins, Relation to Photosynthesis and Retrieval

**C Frankenberg**, California Institute of Technology, Division of Geological and Planetary Sciences, Pasadena, USA; and Jet Propulsion Laboratory, California Institute of Technology, Pasadena, USA

**J Berry**, Department of Global Ecology, Carnegie Institution for Science, Stanford, CA

© 2018 Elsevier Inc. All rights reserved.

3.10.1	Introduction	143
3.10.2	Origins of SIF	144
3.10.2.1	Quenching Mechanisms of Excited Chlorophyll	144
3.10.2.1.1	Summary	147
3.10.2.2	SIF at the Canopy Scale	147
3.10.3	Global SIF Observations	148
3.10.4	SIF Retrievals	149
3.10.4.1	Basic Principles of SIF	150
3.10.5	Additional Challenges from Space	156
3.10.5.1	Notes on Quality Control	158
3.10.6	Conclusions and Outlook	159
Acknowledgments		159
References		159

- SIF is retrieved at small wave bands
- Fraunhofer lines: absorption lines in sun spectrum

# Sun-induced fluorescence

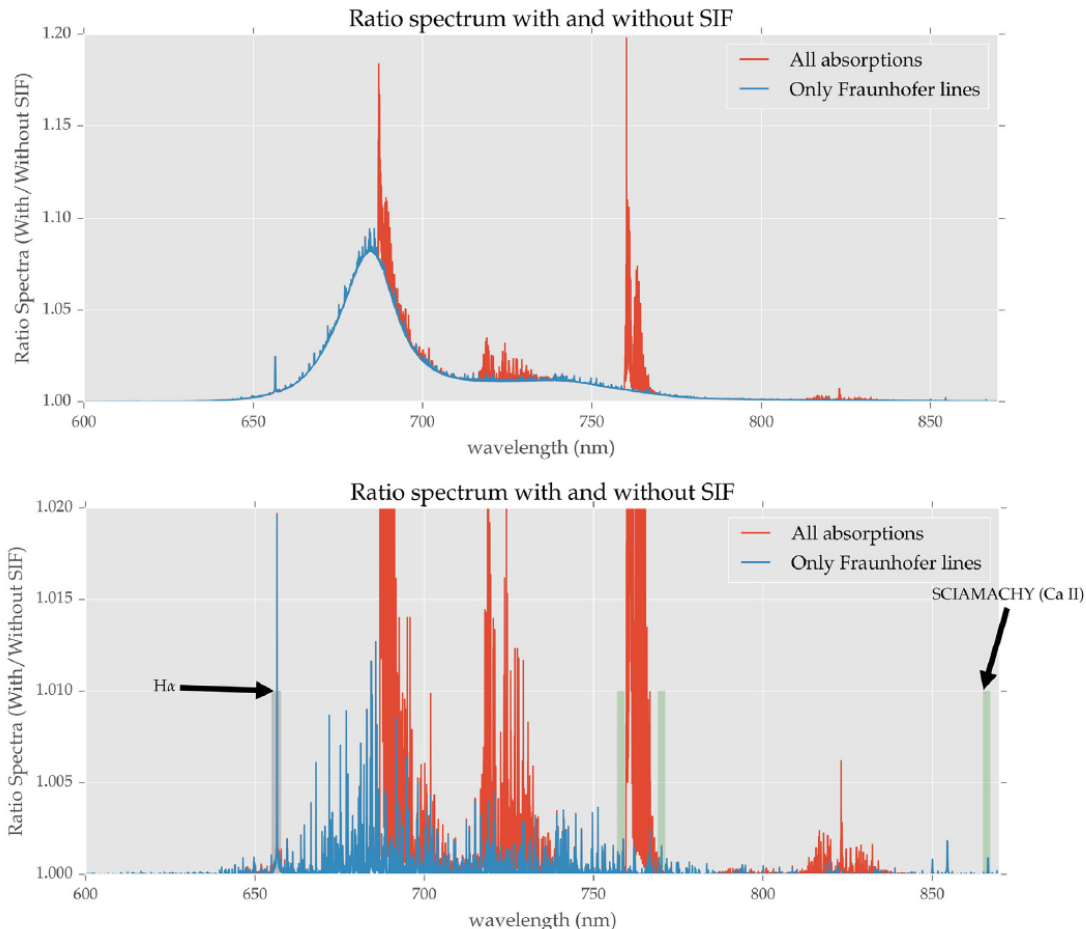


**Fig. 10** This graph shows the impact of an spectrally variable SIF spectrum on the canopy reflectance by computing a ratio spectrum with and without the additive SIF signal. The red curves include both in-filling of  $H_2O$  as well as  $O_2$  lines, while the blue ones only show the impact of Fraunhofer lines. In the bottom-panel, the impact of the broadband change in apparent reflectance is removed to focus on the high-frequent spectral variations, which is the primary way of retrieving SIF. A few specific spectral ranges that are currently being used for satellite-based SIF retrievals are noted by green bars.

## 3.10 Solar Induced Chlorophyll Fluorescence: Origins, Relation to Photosynthesis and Retrieval

C Frankenberg, California Institute of Technology, Division of Geological and Planetary Sciences, Pasadena, USA; and Jet Propulsion Laboratory, California Institute of Technology, Pasadena, USA

J Berry, Department of Global Ecology, Carnegie Institution for Science, Stanford, CA

© 2018 Elsevier Inc. All rights reserved.

3.10.1	Introduction	143
3.10.2	Origins of SIF	144
3.10.2.1	Quenching Mechanisms of Excited Chlorophyll	144
3.10.2.1.1	Summary	147
3.10.2.2	SIF at the Canopy Scale	147
3.10.3	Global SIF Observations	148
3.10.4	SIF Retrievals	149
3.10.4.1	Basic Principles of SIF	150
3.10.5	Additional Challenges from Space	156
3.10.5.1	Notes on Quality Control	158
3.10.6	Conclusions and Outlook	159
Acknowledgments		159
References		159

- SIF is retrieved at small wave bands
- Fraunhofer lines: absorption lines in sun spectrum
- SIF is retrieved from the difference between solar irradiance and reflect surface radiance at Fraunhofer lines

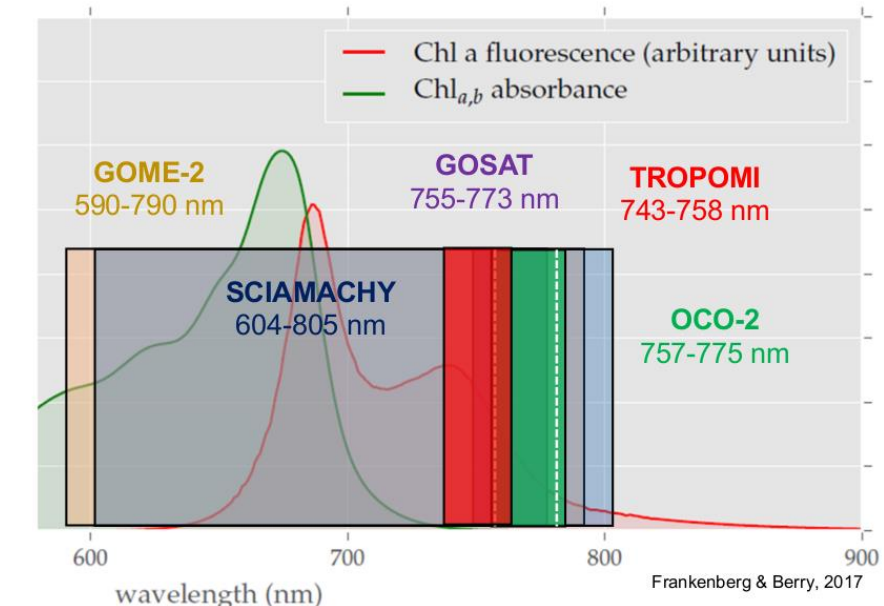
# Overview of existing satellite-based SIF data sets

	SCIAMACHY	GOME-2/MetOp-A	GOSAT-FTS	OCO-2	TROPOMI
Data availability	Aug 2002–Mar 2012	Aug 2007–present	Oct 2009–present	Sep 2014–present	Nov 2017–present
Overpass time	10:00 LST	09:30 LST	13:00 LST	13:30 LST	13:30 LST
Nadir pixel size	30 km × 60 km/ 30 km × 240 km	40 km × 80 km/ 40 km × 40 km	10.5 km diameter	1.3 km × 2.25 km	7 km × 3.5 km
Swath width	960 km	1920 km 960 km	750 km (5 measurements)	10.3 km	2600 km
Revisit time	6 days	1.5 days/3 days	3 days	16 days	almost daily
Spectral coverage (with respect to SIF)	604–805 nm	590–790 nm	755–773 nm	757–775 nm	660–784 nm
Spectral resolution	0.48 nm	0.5 nm	0.025 nm	0.042 nm	0.38
Signal-to-noise ratio (SNR)	< 3000	< 2000	> 300	< 1000	< 5000

Timeline of satellite missions:

- GOME: 1996 - 2003
- SCIAMACHY: 2002 - 2012
- GOME-2: 2007 - present
- GOSAT: 2009 - present
- OCO-2: 2014 - present
- TROPOMI

Timeline scale: 1996 1998 2000 2002 2004 2006 2008 2010 2012 2014 2016 2018 2020



Frankenberg et al., 2011; Joiner et al., 2011; Gauer et al., 2012

Joiner et al., 2013; Gauer et al., 2014; Köhler et al., 2015

Joiner et al., 2012; Köhler et al., 2015

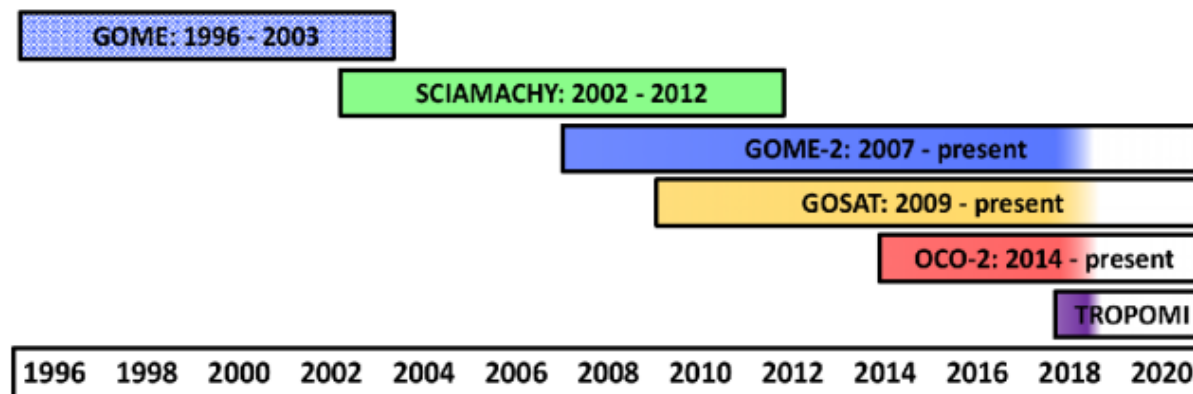
Sun et al., 2017, 2018

Köhler et al., 2018

AGU SIF Workshop

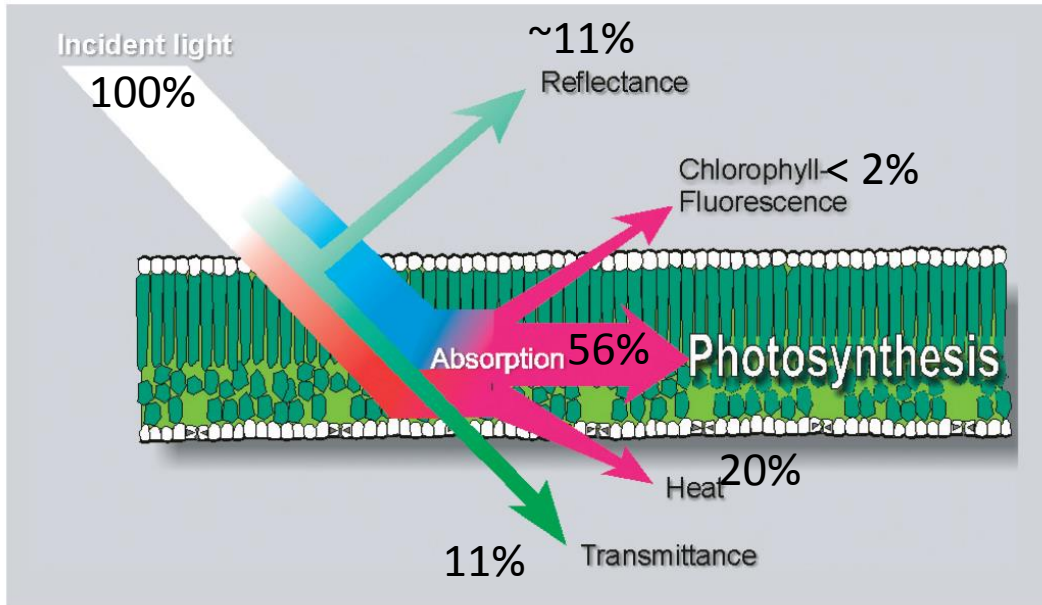
# Overview of existing satellite-based SIF data sets

- Greenhouse Gases Observing Satellite-Fourier Transform Spectrometer (GOSAT-FTS, Frankenberg et al., 2011; Joiner et al. 2011, 2012; Guanter et al. 2012, Köhler et al. 2015a)
- Global Ozone Monitoring Experiment-2 (GOME-2, Joiner et al., 2013, Köhler et al., 2015b; Wolanin et al., 2015,...)
- SCanning Imaging Absorption SpectroMeter for Atmospheric CHartographY (SCIAMACHY , Joiner et al., 2012; Köhler et al., 2015b, Wolanin et al., 2015)
- Orbiting Carbon Observatory-2 (OCO-2, Frankenberg et al., 2014; Sun et al., 2018)
- TROPOspheric Monitoring Instrument (TROPOMI, Köhler et al. 2018, see poster: A33J-3278)
- Global Ozone Monitoring Experiment (GOME, Joiner et al., in prep., see poster: B31N-2689)



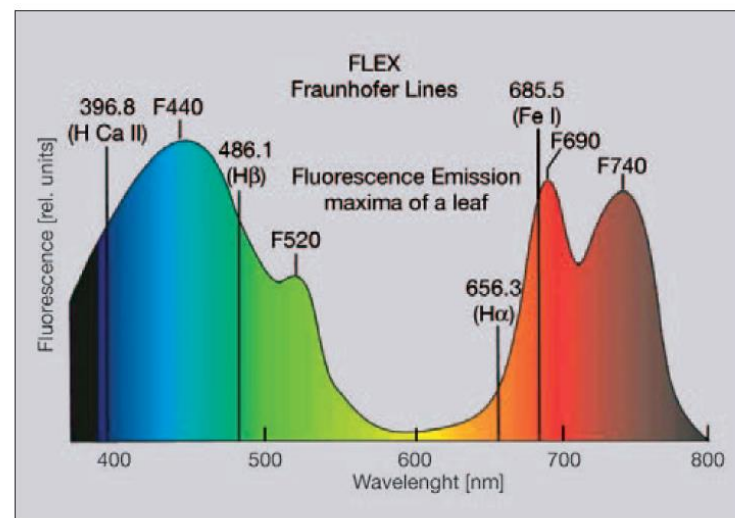
Caltech

# Sun-induced fluorescence

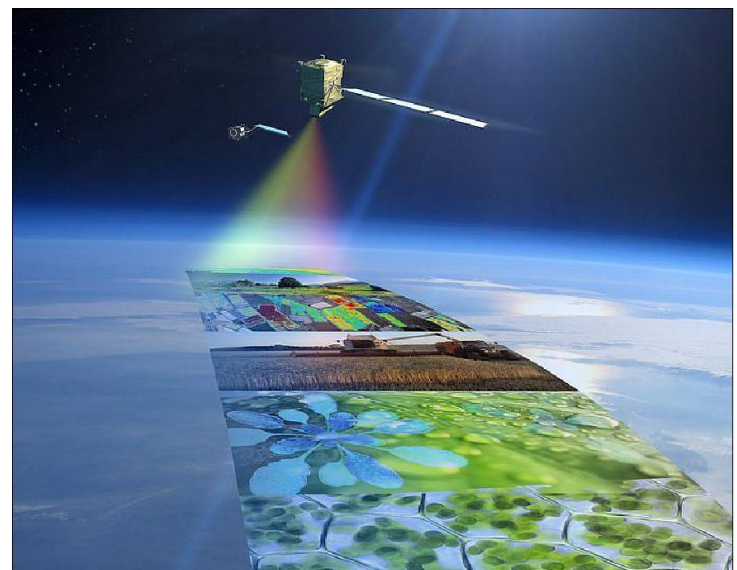


How light energy falling on a leaf is partitioned. About 78% of the incident radiation is absorbed, while the rest is either transmitted or reflected at the leaf's surface. About 20% is dissipated through heat and only 2% emitted as fluorescence, as a by-product of photosynthetic reactions occurring within the leaf itself.

The fluorescence emission spectrum of a leaf as derived from laboratory measurements. The peaks in emission at 440, 520, 690 and 740 nanometres are clearly visible in spectrum.



"FLEX" (ESA Earth explorer 8)  
(Fluorescence Explorer)  
To be launched ~2022



# Sun-induced fluorescence

- SIF is a direct proxy for photosynthesis (GPP)

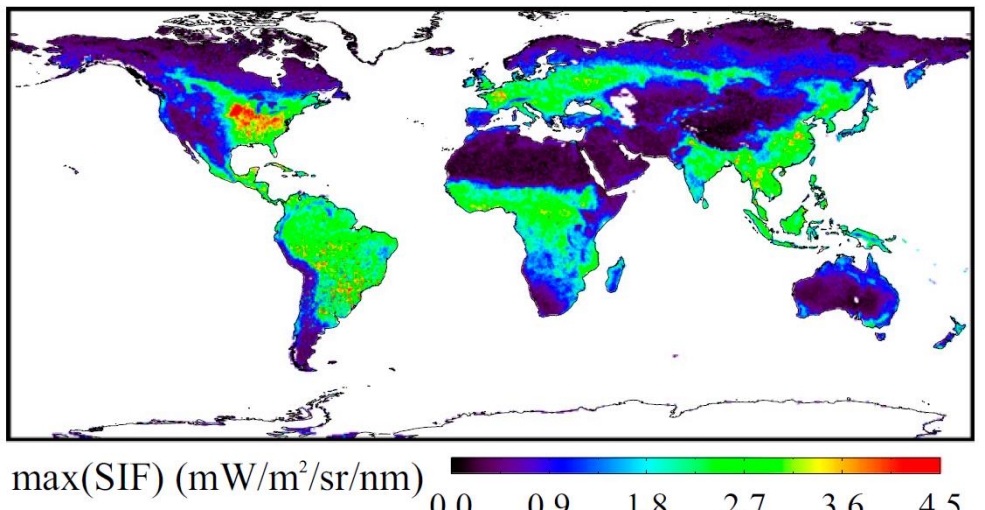


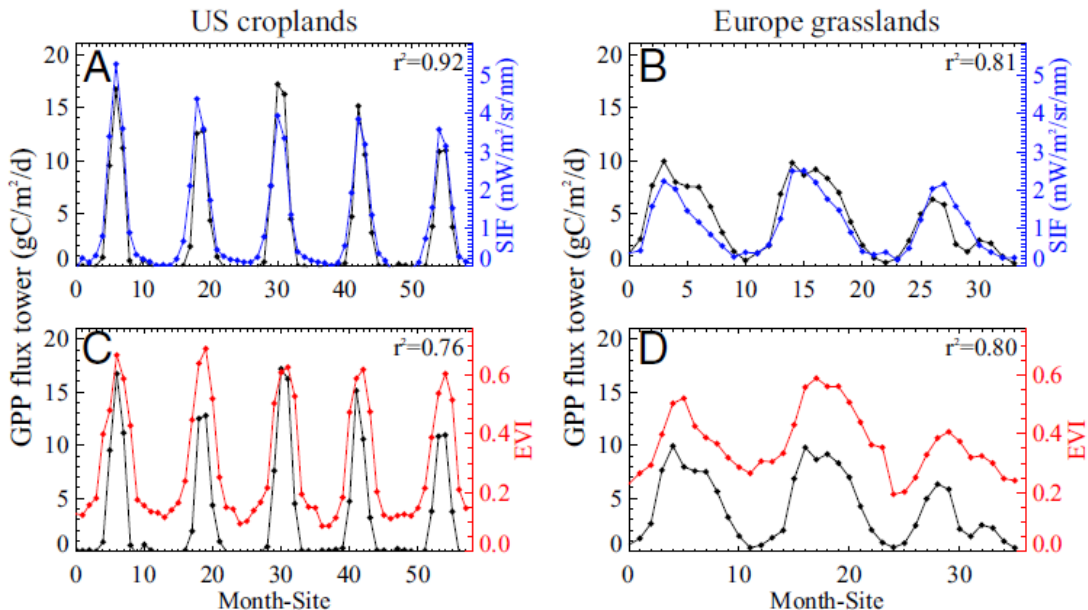
**Fig. 1.** Global map of maximum monthly sun-induced chlorophyll fluorescence (SIF) per  $0.5^\circ$  grid box for 2009. SIF retrievals are performed in a spectral window centered at 740 nm (see *Materials and Methods* and *SI Appendix, SIF Retrievals*). This map illustrates the outstanding SIF signal detected at the US CB, which shows the highest SIF return of all terrestrial ecosystems. The maximum SIF over the largest part of the US CB region is detected in July.

## Global and time-resolved monitoring of crop photosynthesis with chlorophyll fluorescence

Luis Guanter<sup>a,1,2</sup>, Yongguang Zhang<sup>a,1</sup>, Martin Jung<sup>b</sup>, Joanna Joiner<sup>c</sup>, Maximilian Voigt<sup>a</sup>, Joseph A. Berry<sup>d</sup>, Christian Frankenberg<sup>e</sup>, Alfredo R. Huete<sup>f</sup>, Pablo Zarco-Tejada<sup>g</sup>, Jung-Eun Lee<sup>h</sup>, M. Susan Moran<sup>i</sup>, Guillermo Ponce-Campos<sup>j</sup>, Christian Beer<sup>k</sup>, Gustavo Camps-Valls<sup>k</sup>, Nina Buchmann<sup>l</sup>, Damiano Gianelle<sup>m</sup>, Katja Klumpp<sup>n</sup>, Alessandro Cescatti<sup>o</sup>, John M. Baker<sup>p</sup>, and Timothy J. Griffis<sup>q</sup>

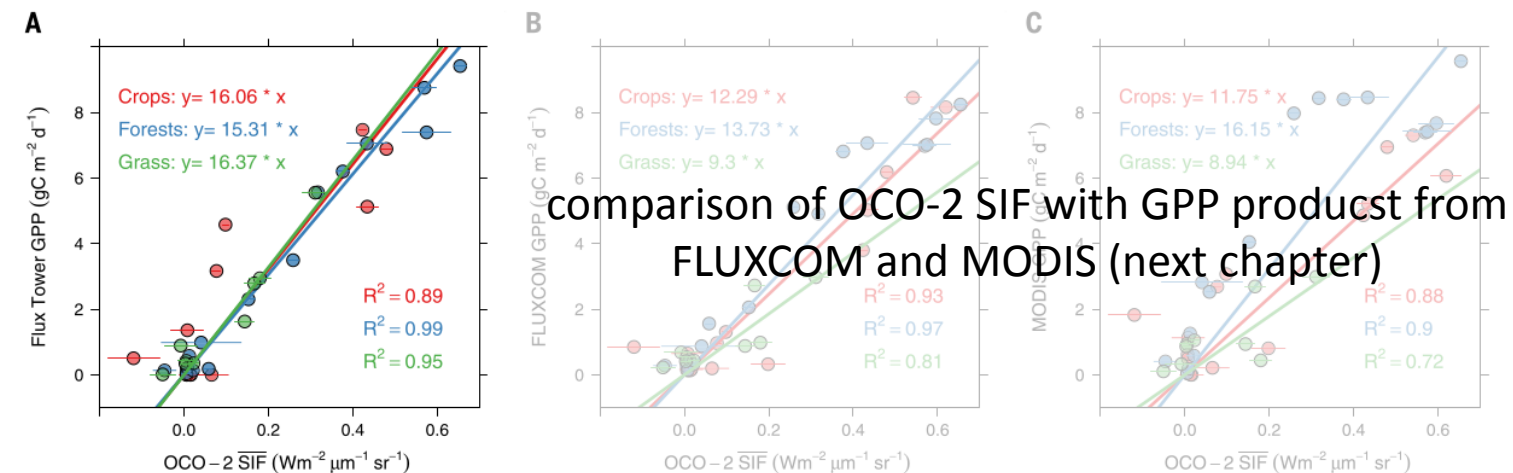
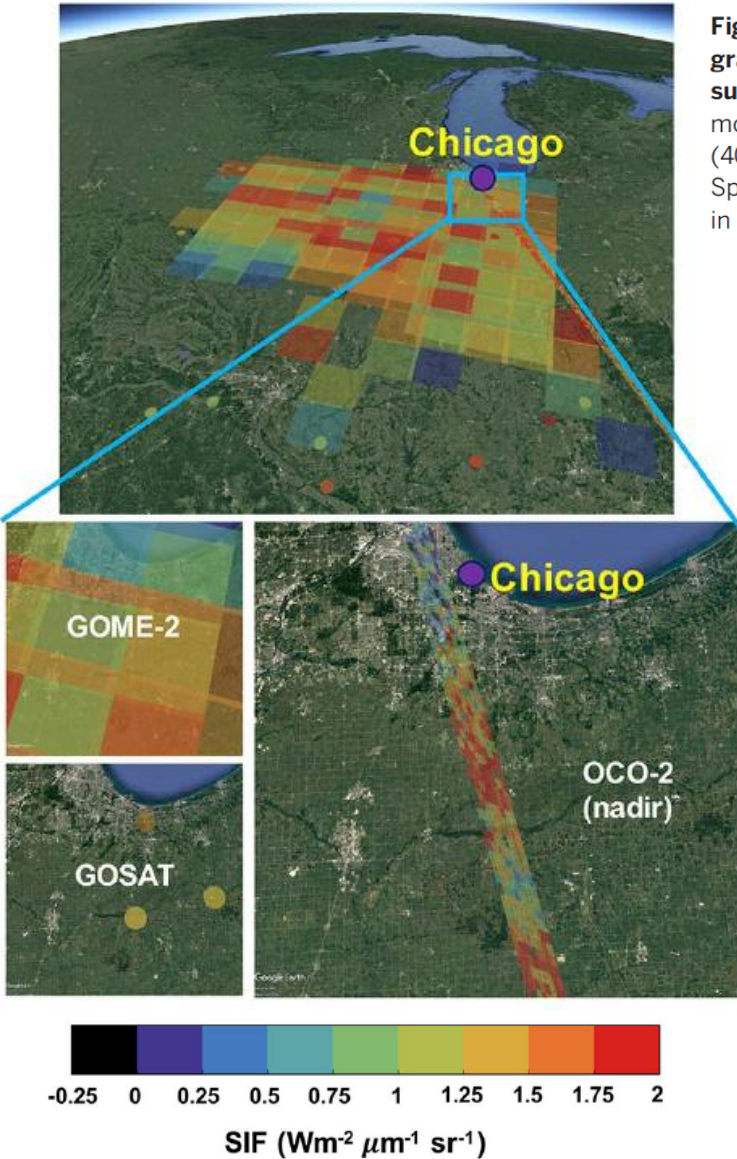
<sup>a</sup>Institute for Space Sciences, Freie Universität Berlin, 12165 Berlin, Germany; <sup>b</sup>Department for Biogeochemical Systems, Max Planck Institute for Biogeochemistry, 07745 Jena, Germany; <sup>c</sup>Laboratory for Atmospheric Chemistry and Dynamics (Code 614) National Aeronautics and Space Administration Goddard Space Flight Center, Greenbelt, MD 20771; <sup>d</sup>Department of Global Ecology, Carnegie Institution for Science, Stanford, CA 94305; <sup>e</sup>Jet Propulsion Laboratory, California Institute of Technology, Pasadena, CA 91109; <sup>f</sup>Plant Functional Biology and Climate Change Cluster, University of Technology Sydney, Sydney, 2007, Australia; <sup>g</sup>Instituto de Agricultura Sostenible, Consejo Superior de Investigaciones Científicas, 14004 Córdoba, Spain; <sup>h</sup>Geological Sciences, Brown University, Providence, RI 02912; <sup>i</sup>Southwest Watershed Research, Agricultural Research Service, US Department of Agriculture, Tucson, AZ 85719; <sup>j</sup>Department of Applied Environmental Science and Bolin Centre for Climate Research, Agricultural Research Service, US Department of Agriculture, Stockholm, Sweden; <sup>k</sup>Image Processing Laboratory, Universitat de València, 46980 València, Spain; <sup>l</sup>Agricultural Sciences, Eidgenössische Technische Hochschule Zürich, 8092 Zürich, Switzerland; <sup>m</sup>Sustainable Agro-ecosystems and Bioresources Department, Research and Innovation Centre, Fondazione Edmund Mach, 38010 San Michele all'Adige, Italy; <sup>n</sup>Grassland Ecosystems Research Unit, Institut National de la Recherche Agronomique, Clermont-Ferrand, France 63122; <sup>o</sup>Institute for Environment and Sustainability, Joint Research Centre, European Commission, 21027 Ispra, Italy; <sup>p</sup>Soil and Water Management Research, Agricultural Research Service, US Department of Agriculture, St. Paul, MN 55108; and <sup>q</sup>Department of Soil, Water, and Climate, University of Minnesota, St. Paul, MN 55108

Edited by Gregory P. Asner, Carnegie Institution for Science, Stanford, CA, and approved February 25, 2014 (received for review October 24, 2013)



**Fig. 4.** Time series of flux tower-based GPP compared with SIF retrievals (A and B) and the MODIS MOD13C2 EVI (C and D) for the same cropland and grassland sites and spatiotemporal averages as in Fig. 3 (monthly averages in  $0.5^\circ$  grid boxes and the 2007–2011 period). SIF and EVI are plotted with the same vertical scale for cropland and grassland sites.

# Sun-induced fluorescence

**A****Footprint**

**Fig. 3. SIF-GPP relationships.** The relationship between GPP and OCO-2 SIF (daily mean value, denoted as  $\overline{SIF}$ , converted from instantaneous measurements) at three flux tower sites representative of three different biomes: crops (Minnesota Tall Tower KCMP) (30), grass (Stuart Plain in Australia) (31), and deciduous temperate forests [Missouri Ozark site (US\_MOz)]. The first two sites are selected because they are in the direct underpass of OCO-2 orbital tracks; for the US\_MOz site, OCO-2 SIF retrievals are obtained from representative forests in the vicinity of the tower. The KCMP footprint covers a mixture of corn, soybean, and grasses but is dominated by the two major crops. Error bars represent the SE of

the OCO-2 SIF retrieval. Daily GPP in the 2015 growing season is obtained during the OCO-2 overpasses from (A) eddy covariance measurements, (B) FLUXCOM products, and (C) MODIS products, sampled at these three flux sites. Both FLUXCOM and MODIS GPP are 8-day products and are linearly interpolated to the OCO-2 overpass dates. The site-specific FLUXCOM GPP value is extracted from the grid cell ( $0.083^\circ$  by  $0.083^\circ$ ) that corresponds to the latitude and longitude of the tower location. The site-specific MODIS (MOD17A2) GPP value is the average of nine adjacent pixels (1 km by 1 km) centered at the tower location. Both are roughly equivalent to  $\sim 9\text{-km}^2$  area.

**RESEARCH ARTICLE****CARBON CYCLE**

## OCO-2 advances photosynthesis observation from space via solar-induced chlorophyll fluorescence

Y. Sun,<sup>1,\*†</sup> C. Frankenberg,<sup>2,1\*</sup> J. D. Wood,<sup>3</sup> D. S. Schimel,<sup>1</sup> M. Jung,<sup>4</sup> L. Guanter,<sup>5</sup> D. T. Drewry,<sup>1,6</sup> M. Verma,<sup>7</sup> A. Porcar-Castell,<sup>8</sup> T. J. Griffis,<sup>9</sup> L. Gu,<sup>10</sup> T. S. Magney,<sup>1</sup> P. Köhler,<sup>2</sup> B. Evans,<sup>11</sup> K. Yuen<sup>1</sup>

- SIF is strongly linearly related to GPP

Overview of Solar-Induced chlorophyll Fluorescence (SIF) from the Orbiting Carbon Observatory-2: Retrieval, cross-mission comparison, and global monitoring for GPP

Ying Sun<sup>a,b,\*</sup>, Christian Frankenberg<sup>c,a,\*\*</sup>, Martin Jung<sup>d</sup>, Joanna Joiner<sup>e</sup>, Luis Guanter<sup>f</sup>, Philipp Köhler<sup>c</sup>, Troy Magney<sup>a</sup>

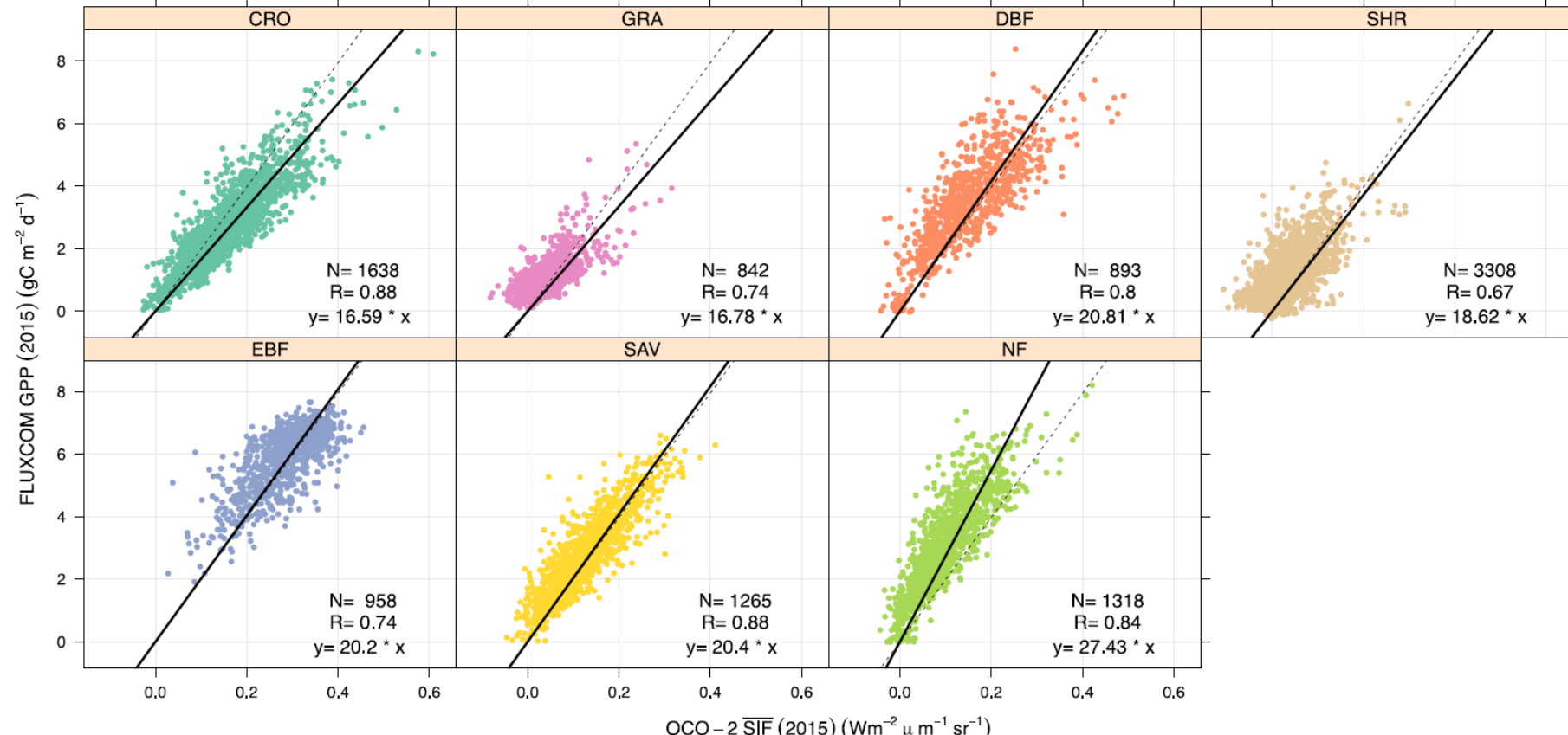


**Fig. 12.** The relationships between the annual mean OCO-2 SIF and FLUXCOM GPP in 2015 for different biomes. Each scatter represents a grid-cell. The fitted linear regression lines passing through the origin are displayed (solid), along with the regression line fitted with all biomes (dotted). The ordinary least square (OLS) regression is used here for the fitting. Biomes are denoted as: CRO for croplands, GRA for grasslands, DBF for deciduous broadleaf forests, SHR for shrublands, EBF for evergreen broadleaf forests, SAV for savannas, NF for needleleaf forests, respectively.

# **Estimation of photosynthesis (GPP and NPP)**

- Gross primary production (GPP) cannot be measured but only estimated with different approaches:
  - › Leaf-to-canopy scaling by using the vertical profile of LAI and light absorptio
  - › Separating GPP and Reco from eddy covariance measurements of NEE
    - Upscaling of local GPP estimates to larger regions/globe with machine learning approaches (e.g. FLUXCOM)
  - › **Light-use efficiency models** (e.g. MODIS MOD17 algorithm)
  - › Empirical relationships or models based on SIF
  - › Process-based models of photosynthesis (see Bonan et al. 2016, p 247-254)
    - **Farquhar model** for photosynthesis (Farquhar et al. 1982)
      - <http://biocycle.atmos.colostate.edu/shiny/photosynthesis/>
    - **Ball-Berry model** for stomatal conductance (Ball et al. 1987)
    - **Collatz model** for stomatal conductance and photosynthesis (Collatz et al. 1991, 1992)

# Light-use efficiency models: MOD17

- MOD17 algorithm to estimate GPP and NPP
  - ›  $GPP = PAR * fAPAR * LUE$
  - › LUE light-use efficiency
    - $LUE = LUEmax * f(\text{temperature}) * f(VPD)$
  - › Respiration model to derive NPP
    - $NPP = GPP - Ra$

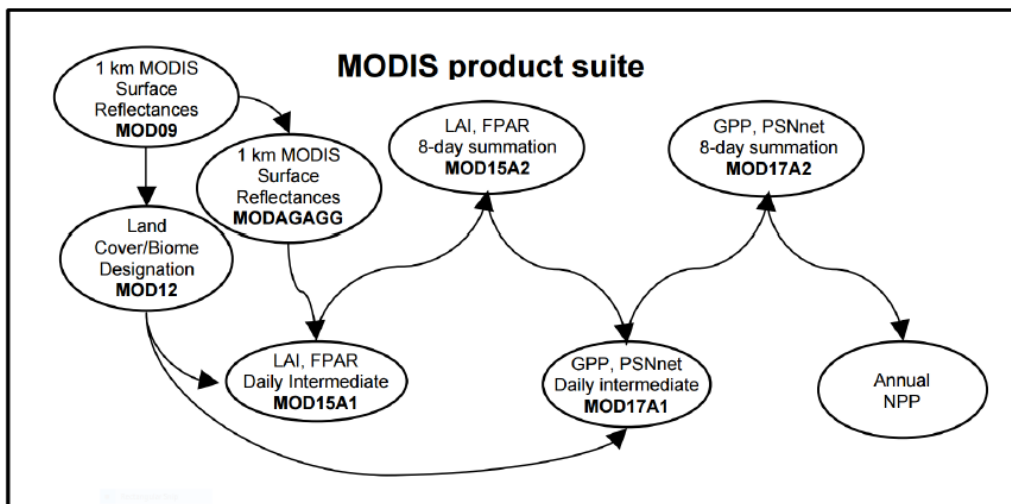


Figure 2.1. The linkages among MODIS land products.

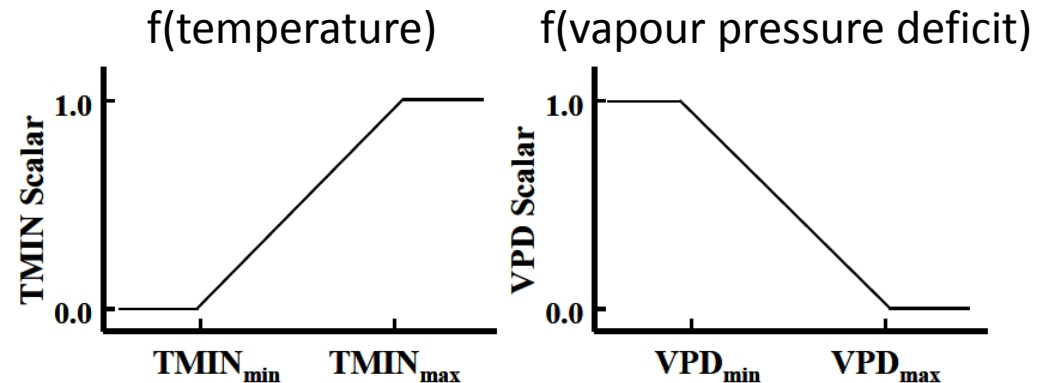
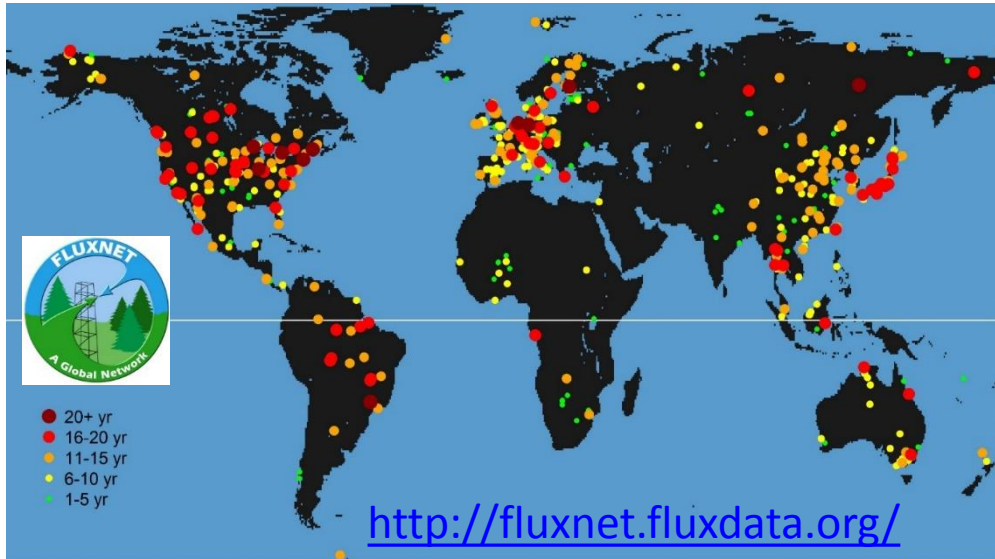


Figure 1.2. The TMIN and VPD attenuation scalars are simple linear ramp functions of daily TMIN and VPD.

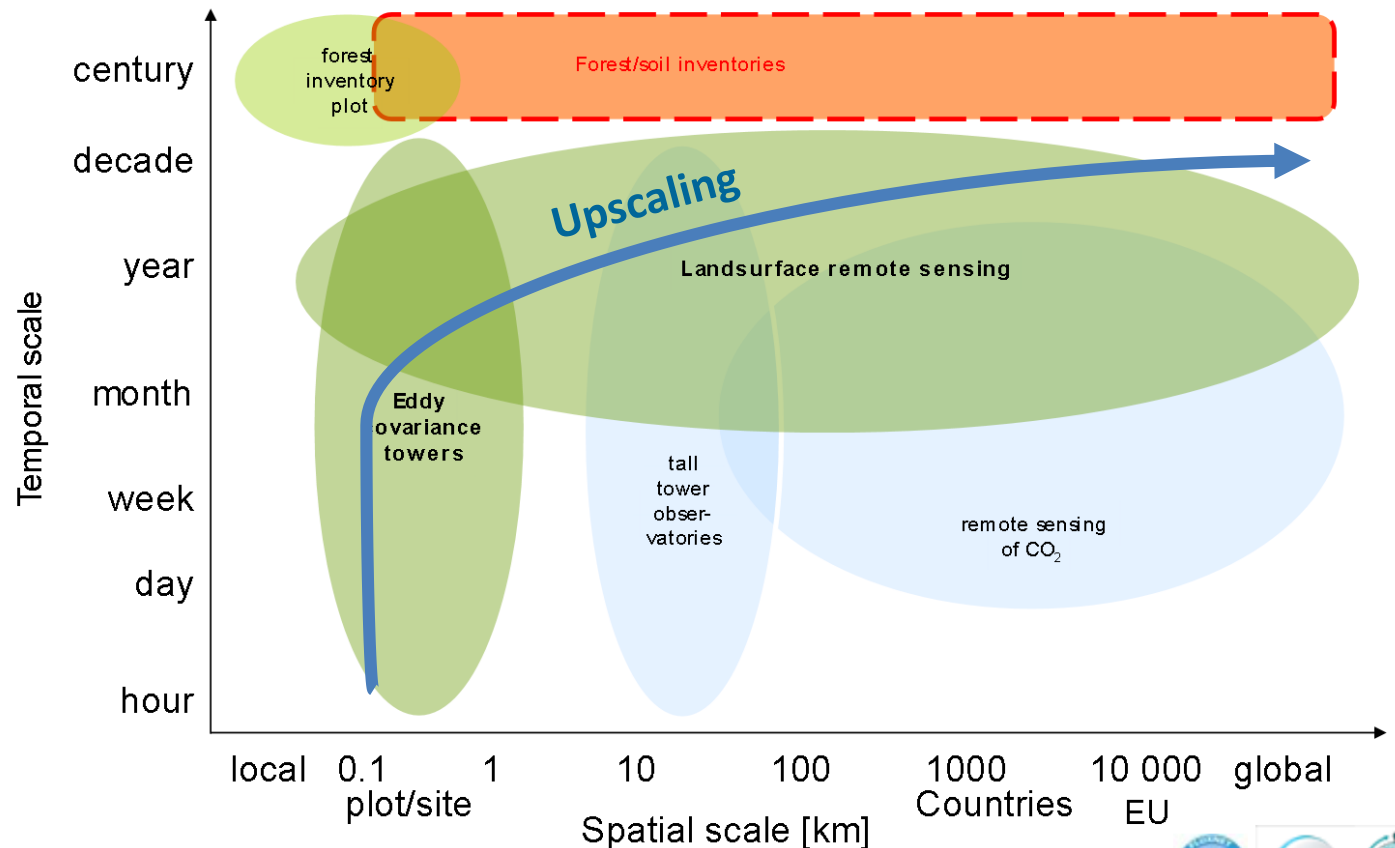
Table 2.2. Biome-Property-Look-Up-Table (BPLUT) for MODIS GPP/NPP algorithm with NCEP-DOE reanalysis II and the Collection 5 FPAR/LAI as inputs. The full names for the University of Maryland land cover classification system (UMD\_VEG\_LC) in MOD12Q1 dataset (fieldname: Land\_Cover\_Type\_2) are, Evergreen Needleleaf Forest (ENF), Evergreen Broadleaf Forest (EBF), Deciduous Needleleaf Forest (DNF), Deciduous Broadleaf Forest (DBF), Mixed forests (MF), Closed Shrublands (CShrub), Open Shrublands (OShrub), Woody Savannas (WSavanna), Savannas (Savanna), Grassland (Grass), and Croplands (Crop).

UMD_VEG_LC	ENF	EBF	DNF	DBF	MF	CShrub	OShrub	WSavanna	Savanna	Grass	Crop
LUEmax (KgC/m <sup>2</sup> /d/MJ)	0.000962	0.001268	0.001086	0.001165	0.001051	0.001281	0.000841	0.001239	0.001206	0.000860	0.001044
Tmin_min (C)	-8.00	-8.00	-8.00	-6.00	-7.00	-8.00	-8.00	-8.00	-8.00	-8.00	-8.00
Tmin_max (C)	8.31	9.09	10.44	9.94	9.50	8.61	8.80	11.39	11.39	12.02	12.02
VPD_min (Pa)	650.0	800.0	650.0	650.0	650.0	650.0	650.0	650.0	650.0	650.0	650.0
VPD_max (Pa)	4600.0	3100.0	2300.0	1650.0	2400.0	4700.0	4800.0	3200.0	3100.0	5300.0	4300.0

# Upscaling of eddy covariance observations



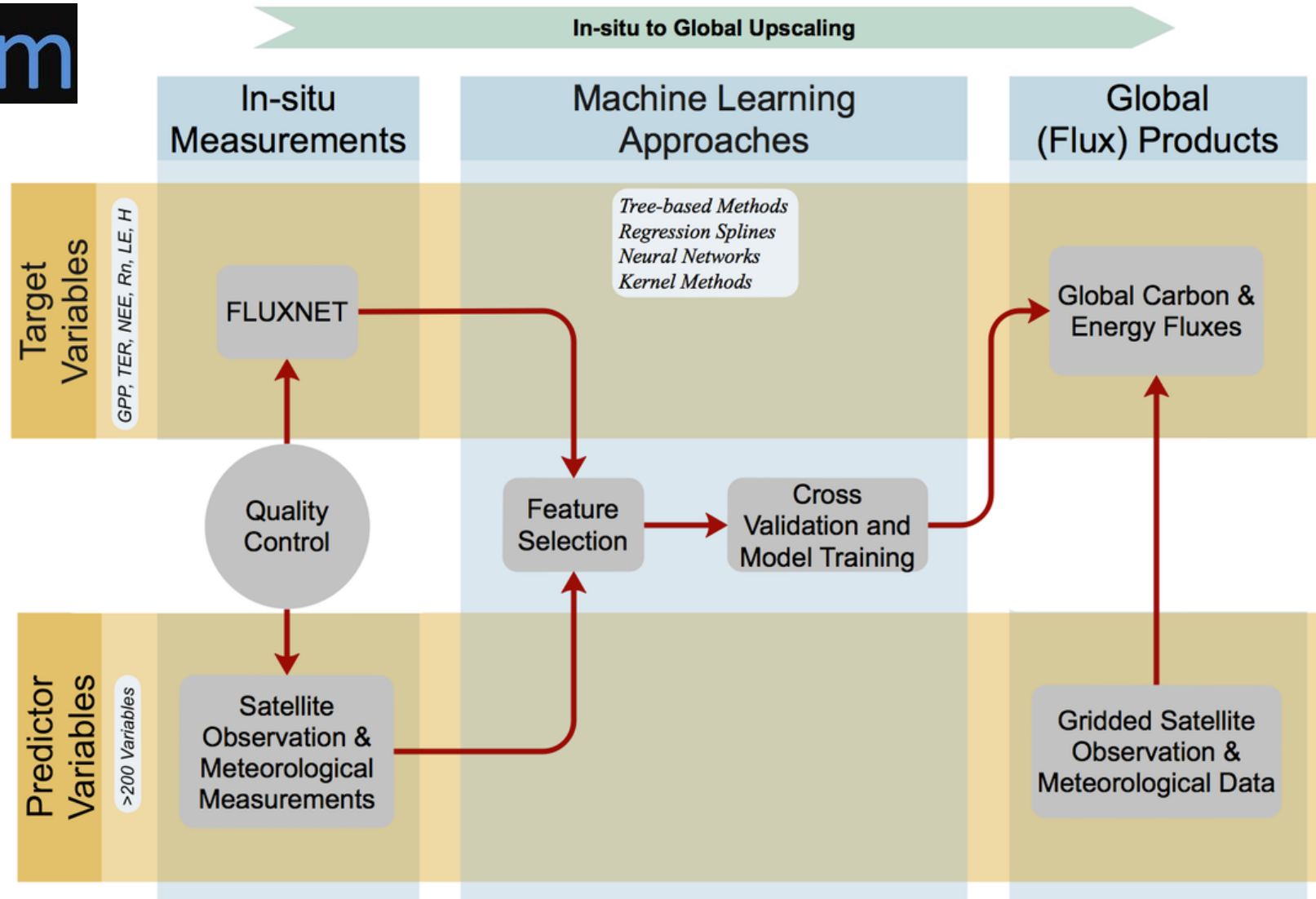
From point to globe via integration with remote sensing



[© Markus Reichstein]



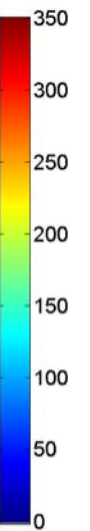
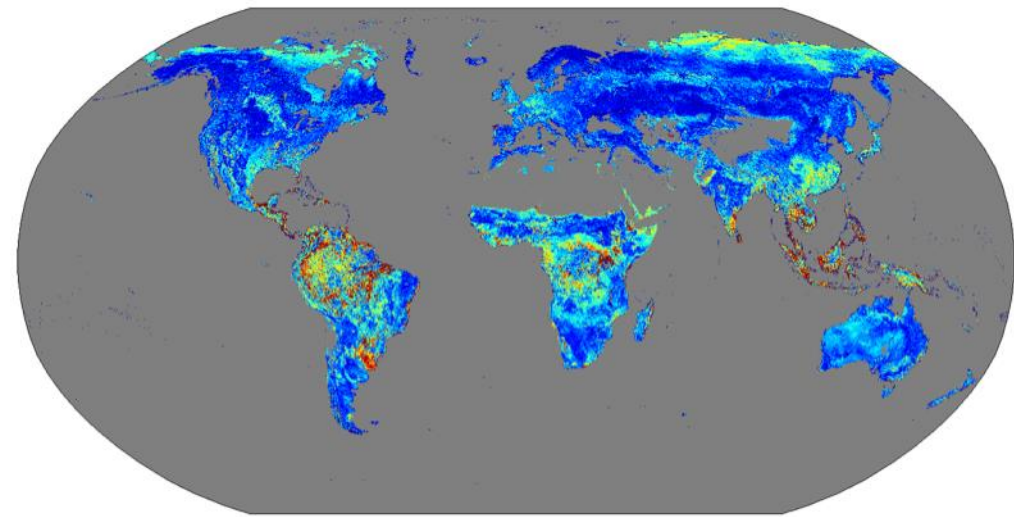
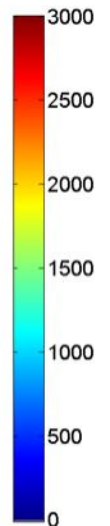
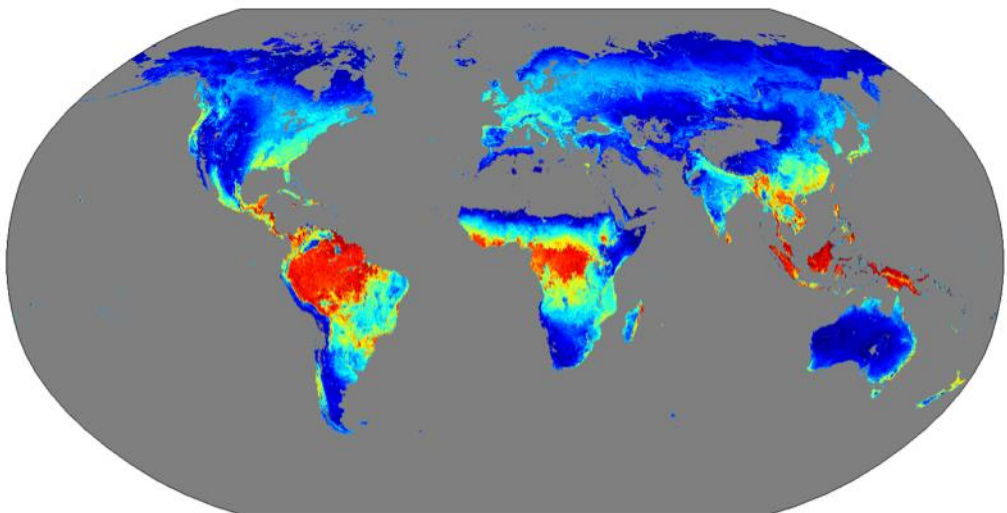
# Upscaling of eddy covariance observations



# Upscaling of eddy covariance observations



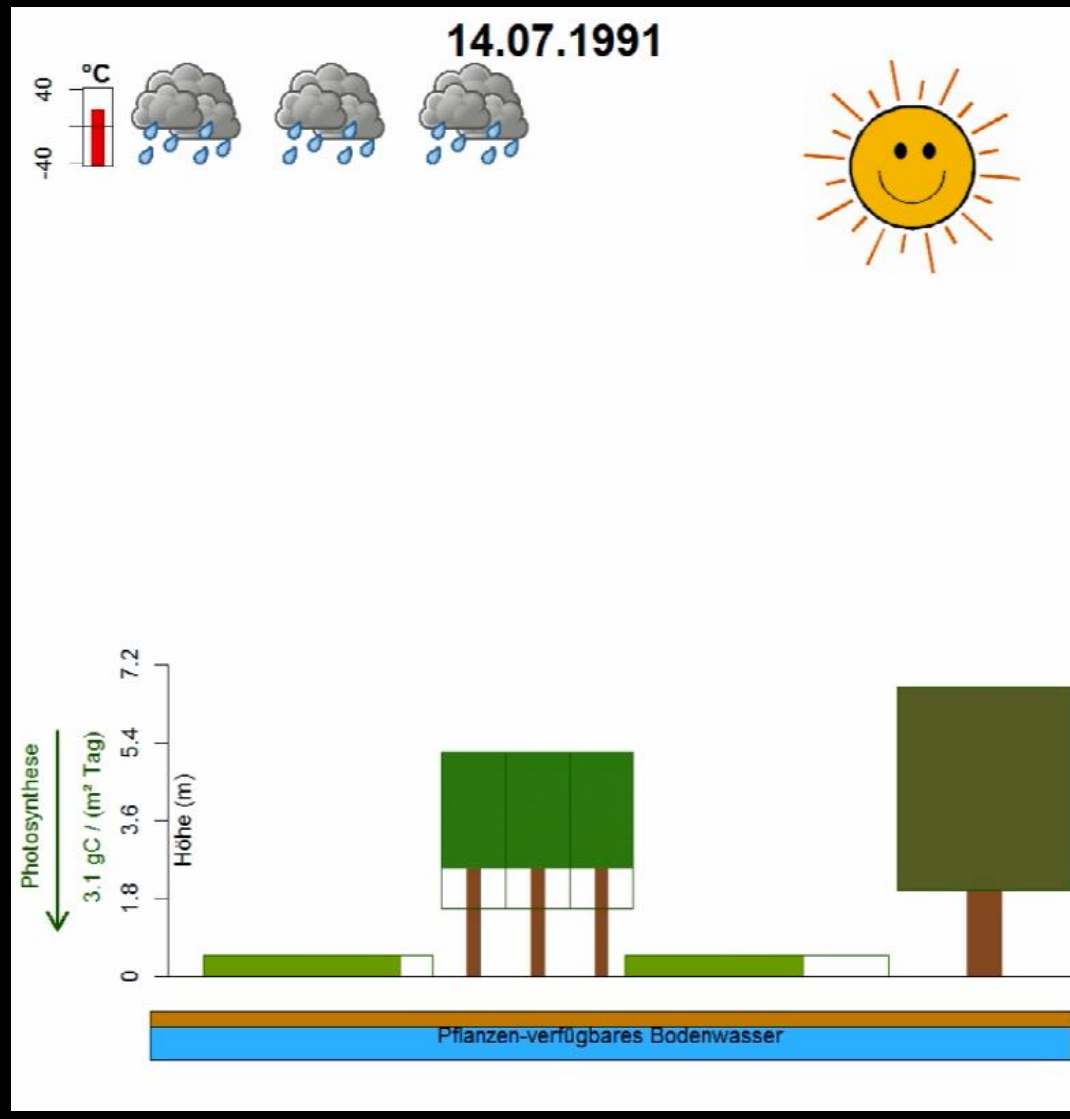
Mean annual GPP and uncertainty (gC m<sup>-2</sup> yr<sup>-1</sup>)



# Ecosystem models

# Modelling

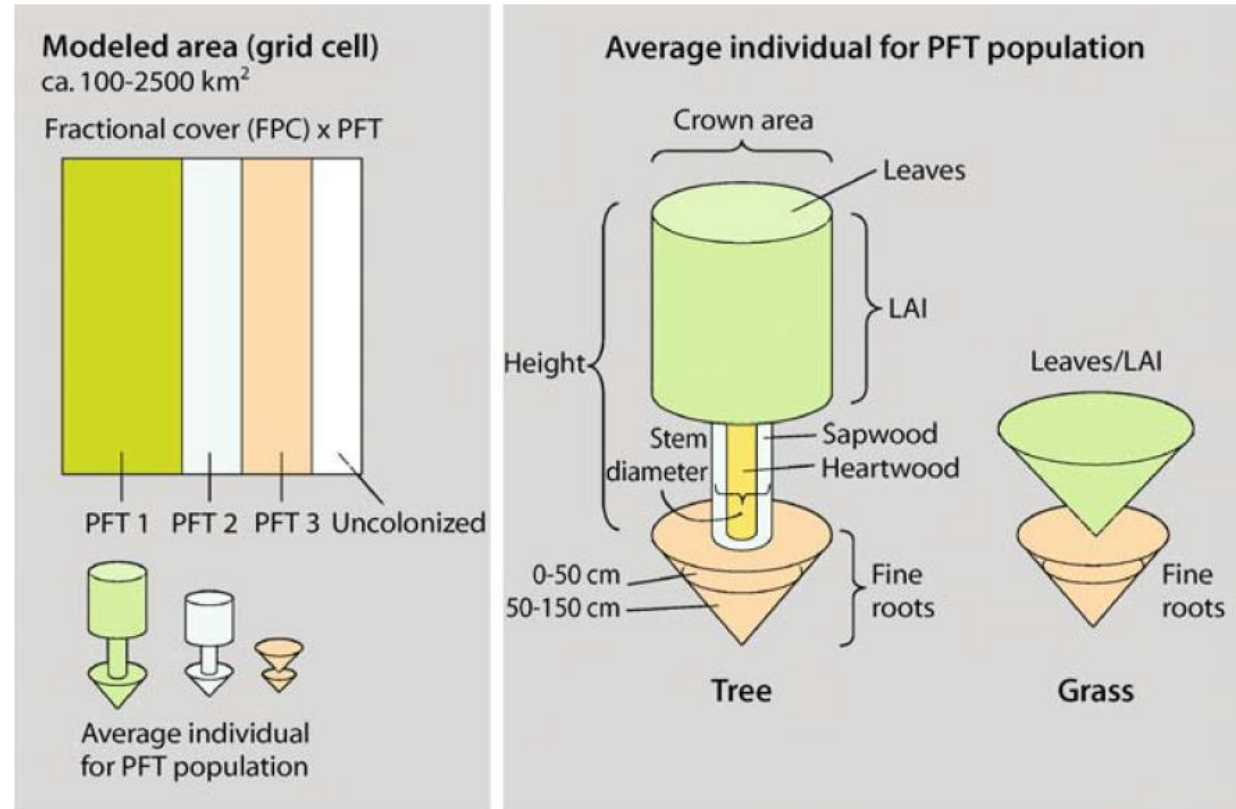
- What is a model?
- Which components has every simulation model?



# Ecosystem models

Fig. 15.3.

Each DGVM has adopted a different large-area parameterization for vegetation dynamics. This figure depicts one example (Sitch et al. 2003). Here, each PFT occupies a fraction of the modeled area (grid cell). Structural properties for one *average individual* for each PFT vary dynamically depending on carbon allocation, tissue turnover and allometric relationships. Population density scales PFT properties from the average individual to the grid cell



## Chapter 15

### Dynamic Global Vegetation Modeling: Quantifying Terrestrial Ecosystem Responses to Large-Scale Environmental Change

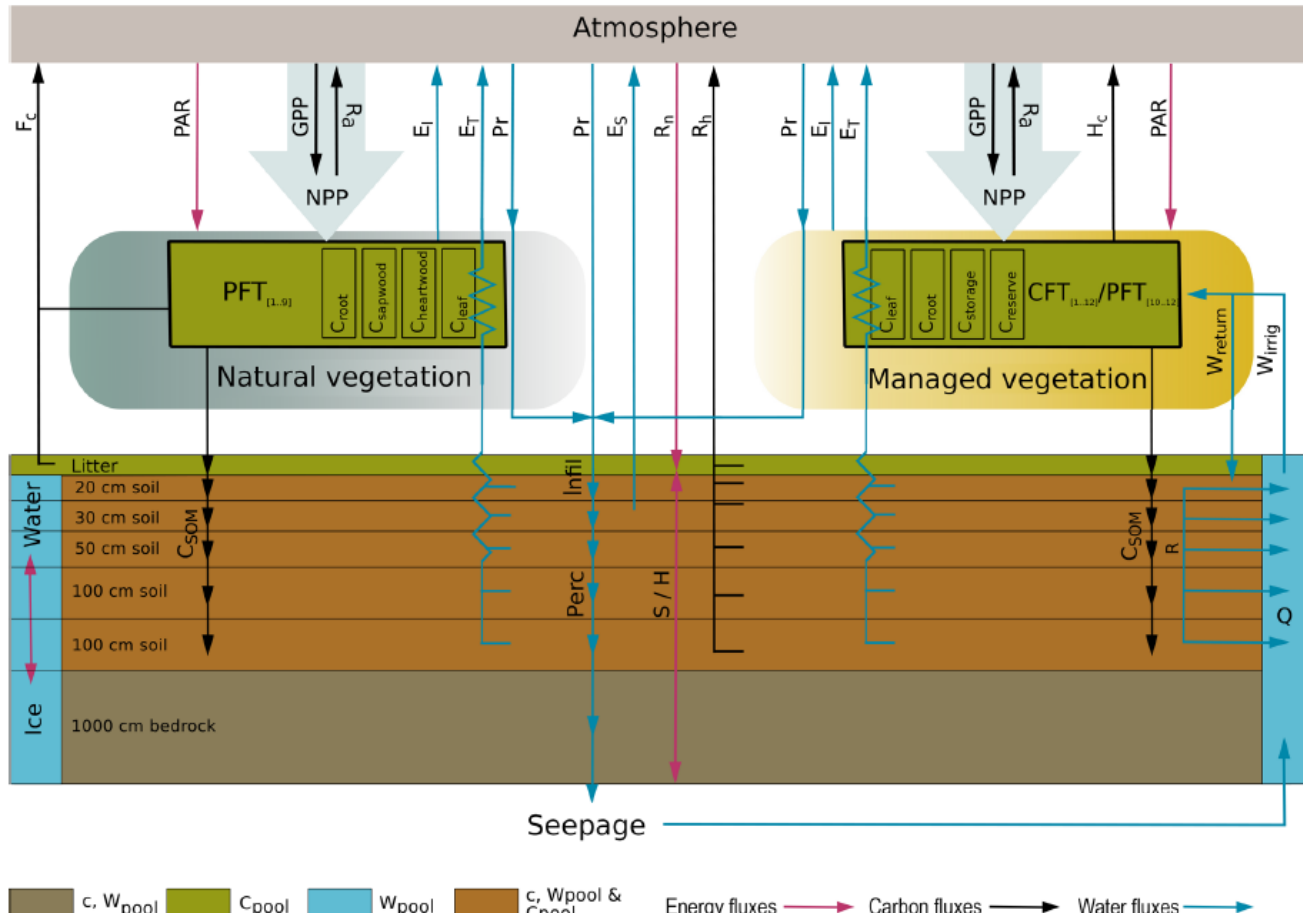
I. Colin Prentice · Alberte Bondeau · Wolfgang Cramer · Sandy P. Harrison · Thomas Hickler · Wolfgang Lucht  
Stephen Sitch · Ben Smith · Martin T. Sykes

Prentice et al. 2007

# Example: LPJmL dynamic global vegetation model

Geosci. Model Dev., 11, 1343–1375, 2018  
<https://doi.org/10.5194/gmd-11-1343-2018>  
 © Author(s) 2018. This work is distributed under the Creative Commons Attribution 4.0 License.

Geoscientific  
Model Development  

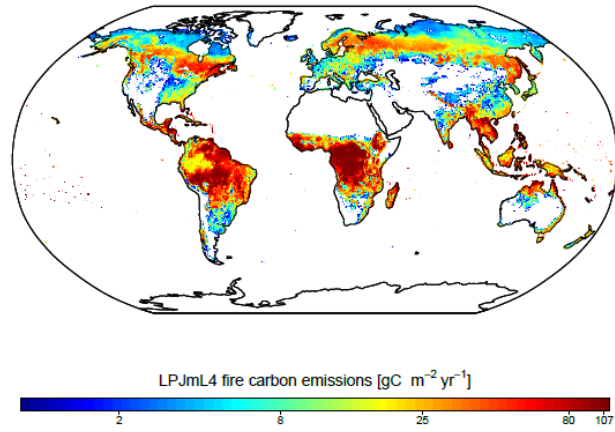
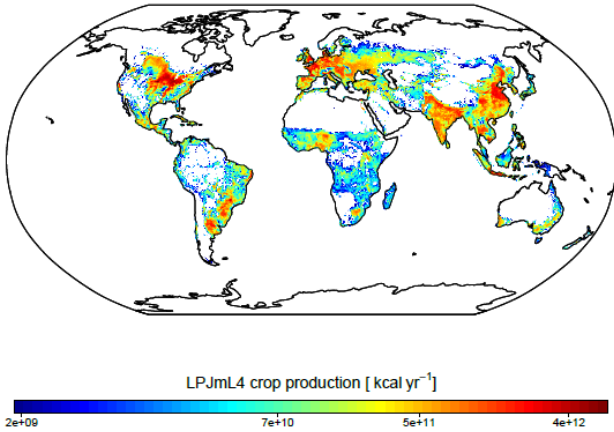
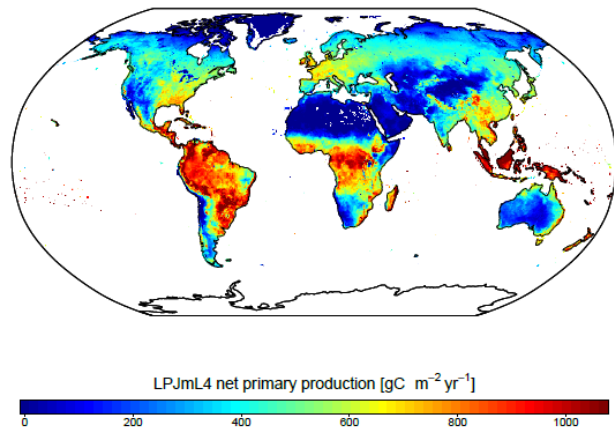
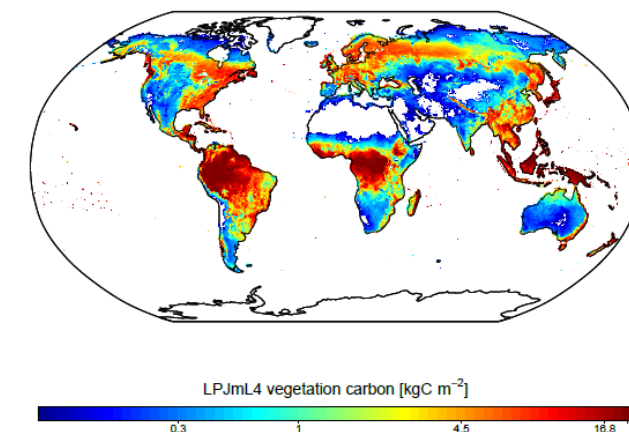
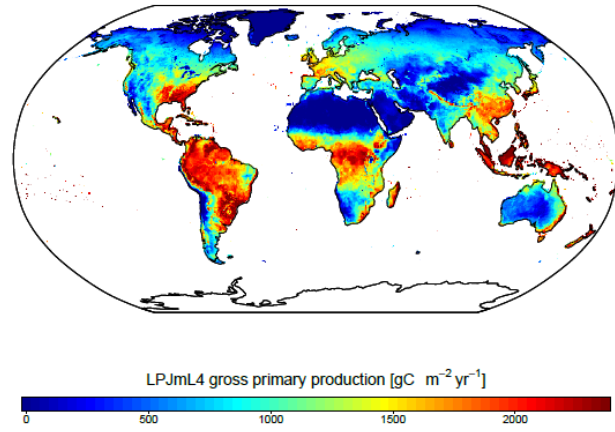
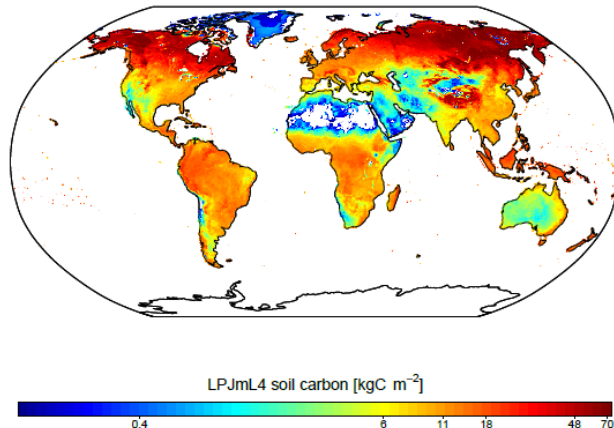



## LPJmL4 – a dynamic global vegetation model with managed land – Part 1: Model description

Sibyll Schaphoff<sup>1</sup>, Werner von Bloh<sup>1</sup>, Anja Rammig<sup>2</sup>, Kirsten Thonicke<sup>1</sup>, Hester Biemans<sup>3</sup>, Matthias Forkel<sup>4</sup>, Dieter Gerten<sup>1,5</sup>, Jens Heinke<sup>1</sup>, Jonas Jägermeyr<sup>1</sup>, Jürgen Knauer<sup>6</sup>, Fanny Langerwisch<sup>1</sup>, Wolfgang Lucht<sup>1,5</sup>, Christoph Müller<sup>1</sup>, Susanne Rolinski<sup>1</sup>, and Katharina Waha<sup>1,7</sup>

**Figure 1.** LPJmL4 scheme for carbon, water, and energy fluxes represented by the model. C – carbon; W – water; S – sensible heat conduction; H – latent heat convection; c – energy conduction;  $R_n$  – net downward radiation (input); PAR – photosynthetic active radiation;  $E_i$  – interception;  $E_T$  – transpiration;  $E_S$  – evaporation; Infil – infiltration; Perc – percolation; Pr – precipitation (input); GPP – gross primary production; NPP – net primary production;  $R_a$  – autotrophic respiration;  $R_h$  – heterotrophic respiration;  $H_c$  – carbon harvested;  $F_c$  – carbon emitted by fire; SOM – soil organic matter; R – run-off; Q – discharge.

# Example: LPJmL dynamic global vegetation model



Geosci. Model Dev., 11, 1343–1375, 2018  
<https://doi.org/10.5194/gmd-11-1343-2018>  
© Author(s) 2018. This work is distributed under the Creative Commons Attribution 4.0 License.



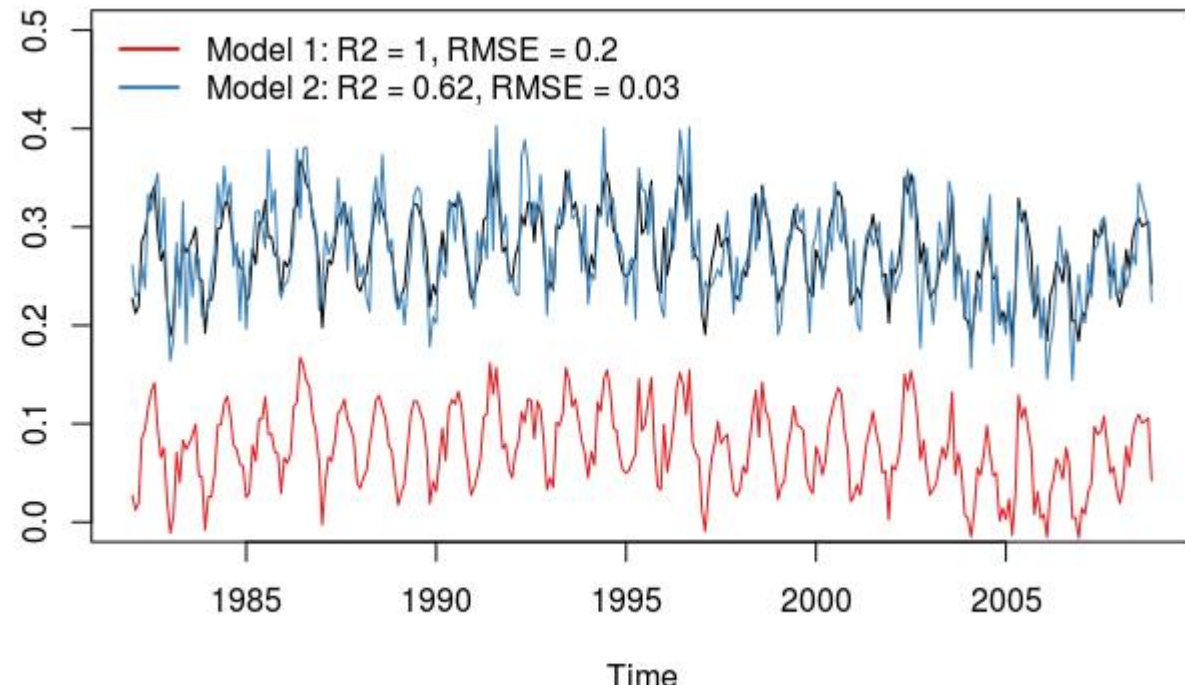
## LPJmL4 – a dynamic global vegetation model with managed land – Part 1: Model description

Sibyll Schaphoff<sup>1</sup>, Werner von Bloh<sup>1</sup>, Anja Rammig<sup>2</sup>, Kirsten Thonicke<sup>1</sup>, Hester Biemans<sup>3</sup>, Matthias Forkel<sup>4</sup>, Dieter Gerten<sup>1,5</sup>, Jens Heinke<sup>1</sup>, Jonas Jägermeyr<sup>1</sup>, Jürgen Knauer<sup>6</sup>, Fanny Langerwisch<sup>1</sup>, Wolfgang Lucht<sup>1,5</sup>, Christoph Müller<sup>1</sup>, Susanne Rolinski<sup>1</sup>, and Katharina Waha<sup>1,7</sup>

# Model evaluation

# Model evaluation

Which one is the better model?



$R^2$  = coefficient of determination = correlation<sup>2</sup> → perfect model == 1

RMSE (RMSD) = root mean squared error/difference → perfect model == 0

# Model evaluation

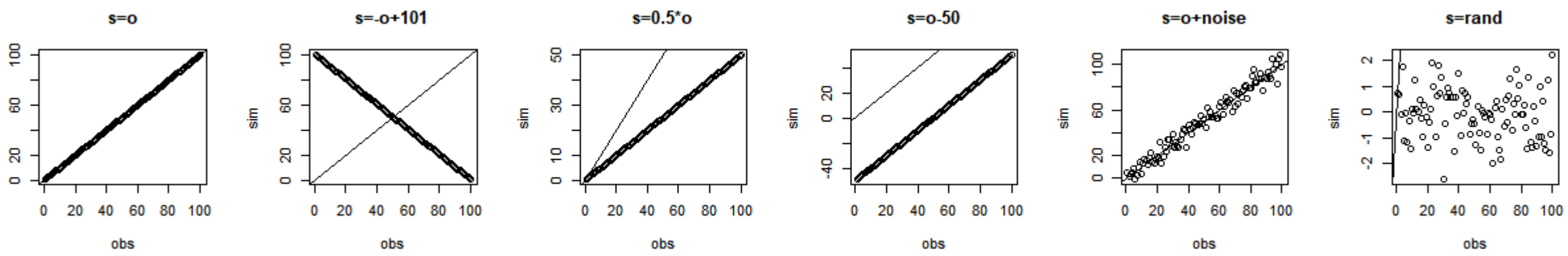
Model performance measures  
(objective functions)

(Janssen & Heuberger 1995)

Table 1  
Performance measures for comparing model predictions and observations

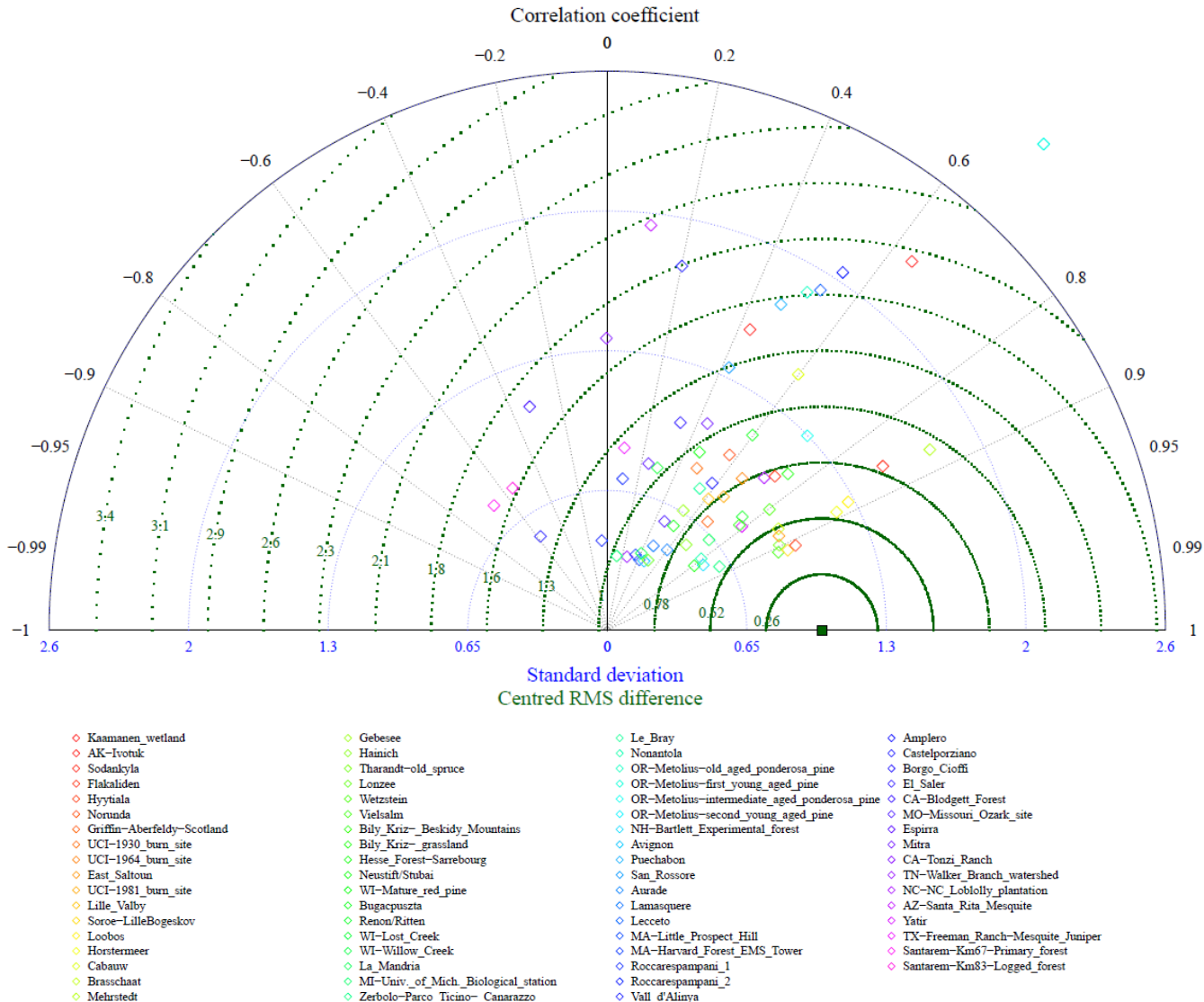
Criterion	Symbol	Formulation
Average error	AE	$\frac{\sum_{i=1}^N (P_i - O_i)}{n} = \bar{P} - \bar{O}$
Normalized average error	NAE	$\frac{(\bar{P} - \bar{O})}{\bar{O}}$
Fractional mean bias	FB	$\frac{(\bar{P} - \bar{O})}{\frac{1}{2}(\bar{P} + \bar{O})}$
Relative mean bias	rB	$\frac{(\bar{P} - \bar{O})}{S_O}$
Fractional variance	FV	$\frac{(S_P^2 - S_O^2)}{\frac{1}{2}(S_P^2 + S_O^2)}$
Variance ratio	VR	$\frac{S_P^2}{S_O^2}$
Kolmogorov-Smirnov	KS	$\max_x( F_P(x) - F_O(x) )$
Root mean square error	RMSE	$\sqrt{\frac{\sum_{i=1}^N (P_i - O_i)^2}{N}}$
Normalized RMSE	NRMSE	$\frac{\text{RMSE}}{\bar{O}}$
Index of agreement	IoA	$1 - \frac{\sum_{i=1}^N (P_i - O_i)^2}{\sum_{i=1}^N ( P_i  +  O_i )^2}$
Alternative index of agreement	AIoA	$1 - \frac{\sum_{i=1}^N  P_i - O_i }{\sum_{i=1}^N ( P_i  +  O_i )}$
Mean absolute error	MAE	$\frac{\sum_{i=1}^N  P_i - O_i }{N}$
Normalized mean absolute error	NMAE	$\frac{\text{MAE}}{\bar{O}}$
Maximal absolute error	MaxAE	$\max_{i=1, \dots, N}( P_i - O_i )$
Median absolute error	MedAE	$\text{median}( P_i - O_i )$
Upper quartile absol. error	UppAE	75-th percentile(  $P_i - O_i )$
Ratio of scatter	RS	$\frac{[\sum_{i=1}^N (O_i - \bar{O})^2]}{[\sum_{i=1}^N (P_i - \bar{O})^2]}$
Modelling efficiency	ME	$\frac{[\sum_{i=1}^N (O_i - \bar{O})^2 - \sum_{i=1}^N (P_i - O_i)^2]}{[\sum_{i=1}^N (O_i - \bar{O})^2]}$
Regression quantities	$\alpha, \beta, R^2$	$O_i = \alpha + \beta \cdot P_i + \varepsilon_i$

$P_i$  and  $O_i$  denote the predicted value and observed value  $i$ ;  $\bar{P}$ ,  $\bar{O}$  and  $S_P^2$ ,  $S_O^2$  are their means and variances;  $F_P$ ,  $F_O$  denote the cumulative empirical distribution functions;  $P'_i = P_i - \bar{O}$  and  $O'_i = O_i - \bar{O}$ .



	obs	obs	obs	obs	obs	obs
	s=0	s=-0.1+101	s=0.5*s	s=0-50	s=0+noise	s=rand
<b>Correlation-based metrics:</b>						
Correlation coefficient	Cor = 1.000	-1.000	1.000	1.000	0.984	-0.128
Spearman correlation	Spearman = 1.000	-1.000	1.000	1.000	0.985	-0.152
Regression slope	Slope = 1.000	-1.000	2.000	1.000	0.963	-3.881
Coefficient of determination	R2 = 1.0000	1.0000	1.0000	1.0000	0.9680	0.0165
<b>Bias-based metrics:</b>						
Average error	AE = 0.000	0.000	-25.250	-50.000	0.596	-50.576
Normalized average error	NAE = 0.0000	0.0000	-0.5000	-0.9901	0.0118	-1.0015
Fractional mean bias	FB = 0.0000	0.0000	-0.6667	-1.9608	0.0117	-2.0060
Relative mean bias	rB = 0.0000	0.0000	-0.8703	-1.7235	0.0206	-1.7433
Percent bias	Pbias = 0.00	0.00	-50.00	-99.01	1.18	-100.15
<b>Variance-based metrics:</b>						
Fractional variance	FV = 0.0000	0.0000	-1.2000	0.0000	0.0425	-1.9956
Variance ratio	VR = 1.00000	1.00000	0.25000	1.00000	1.04342	0.00109
<b>Squared error metrics:</b>						
Sum squared error	SSE = 0	333300	84588	250000	2822	339917
Mean squared error	MSE = 0.0	3333.0	845.9	2500.0	28.2	3399.2
Root mean squared error	RMSE = 0.00	57.73	29.08	50.00	5.31	58.30
Normalized RMSE	NRMSE = 0.000	1.143	0.576	0.990	0.105	1.155
<b>Absolute error metrics:</b>						
Mean absolute error	MAE = 0.00	50.00	25.25	50.00	4.27	50.58
Normalized mean absolute error	NMAE = 0.0000	0.9901	0.5000	0.9901	0.0845	1.0015
Median absolute error	MedAE = 0.0	50.0	25.2	50.0	3.5	51.1
Upper quartile absolute error	UpAE = 0.00	75.00	37.62	50.00	6.41	74.86
Maximal absolute error	MaxAE = 0.0	99.0	50.0	50.0	13.9	99.8
<b>Distribution-based metrics:</b>						
Ratio of scatter	RS = 1.000	1.000	0.985	0.250	0.958	0.326
Kolmogorov-Smirnov statistic	KS = 0.000	0.000	0.500	0.500	0.040	0.980
<b>Efficiency metrics:</b>						
Index of agreement	IoA = 1.000	0.000	0.712	0.625	0.992	0.426
Modelling/Nash-Sutcliffe eff.	MEF = 1.0000	-3.0000	-0.0152	-2.0003	0.9661	-3.0794
Kling-Gupta efficiency	KGE = 1.0000	-1.0000	0.2929	0.0099	0.9706	-0.7919

# Example: LPJmL dynamic global vegetation model



Geosci. Model Dev., 11, 1377–1403, 2018  
<https://doi.org/10.5194/gmd-11-1377-2018>  
 © Author(s) 2018. This work is distributed under the Creative Commons Attribution 4.0 License.



Geoscientific  
Model Development

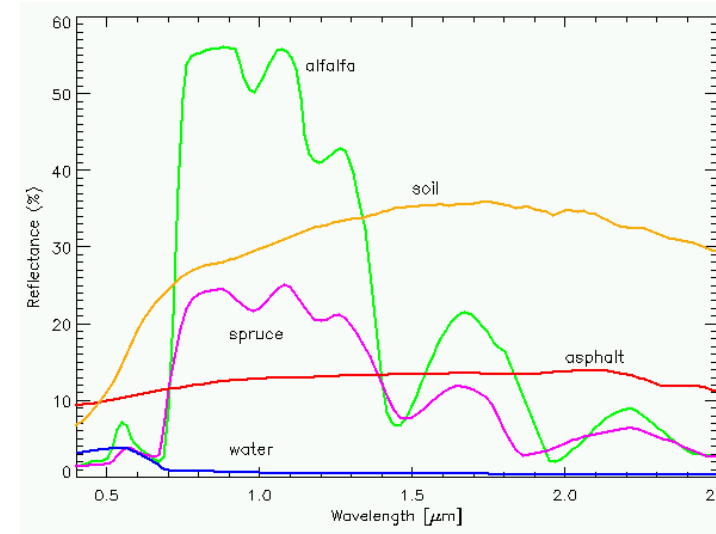
## LPJmL4 – a dynamic global vegetation model with managed land – Part 2: Model evaluation

Sibyll Schaphoff<sup>1</sup>, Matthias Forkel<sup>2</sup>, Christoph Müller<sup>1</sup>, Jürgen Knauer<sup>3</sup>, Werner von Bloh<sup>1</sup>, Dieter Gerten<sup>1,4</sup>, Jonas Jägermeyr<sup>1</sup>, Wolfgang Lucht<sup>1,4</sup>, Anja Rammig<sup>5</sup>, Kirsten Thonicke<sup>1</sup>, and Katharina Waha<sup>1,6</sup>

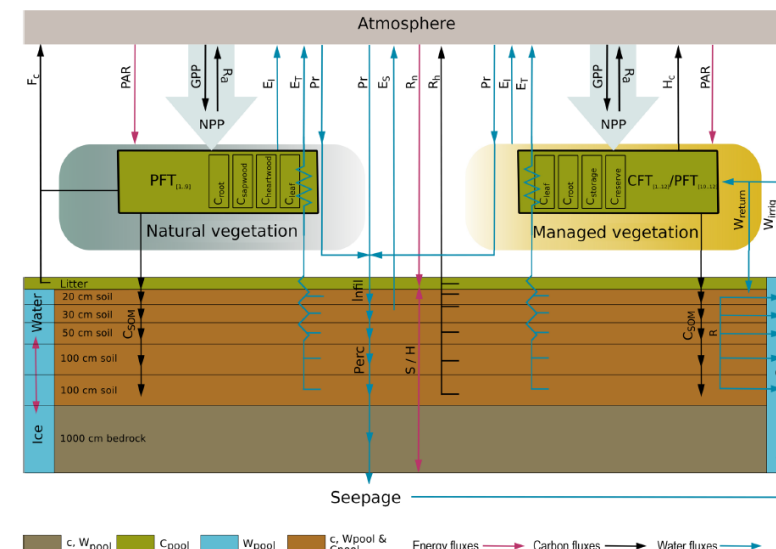
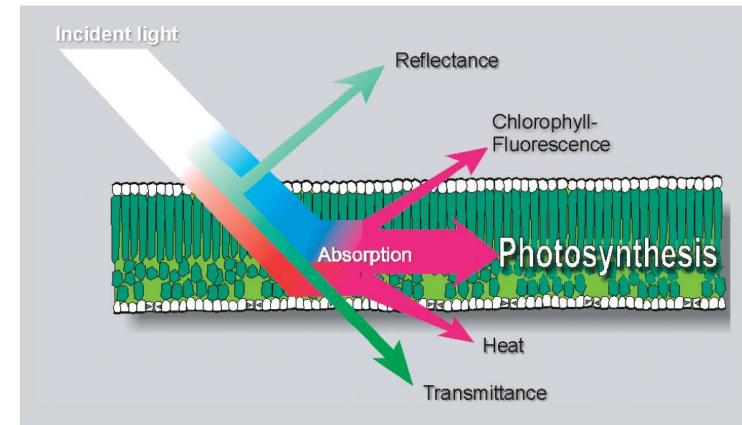
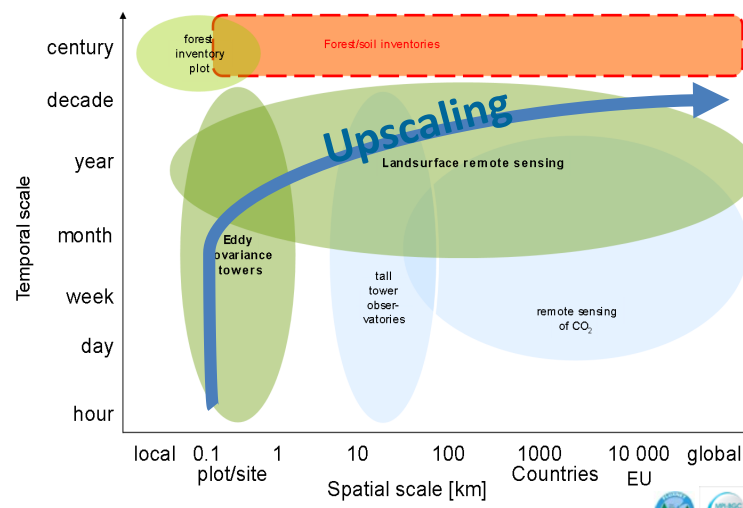
**Taylor diagram** visualize  
multiple model performance  
metrics

Figure 3. Net ecosystem exchange rate measured at eddy flux towers: ORNL DAAC (2011). Available online at FLUXNET (<http://fluxnet.fluxdata.org/data/la-thuile-dataset/>). Sites (colours) are ordered from north to south.

# Conclusions



From point to globe via integration with remote sensing



e 1. LPJmL4 scheme for carbon, water, and energy fluxes represented by the model. C – carbon; W – water; S – sensible heat convection; H – latent heat convection; c – energy conduction; R<sub>n</sub> – net downward radiation (input); PAR – photosynthetic active radiation interception; E<sub>I</sub> – transpiration; E<sub>S</sub> – evaporation; Infil – infiltration; Perc – percolation; Pr – precipitation (input); GPP – gross primary production; NPP – net primary production; R<sub>a</sub> – autotrophic respiration; R<sub>h</sub> – heterotrophic respiration; H<sub>c</sub> – carbon harvested; F<sub>c</sub> – carbon emitted by fire; SOM – soil organic matter; R – run-off; Q – discharge.

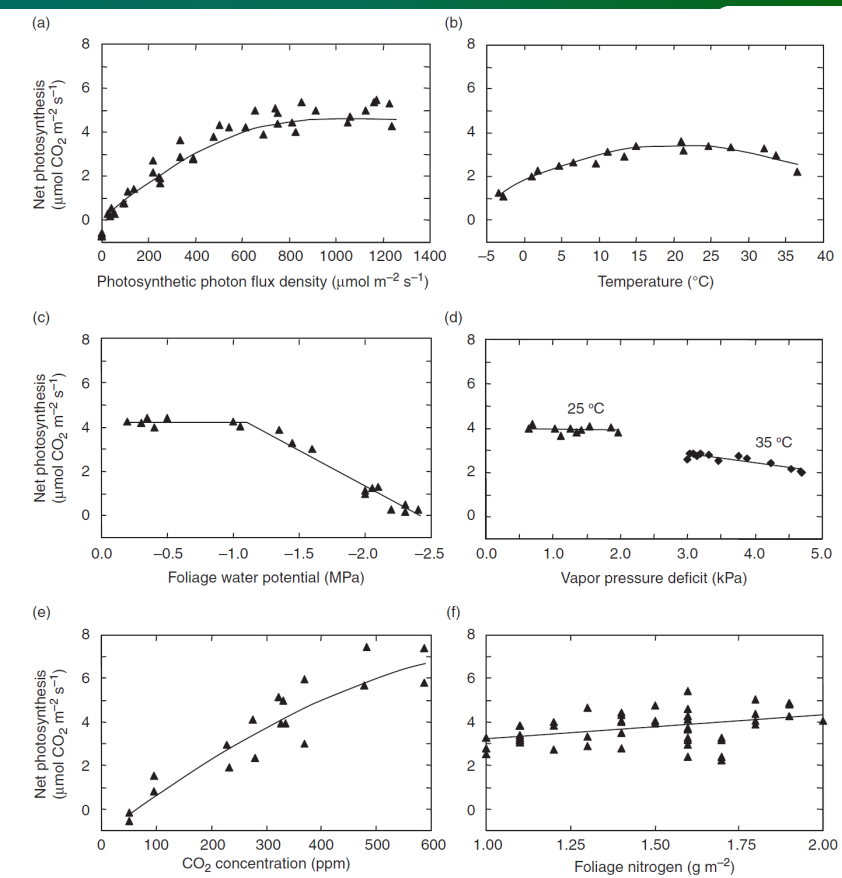


Table 1  
Performance measures for comparing model predictions and observations

Criterion	Symbol	Formulation
Average error	AE	$\frac{\sum_{i=1}^N (P_i - O_i)}{n} = \bar{P} - \bar{O}$
Normalized average error	NAE	$\frac{(\bar{P} - \bar{O})}{\bar{O}}$
Fractional mean bias	FB	$\frac{1}{2} (\bar{P} + \bar{O})$
Relative mean bias	rB	$\frac{(\bar{P} - \bar{O})}{\bar{O}}$
Fractional variance	FV	$\frac{1}{2} (\bar{S}_P^2 + \bar{S}_O^2)$
Variance ratio	VR	$\frac{\bar{S}_P^2}{\bar{S}_O^2}$
Kolmogorov–Smirnov	KS	$\max_x  (F_P(x) - F_O(x)) $
Root mean square error	RMSE	$\sqrt{\frac{\sum_{i=1}^N (P_i - O_i)^2}{N}}$
Normalized RMSE	NRMSE	$\frac{\text{RMSE}}{\bar{O}}$
Index of agreement	IoA	$1 - \frac{\sum_{i=1}^N (P_i - O_i)^2}{\sum_{i=1}^N (P_i + O_i)^2}$
Alternative index of agreement	AIoA	$1 - \frac{\sum_{i=1}^N  P_i - O_i }{\sum_{i=1}^N (P_i + O_i)}$
Mean absolute error	MAE	$\frac{\sum_{i=1}^N  P_i - O_i }{n}$

# Exercise 3

## 120.081 Climate and Environmental Remote Sensing (VU, 2019S) – Exercise 3: Ecosystem model-data integration

Wouter Dorigo, Matthias Forkel, and Leander Mössinger

Climate and Environmental Remote Sensing Group, Department of Geodesy and Geoinformation, Technische Universität Wien, Gusshausstraße 27-29, 1040 Vienna, Austria

Correspondence to: Matthias Forkel ([matthias.forkel@geo.tuwien.ac.at](mailto:matthias.forkel@geo.tuwien.ac.at), for general questions regarding the exercise), Leander Mössinger ([leander.moessinger@geo.tuwien.ac.at](mailto:leander.moessinger@geo.tuwien.ac.at), for Python-related questions)

### 1 Introduction

Dynamic global vegetation models (DGVMs) are used to quantify past, present, and future dynamics of global ecosystems such as vegetation distribution, carbon and water cycling, and land management. Widely used is the LPJ (Lund-Potsdam-Jena) DGVM (Sitch et al., 2003) that in its most recent version (LPJmL4) represents carbon, water and energy fluxes in natural and managed vegetation and includes improved representations of permafrost and soil hydrology, fire, phenology, irrigation and water reservoirs, crop types and bioenergy plants (Schaphoff et al., 2018a) (Figure 1). LPJmL has been evaluated against various satellite and in-situ observations (Schaphoff et al., 2018b). Moreover, satellite observations have been used to estimate model parameters that govern the simulated phenology and gross primary production (Forkel et al., 2014).

The aim of this exercise is to analyse and evaluate LPJmL model results against satellite datasets of the fraction of absorbed photosynthetic active radiation (FAPAR), sun-induced fluorescence (SIF), and surface soil moisture (SSM) for some selected grid cells. Furthermore, the sensitivity of model parameters will be assessed for a grid cell in a Savannah ecosystem and an optimal model parameter set will be estimated.

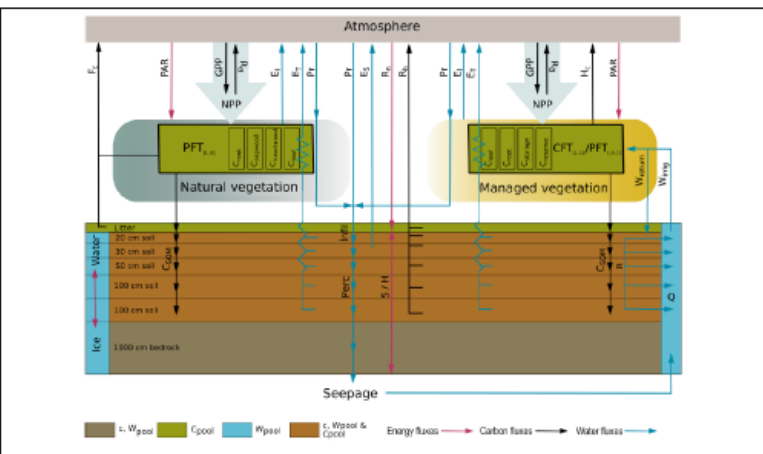


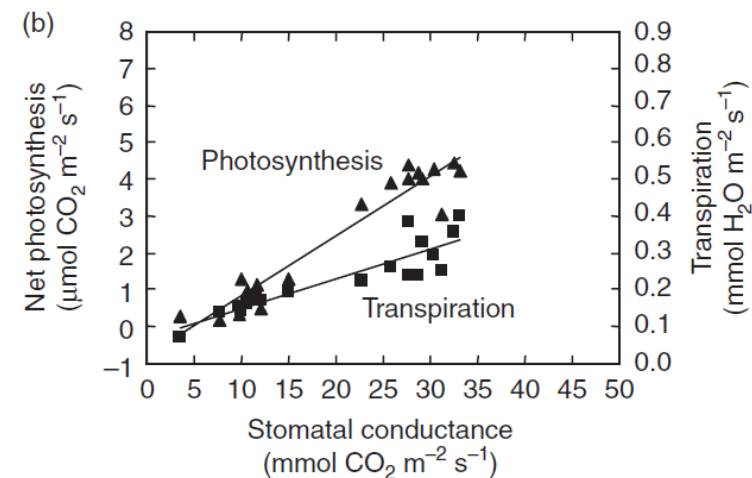
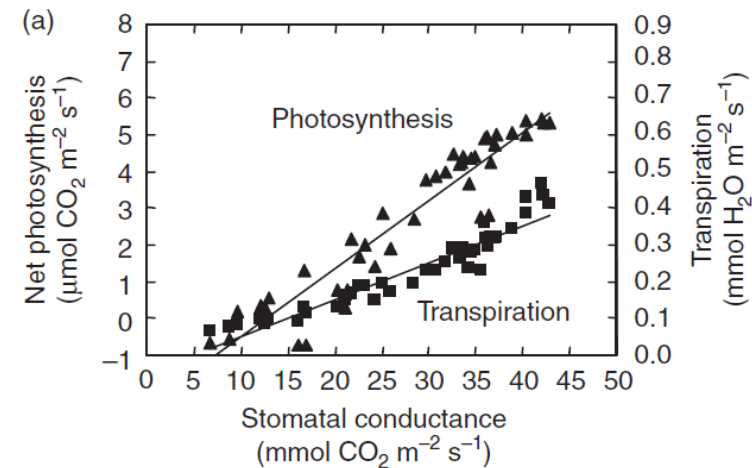
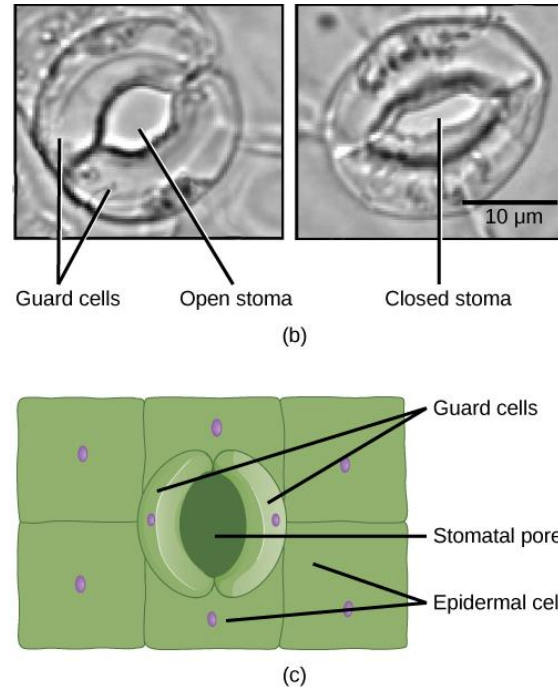
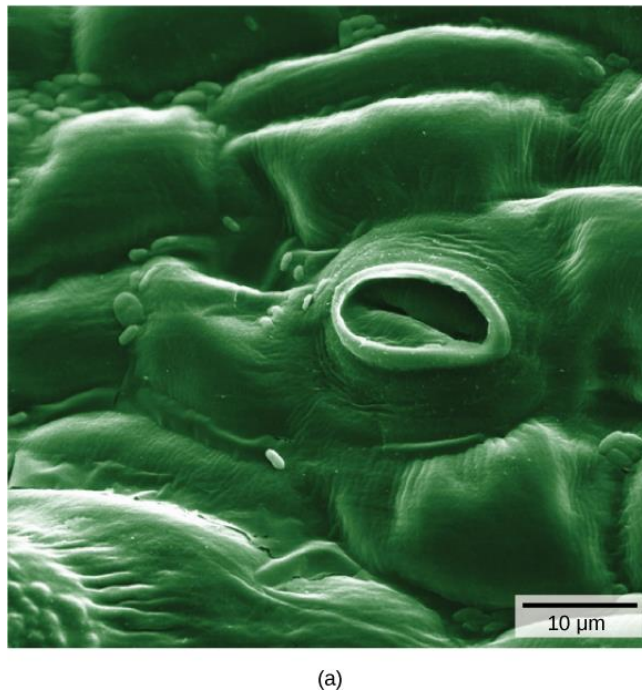
Figure 1. LPJmL4 scheme for carbon, water, and energy fluxes represented by the model. C – carbon; W – water; S – sensible heat conduction; H – latent heat convection; c – energy conduction; R<sub>d</sub> – net downward radiation (input); PAR – photosynthetic active radiation; E<sub>i</sub> – interception; E<sub>v</sub> – transpiration; Infilt – infiltration; Perc – percolation; Pr – precipitation (input); GPP – gross primary production; NPP – net primary production; R<sub>h</sub> – autotrophic respiration; R<sub>h</sub> – heterotrophic respiration; H<sub>c</sub> – carbon harvested; F<sub>c</sub> – carbon emitted by fire; SOM – soil organic matter; R – run-off; Q – discharge.

Figure 1: Structure of the LPJmL4 model (Schaphoff et al., 2018a).

# Unused slides

# Stomatal conductance – water-use efficiency

- Stomata regulate carbon and water exchange
- Open stomata = high stomatal conductance
- Plants try to maximize carbon gain and minimize water loss
- Water-use efficiency
  - WUE = CO<sub>2</sub> assimilation / transpiration



**Fig. 16.7** Relationship between photosynthesis, transpiration, and stomatal conductance for jack pine.  
(a) Light response over a range of 0 to 1250  $\mu\text{mol photon m}^{-2} \text{ s}^{-1}$ . (b) Foliage water potential response over a range of -0.2 to -2.4 MPa. Data from Dang et al. (1997a,b, 1998).

# Canopy light absorption

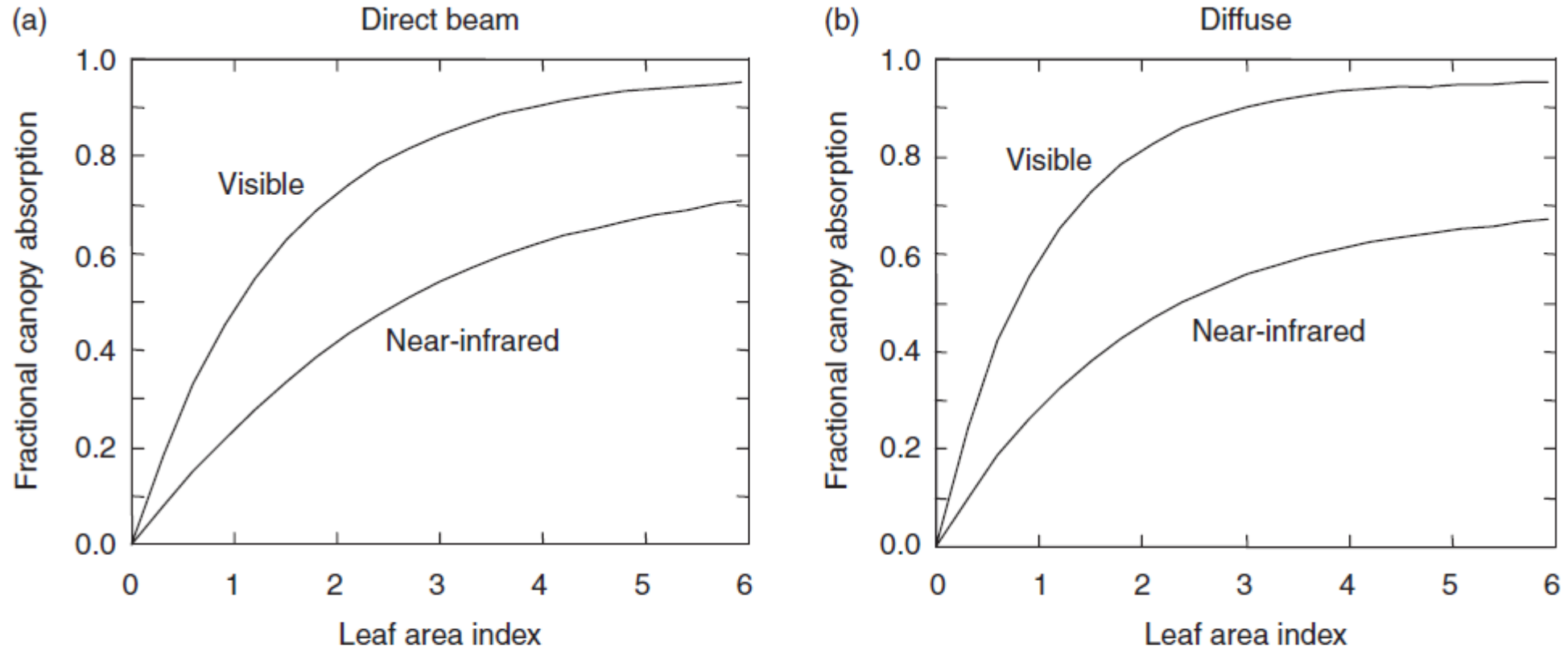
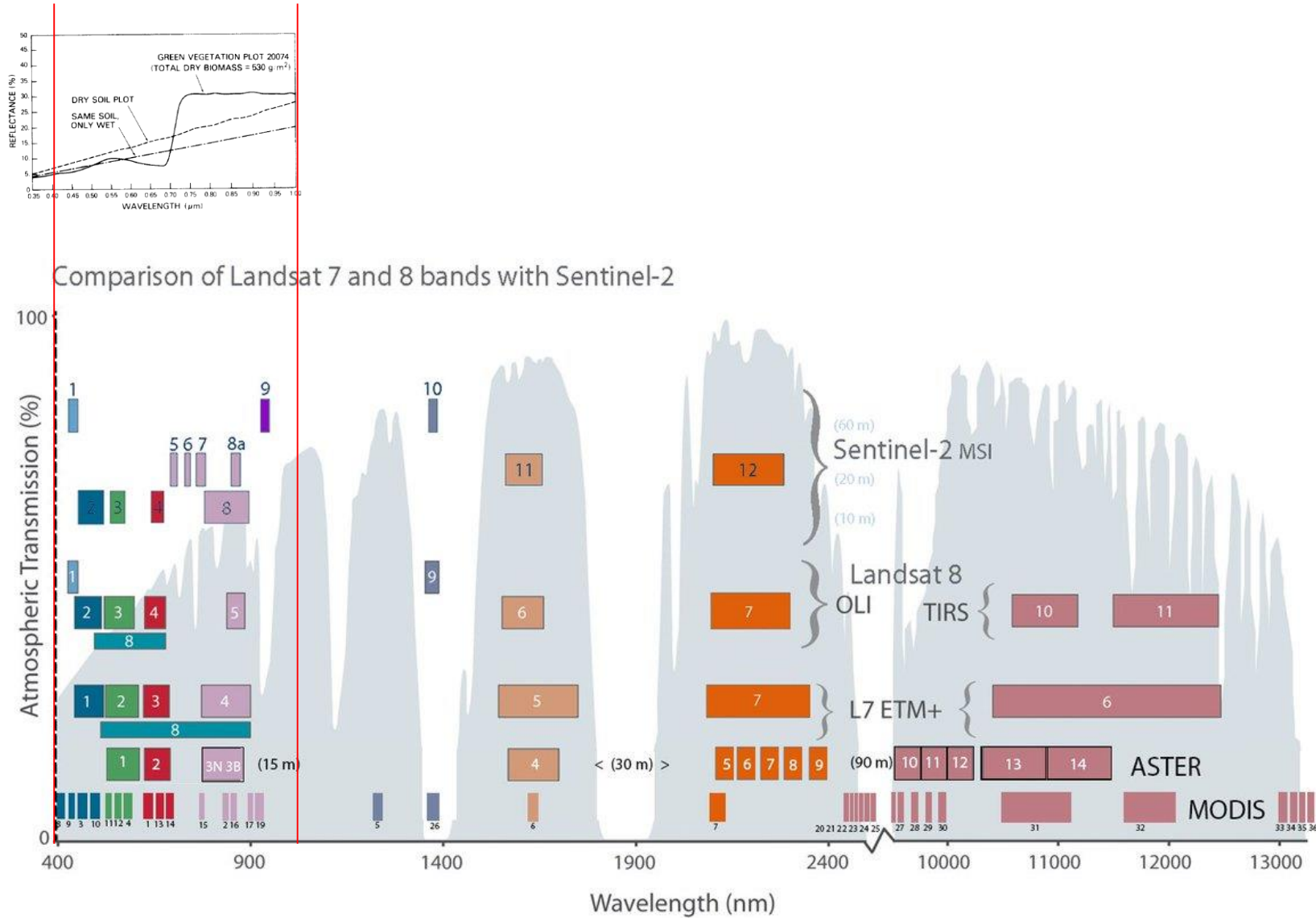


**Fig. 17.3** Radiative transfer in a broadleaf forest with spherical leaf orientation in relation to leaf area index. Shown for the visible and near-infrared wavebands are (a) the fraction of direct beam solar radiation and (b) the fraction of diffuse solar radiation absorbed by the canopy using the radiative transfer model of Sellers (1985). The zenith angle is 45° and soil albedos are 0.10 (visible) and 0.20 (near-infrared). Leaf optical properties are from Table 17.1.

# Vegetation indices from multiple sensors



$$NDVI = \frac{NIR - red}{NIR + red}$$

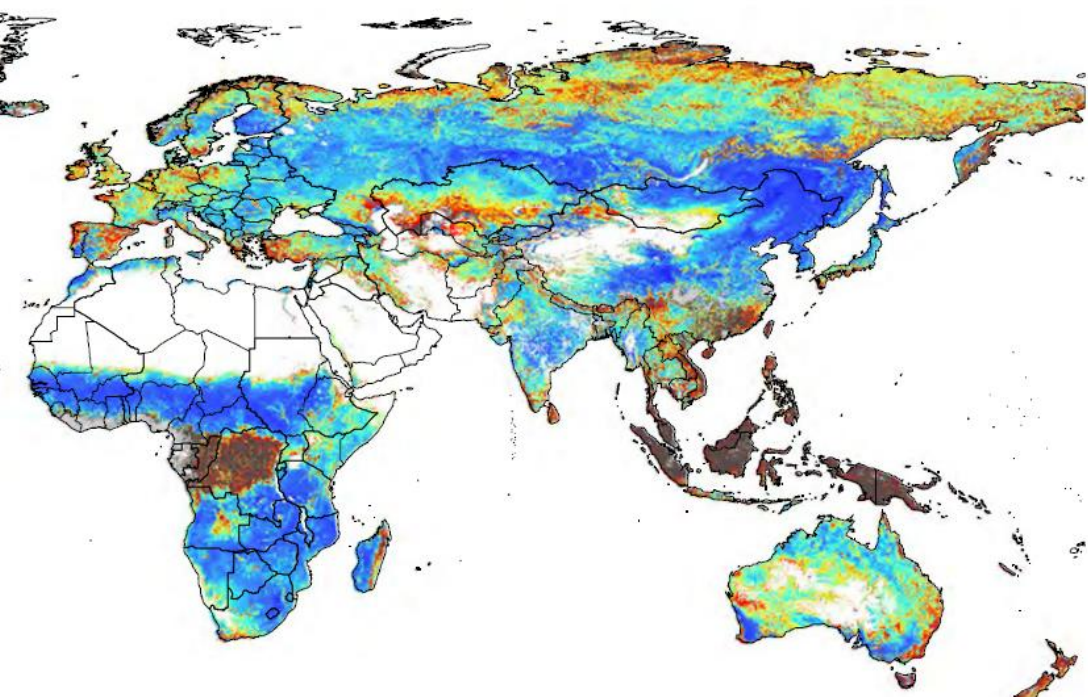
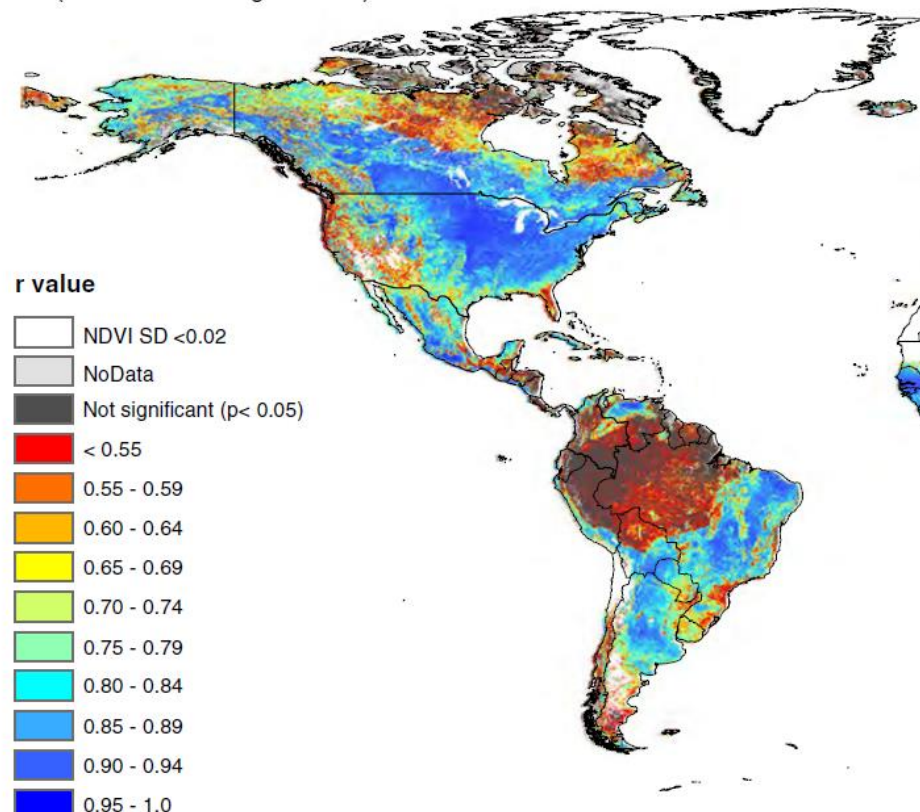
$$FAPAR = f(NDVI, \dots)$$

$$= f(NIR, red, \dots)$$

## Correlation between NDVI time series

**A**

MODIS/GIMMS NDVI linear correlation  
2000-2010 monthly observations  
(QA data screening included)



Contents lists available at SciVerse ScienceDirect

Remote Sensing of Environment

journal homepage: [www.elsevier.com/locate/rse](http://www.elsevier.com/locate/rse)

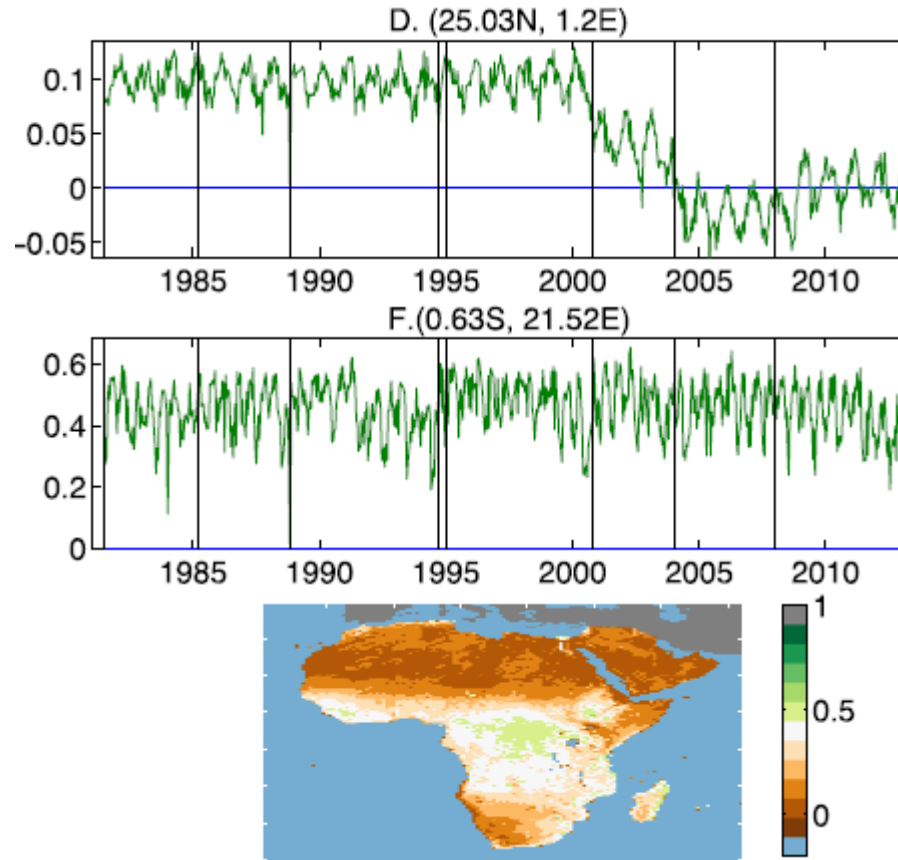


Evaluation of Earth Observation based global long term vegetation trends – Comparing GIMMS and MODIS global NDVI time series  
Rasmus Fensholt\*, Simon R. Proud

Fig.: Correlation between MODIS and GIMMS NDVI (monthly, 2000-2010)  
(Fensholt and Proud 2012).

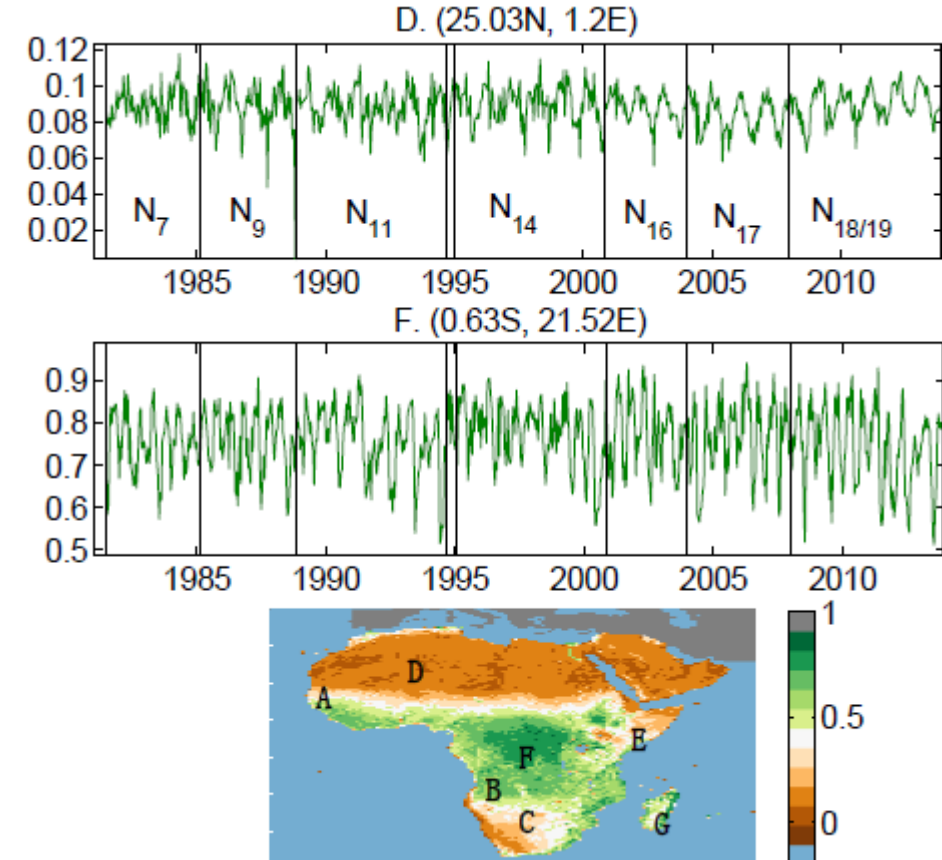
# Multi-sensor harmonisation

- NOAA AVHRR (advanced very high resolution radiometer)
- GIMMS NDVI (3g) dataset 1981-2011(2015)

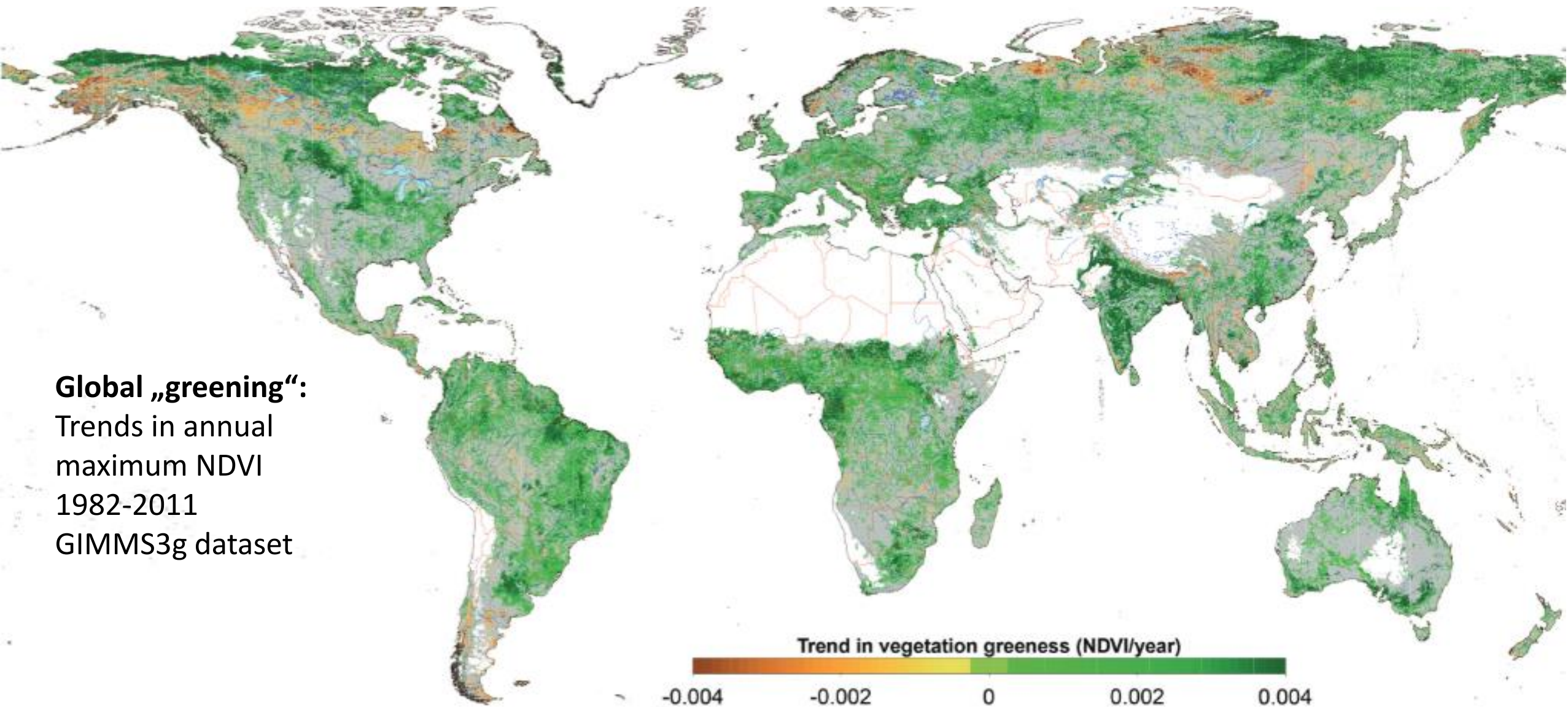


## A Non-Stationary 1981–2012 AVHRR NDVI<sub>3g</sub> Time Series

Jorge E. Pinzon <sup>1,\*</sup> and Compton J. Tucker <sup>2</sup>



# Global NDVI trends



# MOD17 algorithm

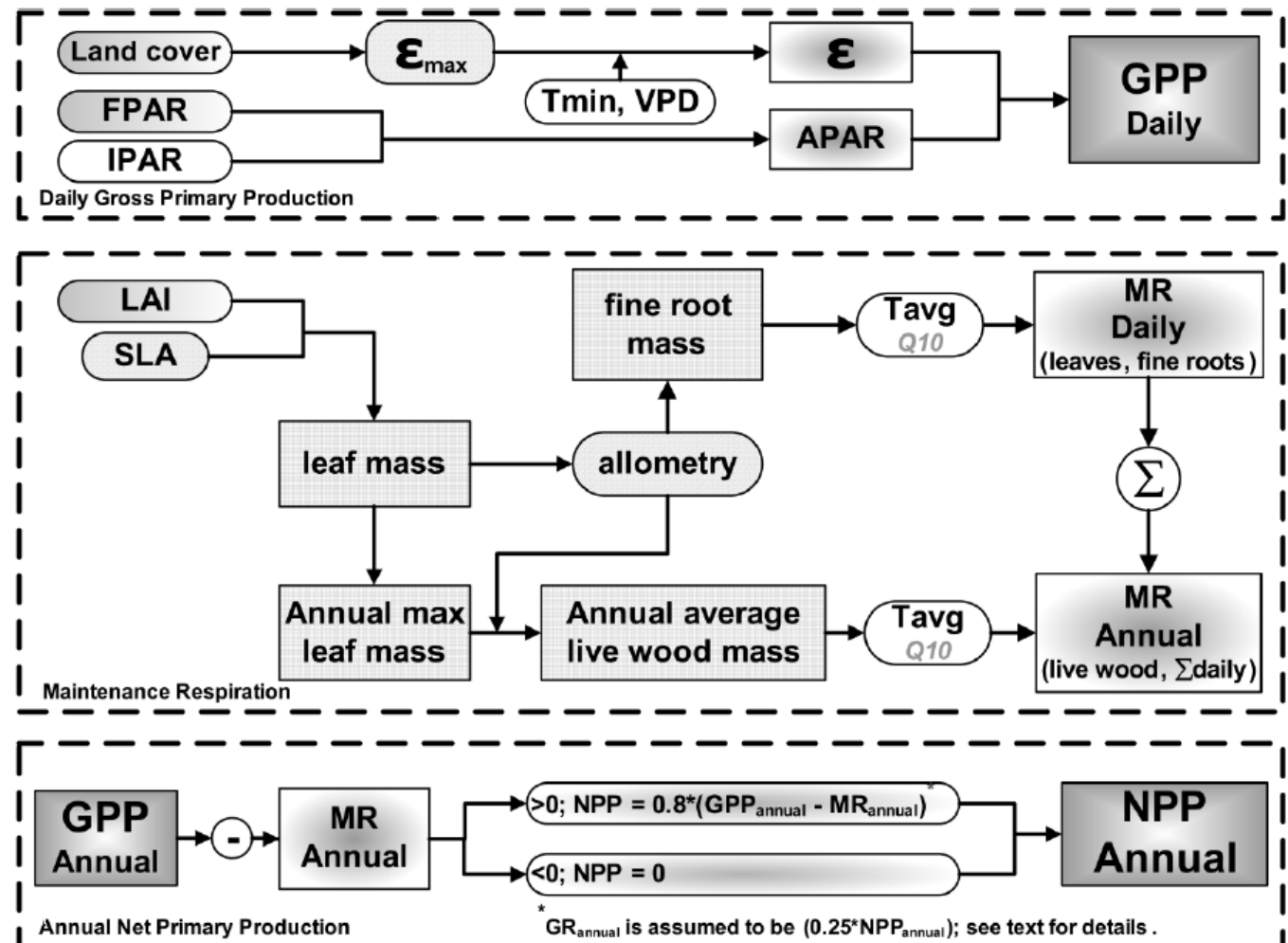


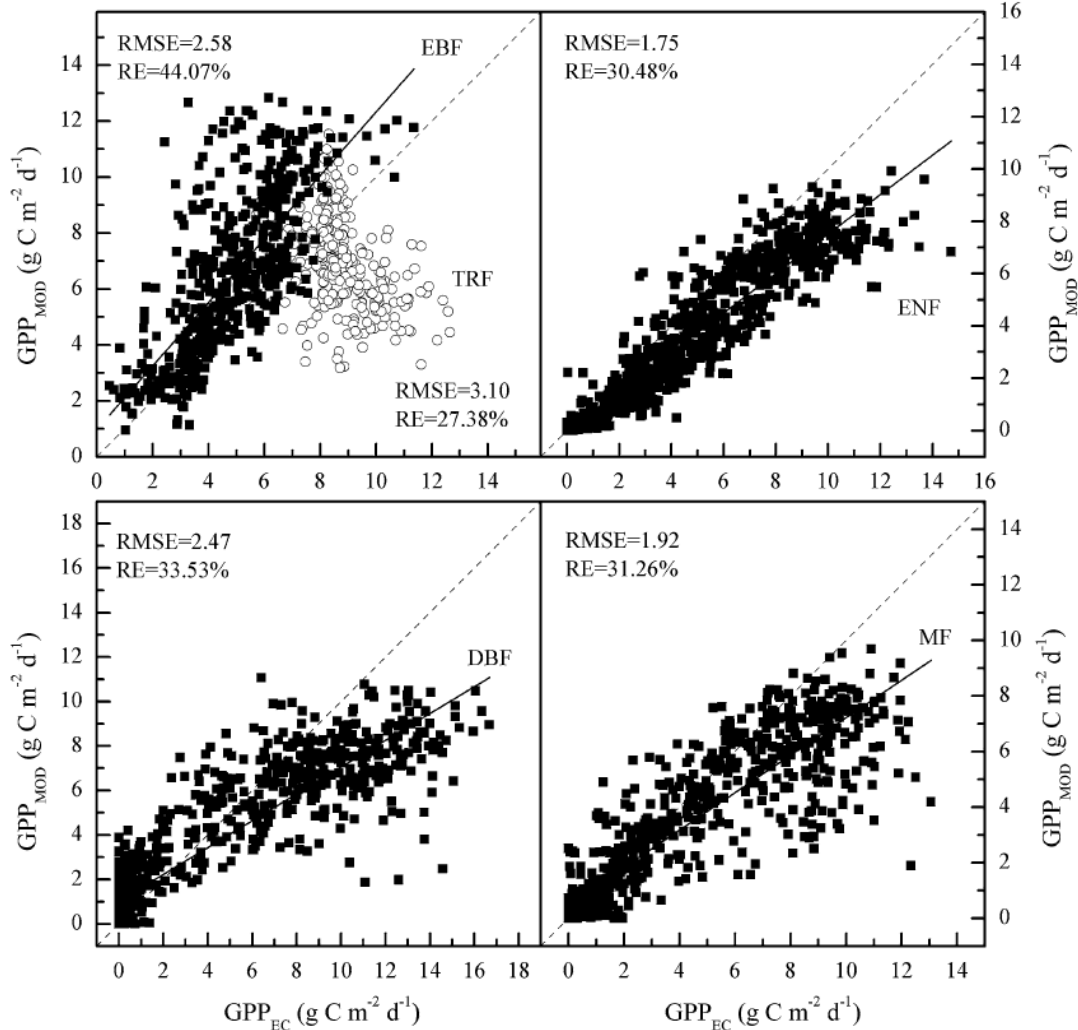
*Figure 1.1. Flowcharts showing the logic behind the MOD17 Algorithm in calculating both 8-day average GPP and annual NPP.*

# Performance of MOD17

Environ Earth Sci (2015) 74:5907–5918  
DOI 10.1007/s12665-015-4615-0

ORIGINAL ARTICLE

## Evaluation of MOD17 GPP



## A comprehensive assessment of MODIS-derived GPP for forest ecosystems using the site-level FLUXNET database

Xuguang Tang<sup>1,2</sup> · Hengpeng Li<sup>1</sup> · Ni Huang<sup>2</sup> · Xinyan Li<sup>1</sup> · Xibao Xu<sup>1</sup> · Zhi Ding<sup>3</sup> · Jing Xie<sup>4</sup>

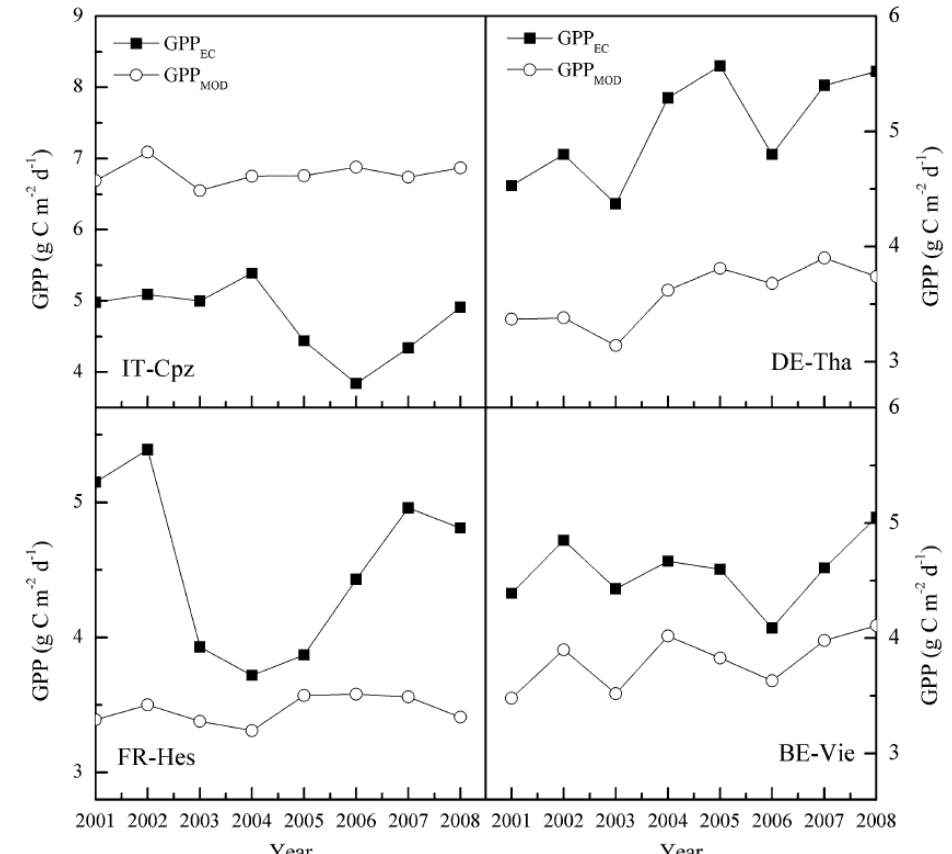




**Table 2.** Selected predictors for both setups for CO<sub>2</sub> fluxes (GPP, TER and NEE) and energy fluxes ( $H$ , LE and Rn). List of acronyms: Enhanced Vegetation Index (EVI), fraction of absorbed photosynthetically active radiation (fAPAR), leaf area index (LAI), daytime land surface temperature (LST<sub>Day</sub>) and nighttime land surface temperature (LST<sub>Night</sub>), middle infrared reflectance (band 7; MIR<sup>1</sup>), Normalized Difference Vegetation Index (NDVI), Normalized Difference Water Index (NDWI), plant functional type (PFT), incoming global radiation ( $R_g$ ), top of atmosphere potential radiation (Rpot), Index of Water Availability (IWA), relative humidity (Rh), Water Availability Index lower (WAI<sub>L</sub>), and upper (WAI<sub>U</sub>) (for details, see Sect. S3), and mean seasonal cycle (MSC). The product between A and B (A × B) is shown as (A, B).

Setup	Type of variability	CO <sub>2</sub> fluxes	Energy fluxes
RS	Spatial	PFT Amplitude of MSC of EVI Amplitude of MSC of MIR <sup>1</sup> Maximum of MSC of LST <sub>Day</sub>	PFT Maximum of MSC of (fAPAR, $R_g$ ) Minimum of MSC of $R_g$
	Spatial and seasonal	MSC LAI	MSC of (EVI, LST <sub>Day</sub> ) Rpot
	Spatial, seasonal and interannual	NDWI LST <sub>Day</sub> LST <sub>Night</sub> (NDVI, $R_g$ )	$R_g$ LST <sub>Day</sub> Anomalies of LST <sub>Night</sub> Anomalies of (EVI, LST <sub>Day</sub> )
RS + METEO	Spatial	PFT Amplitude of MSC of NDVI Amplitude of MSC of band 4 BRDF reflectance <sup>2</sup> Minimum of MSC of NDWI Amplitude of MSC of WAI <sub>L</sub>	PFT Maximum of MSC of WAI <sub>U</sub> Mean of MSC of band 6 BRDF reflectance <sup>2</sup> Max of MSC of (fPAR, $R_g$ )
	Spatial and seasonal	MSC of LST <sub>Night</sub> MSC of (fPAR, LST <sub>Day</sub> ) MSC of (EVI, Rpot)	Rpot MSC of NDWI MSC of LST <sub>Night</sub> MSC of (EVI, $R_g$ )
	Spatial and seasonal and interannual	$T_{air}$ ( $R_g$ , MSC of NDVI) WAI <sub>L</sub>	Rain $R_g$ Rh (MSC of NDVI, $R_g$ , IWA)

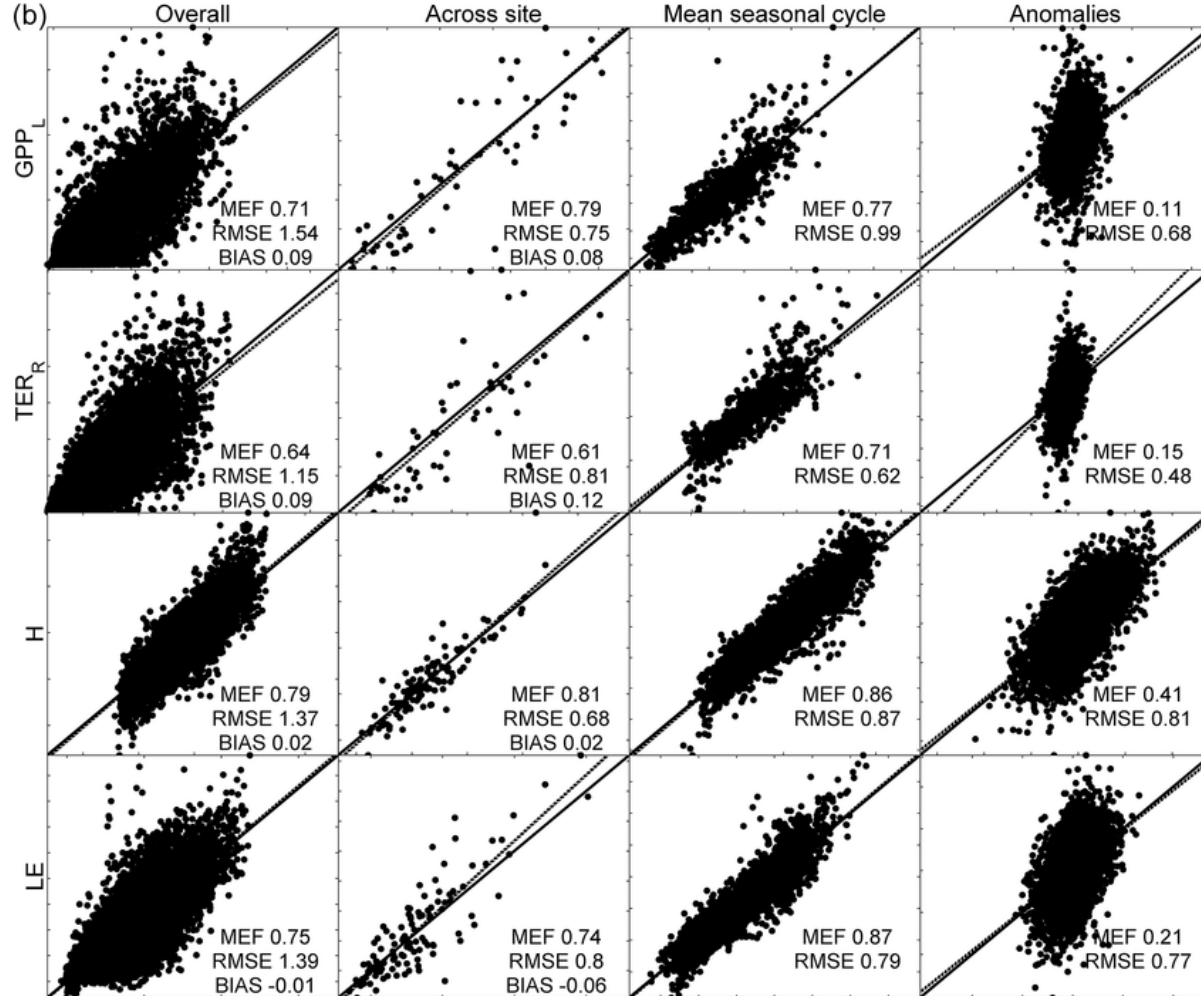
Biogeosciences, 13, 4291–4313, 2016  
[www.biogeosciences.net/13/4291/2016/](http://www.biogeosciences.net/13/4291/2016/)  
doi:10.5194/bg-13-4291-2016  
© Author(s) 2016. CC Attribution 3.0 License.



## Predicting carbon dioxide and energy fluxes across global FLUXNET sites with regression algorithms

Gianluca Tramontana<sup>1</sup>, Martin Jung<sup>2</sup>, Christopher R. Schwalm<sup>3</sup>, Kazuhito Ichii<sup>4,5</sup>, Gustau Camps-Valls<sup>6</sup>,  
Botond Ráduly<sup>1,7</sup>, Markus Reichstein<sup>2</sup>, M. Altaf Arain<sup>8</sup>, Alessandro Cescatti<sup>9</sup>, Gerard Kiely<sup>10</sup>, Lutz Merbold<sup>11,12</sup>,  
Penelope Serrano-Ortiz<sup>13</sup>, Sven Sickert<sup>14</sup>, Sebastian Wolf<sup>11</sup>, and Dario Papale<sup>1</sup>

# Upscaling of eddy covariance observations



Biogeosciences, 13, 4291–4313, 2016  
[www.biogeosciences.net/13/4291/2016/](http://www.biogeosciences.net/13/4291/2016/)  
doi:10.5194/bg-13-4291-2016  
© Author(s) 2016. CC Attribution 3.0 License.



Biogeosciences

Open Access EGU

## Predicting carbon dioxide and energy fluxes across global FLUXNET sites with regression algorithms

Gianluca Tramontana<sup>1</sup>, Martin Jung<sup>2</sup>, Christopher R. Schwalm<sup>3</sup>, Kazuhito Ichii<sup>4,5</sup>, Gustau Camps-Valls<sup>6</sup>, Botond Ráduly<sup>1,7</sup>, Markus Reichstein<sup>2</sup>, M. Altaf Arain<sup>8</sup>, Alessandro Cescatti<sup>9</sup>, Gerard Kiely<sup>10</sup>, Lutz Merbold<sup>11,12</sup>, Penelope Serrano-Ortiz<sup>13</sup>, Sven Sickert<sup>14</sup>, Sebastian Wolf<sup>11</sup>, and Dario Papale<sup>1</sup>

Figure 3. (a) Scatterplots of observed data by eddy-covariance (y axis) and the median ensemble of modeled fluxes by RS setup (x axis). The panels from left to right were the 8-day predictions, the across-site variability, the mean seasonal cycle and the 8-day anomalies. The fluxes considered here were the gross primary production estimated following Lasslop et al. (2010), GPP L (first row); the total ecosystem respiration estimated following Reichstein et al. (2005), TER R (second row); the sensible heat, H (third row); and the latent heat, LE (fourth row). The reference units were g Cm<sup>-2</sup> d<sup>-1</sup> and M Jm<sup>-2</sup> d<sup>-1</sup> for CO<sub>2</sub> fluxes (GPP L and TER R ) and energy fluxes (H and LE), respectively. (b) As in Fig. 3a, but the predictions (x axis) were obtained by the RS + METEO setup.